ALFRED-WEGENER-INSTITUT
HELMHOLTZ-ZENTRUM FÜR POLAR- UND MEERESFORSCHUNG

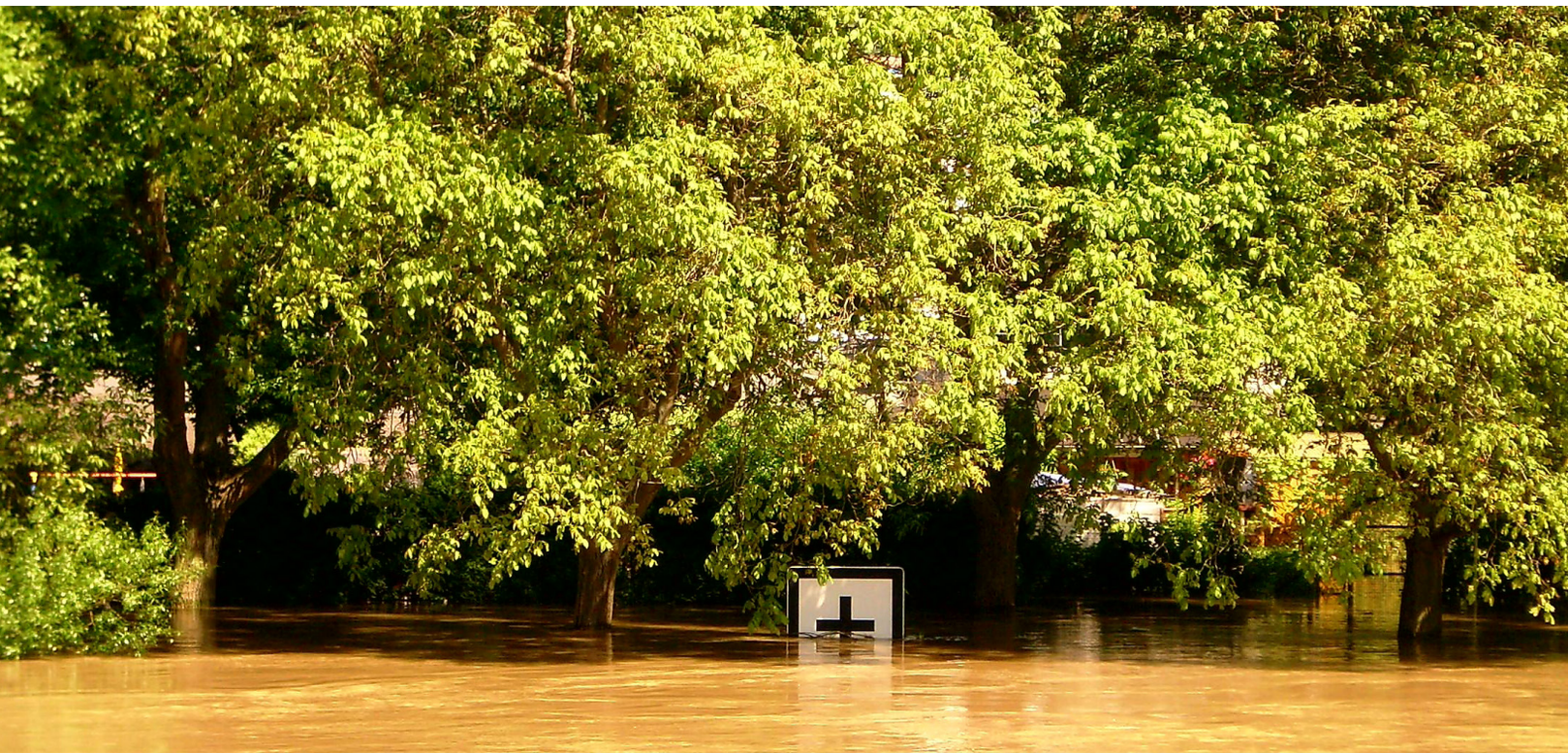

711
2017

Berichte
zur Polar- und Meeresforschung

Reports on Polar and Marine Research

Mid range forecasting of the German Waterways streamflow based on hydrologic, atmospheric and oceanic data

Monica Ionita

HELMHOLTZ GEMEINSCHAFT

Die Berichte zur Polar- und Meeresforschung werden vom Alfred-Wegener-Institut, Helmholtz-Zentrum für Polar- und Meeresforschung (AWI) in Bremerhaven, Deutschland, in Fortsetzung der vormaligen Berichte zur Polarforschung herausgegeben. Sie erscheinen in unregelmäßiger Abfolge.

Die Berichte zur Polar- und Meeresforschung enthalten Darstellungen und Ergebnisse der vom AWI selbst oder mit seiner Unterstützung durchgeführten Forschungsarbeiten in den Polargebieten und in den Meeren.

Die Publikationen umfassen Expeditionsberichte der vom AWI betriebenen Schiffe, Flugzeuge und Stationen, Forschungsergebnisse (inkl. Dissertationen) des Instituts und des Archivs für deutsche Polarforschung, sowie Abstracts und Proceedings von nationalen und internationalen Tagungen und Workshops des AWI.

Die Beiträge geben nicht notwendigerweise die Auffassung des AWI wider.

Herausgeber
Dr. Horst Bornemann

Redaktionelle Bearbeitung und Layout
Birgit Reimann

Alfred-Wegener-Institut
Helmholtz-Zentrum für Polar- und Meeresforschung
Am Handeshafen 12
27570 Bremerhaven
Germany

www.awi.de
www.reports.awi.de

Der Erstautor bzw. herausgebende Autor eines Bandes der Berichte zur Polar- und Meeresforschung versichert, dass er über alle Rechte am Werk verfügt und überträgt sämtliche Rechte auch im Namen seiner Koautoren an das AWI. Ein einfaches Nutzungsrecht verbleibt, wenn nicht anders angegeben, beim Autor (bei den Autoren). Das AWI beansprucht die Publikation der eingereichten Manuskripte über sein Repositorium ePIC (electronic Publication Information Center, s. Innenseite am Rückdeckel) mit optionalem print-on-demand.

The Reports on Polar and Marine Research are issued by the Alfred Wegener Institute, Helmholtz Centre for Polar and Marine Research (AWI) in Bremerhaven, Germany, succeeding the former Reports on Polar Research. They are published at irregular intervals.

The Reports on Polar and Marine Research contain presentations and results of research activities in polar regions and in the seas either carried out by the AWI or with its support.

Publications comprise expedition reports of the ships, aircrafts, and stations operated by the AWI, research results (incl. dissertations) of the Institute and the Archiv für deutsche Polarforschung, as well as abstracts and proceedings of national and international conferences and workshops of the AWI.

The papers contained in the Reports do not necessarily reflect the opinion of the AWI.

Editor
Dr. Horst Bornemann

Editorial editing and layout
Birgit Reimann

Alfred-Wegener-Institut
Helmholtz-Zentrum für Polar- und Meeresforschung
Am Handeshafen 12
27570 Bremerhaven
Germany

www.awi.de
www.reports.awi.de

The first or editing author of an issue of Reports on Polar and Marine Research ensures that he possesses all rights of the opus, and transfers all rights to the AWI, inlcuding those associated with the co-authors. The non-exclusive right of use (einfaches Nutzungsrecht) remains with the author unless stated otherwise. The AWI reserves the right to publish the submitted articles in its repository ePIC (electronic Publication Information Center, see inside page of verso) with the option to "print-on-demand".

Titel: Der Rhein bei Koblenz (Foto von Monica Ionita, Alfred-Wegener-Institut, 5. Juni 2013).

Cover: River Rhine at Koblenz (picture taken by Monica Ionita, Alfred Wegener Institute, 5th June 2013).

Mid range forecasting of the German Waterways streamflow based on hydrologic, atmospheric and oceanic data

Monica Ionita

ISSN 1866-3192

Dr. Monica Ionita

Alfred-Wegener-Institut
Helmholtz-Zentrum für Polar- und Meeresforschung

Am Handelshafen 12
D-27570 Bremerhaven
Germany

✉ monica.ionita@awi.de

Die vorliegende Arbeit ist die inhaltlich unveränderte Fassung eines Abschlussberichts, der 2016 im Kontext des Forschungs- und Entwicklungsvorhabens „Seamless Prediction“ an der Bundesanstalt für Gewässerkunde in Koblenz vorgelegt wurde. Das F&E-Vorhaben wurde durch das Bundesministerium für Verkehr und Digitale Infrastruktur finanziert. Der Bericht evaluiert die Potentiale einer statistischen Vorhersagemethode, die von der Autorin in der Sektion Dynamik des Paleoklimas im Fachbereich Klimawissenschaften des Alfred-Wegener-Instituts, Helmholtz-Zentrum für Polar- und Meeresforschung entwickelt wurde.

Vorwort

Für die Binnenschifffahrt auf frei fließenden Wasserstraßen bilden aktuelle sowie zu erwartende Abflüsse und Wasserstände eine zentrale gewässerkundliche Information und sind eine wichtige Voraussetzung, um die gesamte Logistikkette vom Binnenschiff über die verladende Wirtschaft bis hin zur Anbindung landgebundener Verkehrsträger optimiert zu betreiben. Neben Kurz- und Mittelfristvorhersagen besteht zunehmend auch Bedarf an Prognosen auf monatlichen bis saisonalen Zeitskalen, da hierin ein erhebliches Optimierungspotential von Planungen und Entscheidungen mit längerem zeitlichem Vorlauf innerhalb der wassergebundenen Transportabläufe gesehen wird. Die Bundesanstalt für Gewässerkunde (BfG), die im Auftrag des Bundesministeriums für Verkehr und Digitale Infrastruktur (BMVI) seit mehreren Jahrzehnten operationelle Wasserstandsvorhersagesysteme für die Bundeswasserstraßen im Binnenbereich entwickelt, pflegt und betreibt, widmet sich vor diesem Hintergrund aktuell auch der methodischen Erprobung saisonaler Prognoseverfahren sowie der Entwicklung entsprechender Vorhersageprodukte für schifffahrtsrelevante Pegel an den deutschen Wasserstraßen. Der Fokus liegt dabei auf der Prognose von Niedrigwasserperioden bzw. der entsprechenden schifffahrtsrelevanten Niedrigwasserkenngrößen. Dieser Bericht des Alfred-Wegener-Instituts ist im Kontext des BMVI-finanzierten Forschungs- und Entwicklungsvorhabens der BfG „Seamless Prediction“ entstanden und evaluiert die Potentiale der maßgeblich von Frau Dr. Monica Ionita (AWI) entwickelten statistische Vorhersagemethode für ausgewählte Pegel an den Bundeswasserstraßen Rhein, Elbe und Donau.

Dennis Meißner, 10.05.2017

1. INTRODUCTION

Extreme events became an important research topic in the last years and the study of their variations has been intensified considerably [*Easterling et al., 2000; Gong et al., 2004; Ekström et al., 2005; Palutikof et al., 1999*]. By definition, extreme events are rare, but they do occur and sometimes records are broken. Special attention has also been paid to those extremes related to hydrological variables, like drought or floods, since they produce a huge amount of material losses and human casualties [*Yiou et al., 2006; Mares et al., 2008*]. Between 1998 and 2002, Europe suffered over 100 major damaging floods, including the catastrophic floods along the Danube and Elbe rivers in 2002 [*Ulbrich et al., 2003 a, b; Bronstert et al., 1998*]. Since 1998, floods have caused around 700 fatalities, the displacement of about half a million people and at least € 25 billion in insured economic losses [*European Environment Agency, 2003*]. Extreme events are critical determinants in the evolution and character of many natural and human-influenced systems. From such a perspective, extreme hydro-climatic events, in particular, present society with significant challenges in the context of a rapidly warming world. The capacity of society to respond optimally to hydro-climatic events such as extreme floods or long droughts depends on its ability to understand, predict, prepare for, and respond to extremes.

The availability of water is greatly influenced by climate conditions that vary on seasonal, interannual, and decadal time scales. Characterization of hydrological variability on climatic timescales and identification of connections to climate forcings provide potential improvement for hydrological forecasts when these forcings are predictable or slowly evolving [*Souza and Lall, 2003; Croley, 2003*]. Evidence from long hydrological records shows that period with anomalous hydrological behavior [*Arnell et al., 1993*] are associated with persistent climate anomalies.

Over the last years, interest in seasonal predictability of river discharge variability over Europe has increased markedly [*Trigo et al., 2004; Rimbu et al., 2004; Rimbu et al., 2005; Ionita et al., 2008, 2015, Meissner et al., 2017*]. On seasonal timescales, anomalous atmospheric conditions are often linked with seasonal variations in the rivers streamflow, via variations in precipitation and temperature [*Dettinger and Diaz, 2000; Cullen et al., 2002*]. For example, spring and summer rainfall and temperatures anomalies across Europe may be forecasted from prior knowledge of varying boundary conditions such as anomalous sea surface temperature (SST) in the North Atlantic Ocean [*Colman, 1997; Colman and Davey, 1999; Wilby, 2001*] and/or the tropical Pacific Ocean [*Kiladis and Diaz, 1989; Lloyd-Huges and Saunders, 2002; van Oldenborgh et al., 2000*]. Spring precipitation over central Europe is higher than normal average following warm El Niño events combined with lower SSTs west of Ireland [*Lloyd-Huges and Saunders, 2002*]. Persistent dry (wet) conditions over Europe are usually associated with anticyclonic (cyclonic) circulation, while the sea surface temperatures (SSTs) can play also an important role via the interaction with large-scale climatic or oceanic modes of variability [e.g., North Atlantic oscillation and El Niño–Southern Oscillation, *Ionita et al., 2011, 2015; Schubert et al., 2014*]. Altogether, when favorable phase conditions are met, both large-scale atmospheric as well as oceanic factors could act as precursors to dry (wet) summers over Europe [*Kingston et al., 2013, 2015; Ionita et al., 2012, 2015, 2017*]. Predictability is found to be higher in El Niño-Southern Oscillation (ENSO) extreme years [*Branković and Palmer, 2000*], implying that at least part of the available skill can be attributed to the forcing from the tropical Pacific Ocean.

Two of the most important phenomena that influence streamflow variability are the North Atlantic Oscillation (NAO) and El Niño – Southern Oscillation [*Dettinger and Diaz, 2000; Cullen et al., 2002*]. The NAO refers to a north-south oscillation in atmospheric mass between the Icelandic Low and the Azores High-pressure centers (Walker and Bliss, 1932). The NAO is the dominant pattern of near-surface

atmospheric variability over the North Atlantic, accounting for one third of the total variance in monthly SLP in winter [*Barnston and Livezey, 1987*]. The positive phase of this pattern is associated with higher than normal surface pressure south of 55°N combined with a broad region of anomalously low pressure throughout the Arctic and subarctic. Consequently, this phase is associated with stronger-than-average winds across the mid-latitudes of the Atlantic onto Europe, with anomalously southerly flow over the eastern United States and anomalously northerly flows across Greenland, the northern part of Canada and the Mediterranean region and enhanced easterly trade winds over the sub-tropical North Atlantic. The El Niño Southern Oscillation (ENSO) is an anomalous large scale ocean-atmosphere system associated with strong fluctuations in ocean currents and surface temperatures. It causes abnormal atmospheric and environmental conditions, primarily in equatorial regions within the Pacific Basin [*Barnston and Ropelewski, 1992; Barnston et al., 1997*]. ENSO is a major example of the interrelationship between ocean currents and atmospheric conditions and it consists of two components: El Niño and the Southern Oscillation. ENSO is associated with floods, droughts, and other disturbances in a range of locations around the world. El Niño involves warming of the tropical Pacific surface waters, weakening the usually strong SST gradient across the Pacific, with associated changes in ocean circulation. It's linked atmospheric counterpart, the Southern Oscillation (SO), involves changes in trade winds, tropical circulation and precipitation. The term "Southern Oscillation" refers to the variability of the strength of the Walker Circulation system and is quantified through the Southern Oscillation Index.

The indices of these large-scale climatic patterns are used as predictors for seasonal streamflow anomalies over Europe [*Rimbu et al., 2005, Cullen et al, 2002, Trigo et al., 2004*]. Significant lag-correlations were identified between NAO index and several river streamflow anomalies from Iberian Peninsula [*Trigo et al., 2004*] and Tigris-Euphrates streamflow anomalies [*Cullen et al., 2002*]. *Rimbu et al. [2004]* found significant lag-correlation between NAO and ENSO indices and Danube streamflow. However, the association between NAO and ENSO and streamflow from Iberian Peninsula [*Trigo et al., 2004*] and from south-east Europe [*Rimbu et al., 2004; Cullen et al., 2002*] is non-stationary, i.e. the strength of the correlation between these two phenomena and streamflow anomalies has changed over time. These teleconnection patterns, though they are dominant on a large scale, often fail to provide forecast skill in individual basins [*McCabe and Dettinger, 2002; Grantz et al, 2005*]. The predictability of precipitation and streamflow from Europe using NAO and ENSO as predictors is limited due to non-stationarity. One way to improve the seasonal forecast for streamflow would be to identify stable predictors [*Ionita et al., 2018, 2014*].

A different approach, compared to the one used in the aforementioned studies (e.g. linear regression models) is the use of climate model-based approaches with the purpose of seasonal ensemble hydrological forecasting. In the climate model-based approach, the outputs from global climate models are downscaled to finer resolutions and bias corrected to produce the forcing for the hydrological model [*Wood et al., 2002, 2005*]. *Wood et al. [2002, 2005]* conducted seasonal hydrological predictions for the eastern and western United States by bias correcting and downscaling (spatially and temporally) NCEP Global Spectral Model (GSM) ensemble climate predictions for input into the Variable Infiltration Capacity (VIC) hydrologic model. They found that the initial hydrologic conditions need to be accurately determined, so that the influence of the land surface can be captured in the prediction.

2. STUDY AREA

2.1 Catchment areas

The primary quantities analyzed in this report are the river streamflow and water levels, at gauging stations situated in the catchment areas of three German rivers: Rhine, Elbe and Danube (Figure 1). The European inland waterways offer more than 40,000 km network of canals, rivers and lakes connecting cities and industrial regions across the continent. The German inland waterway network – an integral part of the trans-European waterway system – comprises about 7,350 km, of which approximately 75% are rivers and 25% canals. The major inland waterways with regard to freight transport are the Rhine and the Danube, as well as parts of Elbe and some canals interconnecting the natural waterways. About two third of the German waterways are of international relevance, the contribution of River Rhine being outstanding: with almost 200 million tons transported along the Rhine per year (approximately 2/3 of the European inland waterway volume) the Rhine isn't solely Germany's, but also Europe's most important inland waterway (CCNR 2016).

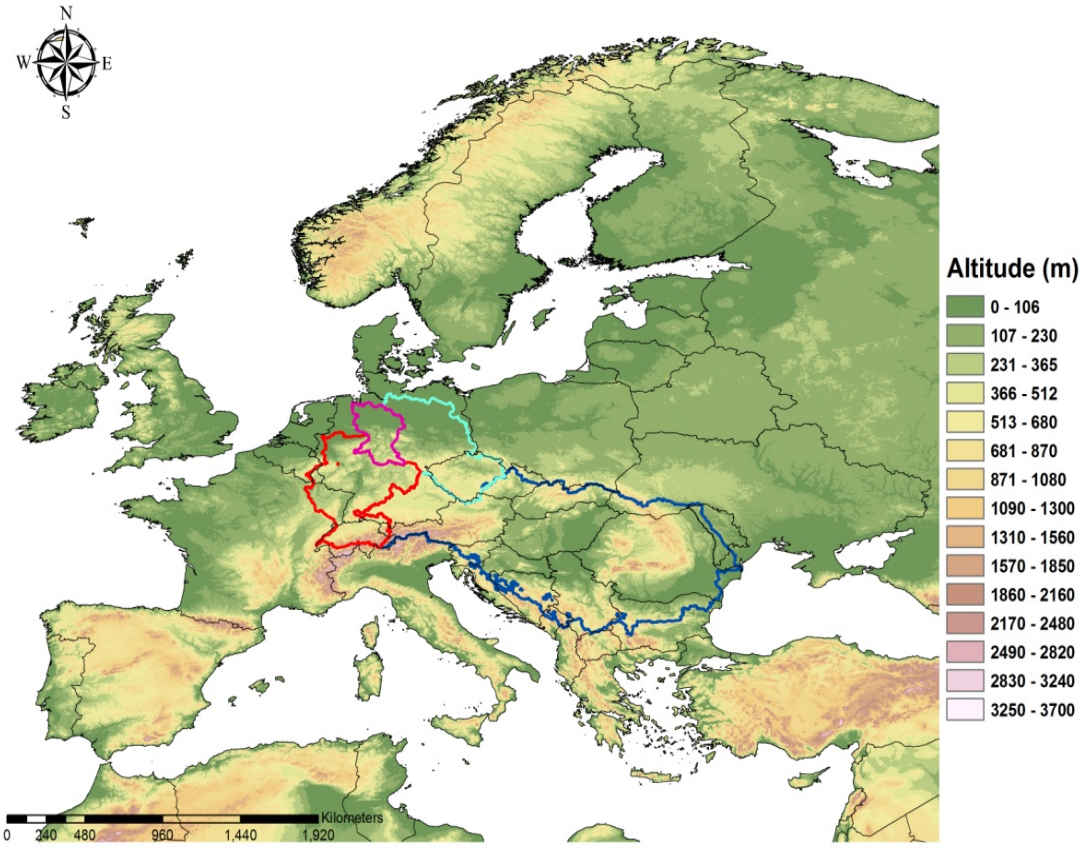

Fig. 1: *The location and elevation of the four catchment areas analyzed: red – Rhine River, green – Elbe River, magenta – Weser River and blue – Danube River*

2.2 Rhine River

River Rhine is one of the major rivers in Western Europe and originates in the Swiss Alps, covering portions of Switzerland, Germany, France and the Netherlands before draining into the North Sea. The Rhine basin (185,000 km^2) can be divided into the Alpine area upstream from Basel (Switzerland) and the middle and lowland parts, downstream. Downstream from Basel, the Rhine is supplied by several large tributaries, such as the Neckar, the Main and the Mosel (Figure 2). Rhine River has been intensively modified by humans during history. The Lower Rhine (where our gauging station is situated), from Bonn downstream through the Netherlands, was channelized during the latter half of the 19th century, with the expansion of this work through the 20th century [*Havinga and Smits, 2000*]. *Pinter et al. [2006]*, testing different mechanism which can affect the Rhine streamflow (e.g. river regulation or land-use and climate change), showed that the regulation of the basin has little or no effect on Rhine streamflow, while the land-use and climate change, over the past 100 years, lead to an increase in the magnitude and frequencies of floods.

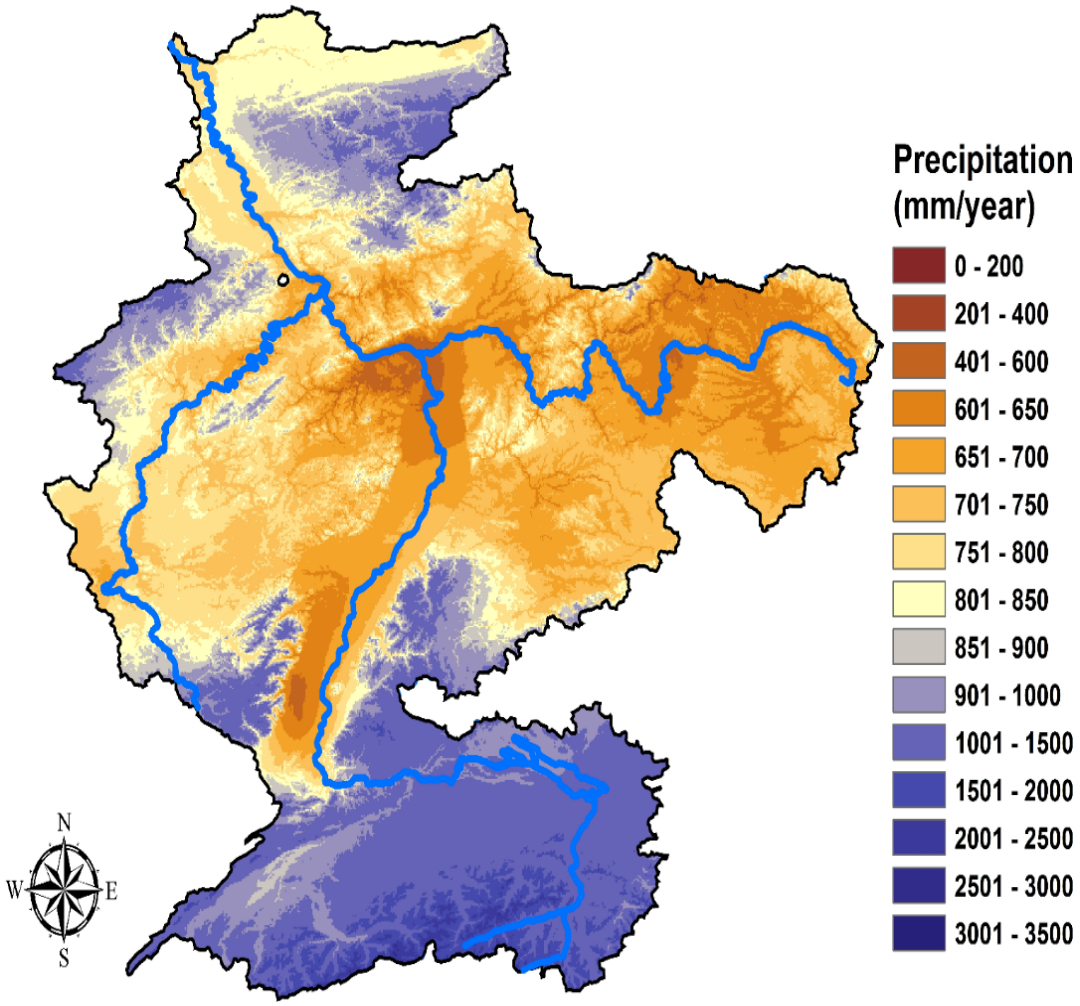

Fig. 2: *Rhine catchment area and the annual precipitation distribution*

a)

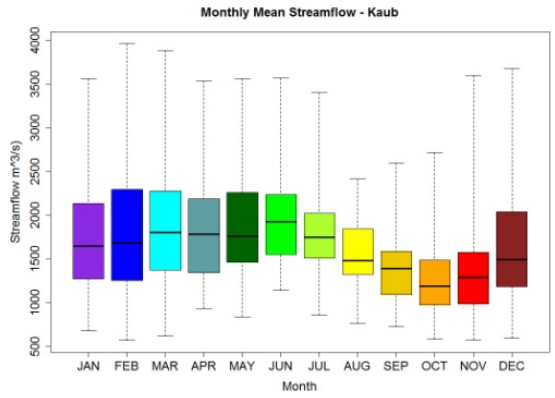

b)

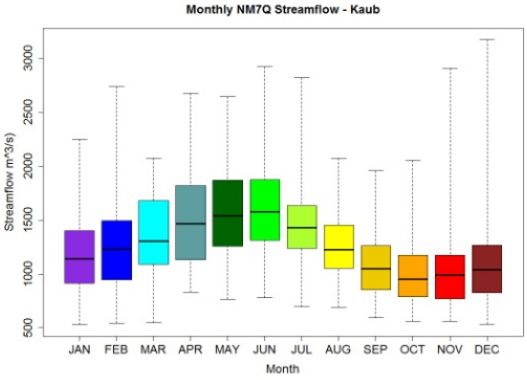

c)

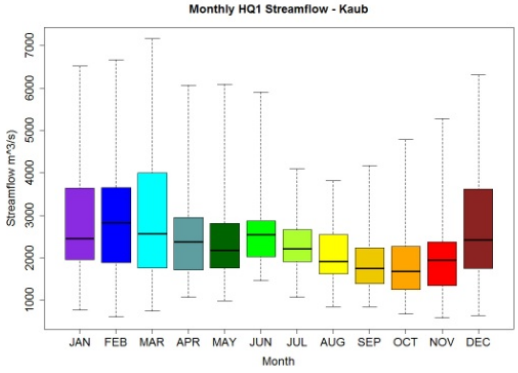

Fig. 3: *a) Boxplot of Rhine's climatological monthly mean streamflow; b) Boxplot of Rhine's climatological monthly low streamflow (NM7Q); c) Boxplot of Rhine's climatological monthly high streamflow (MQ)*

The hydrological discharge regime is characterized by a pronounced seasonal cycle whose rising limb is situated between January and April and the falling one between September and November (Figure 3), the highest values being recorded in February. These high discharge values recorded in the spring months are related to the melting of the snow in the catchment area and the soil humidity.

2.3 Elbe River

The Elbe River rises in the Giant Mountains in Czech Republic at an elevation of 1383 m. The Elbe River basin, comprising the Elbe and its tributaries, has a catchment area of 148,268 km^2, the fourth largest in Europe (Figure 4). The basin spans four countries, with its largest parts in Germany (65.5%) and the Czech Republic (33.7%). Smaller parts lie in Austria (0.6%) and Poland (0.2%). Its length is 1094 km, of which 367 km are located in the Czech Republic and 727 km in Germany. The mouth is in the North Sea and the principal tributaries are: Vltava (Moldau), Havel, Saale, Mulde, Eger and Schwarze Elster. The basin covers different geographical regions from middle mountain ranges in the west and south to large lowlands in the central, northern and eastern part of the catchment.

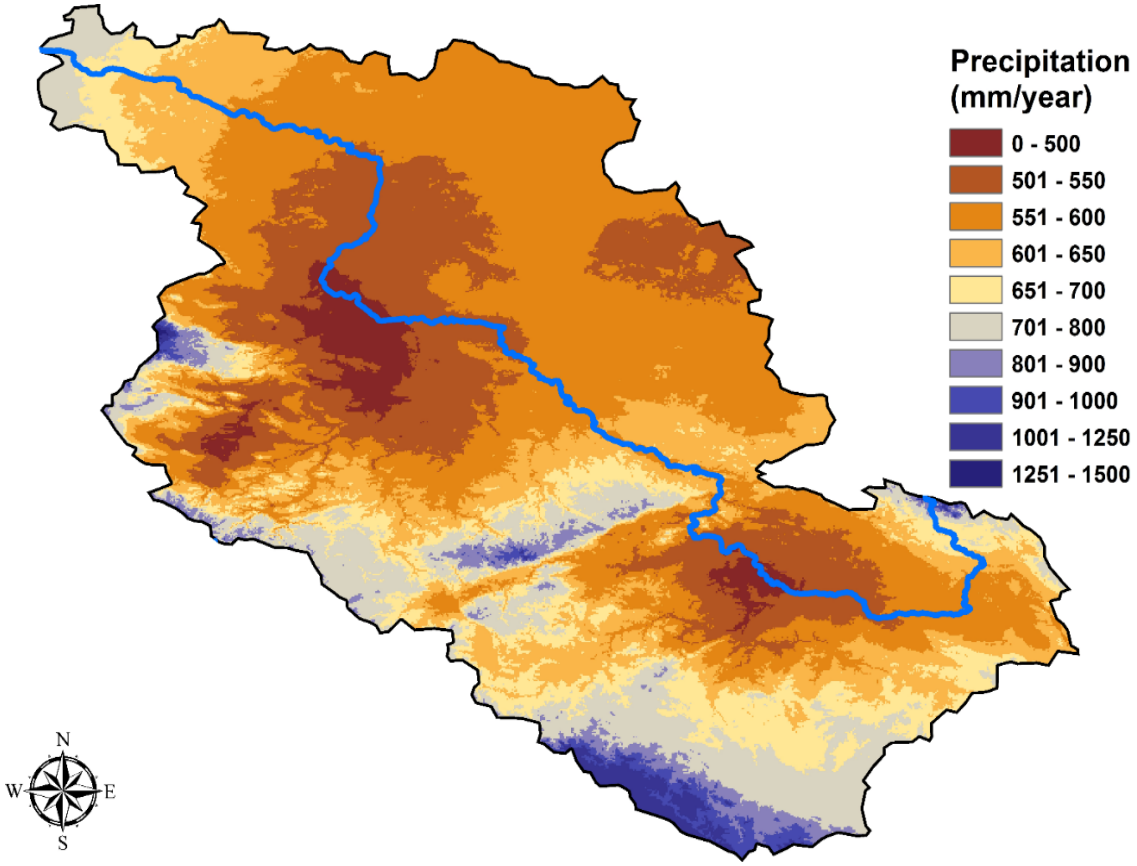

Fig. 4: *Elbe catchment area and the annual precipitation distribution*

The whole basin is formally partitioned into three main sectors, due to the geomorphologic character: the Upper Elbe (463 km), the Middle Elbe (489 km) and the Lower Elbe (142 km). From a climatic point of view, the Elbe river basin is located in a transition zone between the maritime and the continental climate. The temperature shows strong intra-annual variability and this influences the evaporation.
The Elbe river basin is the driest basin in Germany (compared to Rhine, Weser or Danube) due to the low precipitation levels of about 659 mm/year on average. Precipitation is ranging from below 450 mm/year in the central part to 1600 mm/year in the mountain area (Figure 4). The mean annual discharge at the border between the Czech Republic and Germany is approximately 311 m^3/s. At Cuxhaven (Germany), the Elbe discharges into the North Sea. The mean annual discharge at the mouth is around 861 m^3/s. The hydrological regime of Elbe river streamflow has a strong seasonal cycle, with the highest streamflow values occurring during the spring months (February to April, Figure 5) and the lowest ones being recorded during the summer months (July, August and September, Figure 5).

a)

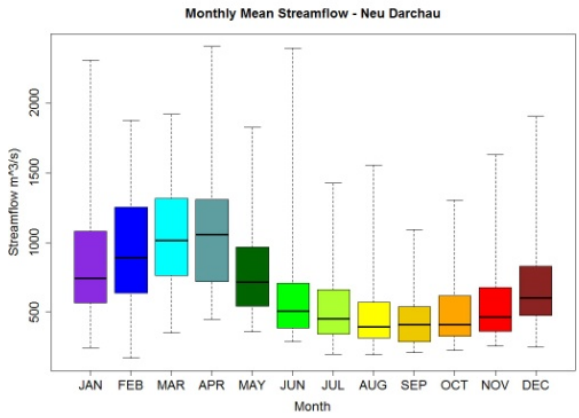

b)

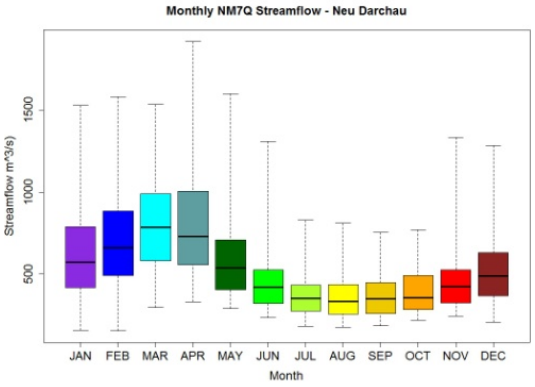

c)

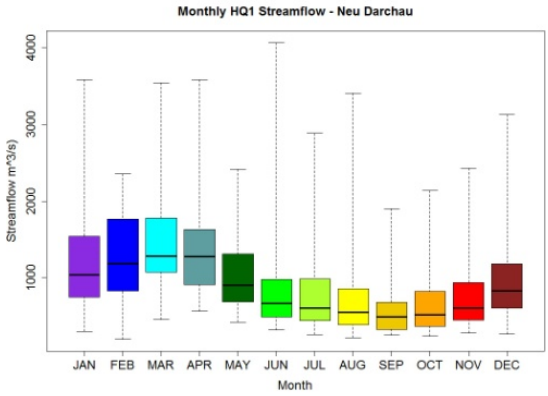

Fig. 5. *a) Boxplot of Elbe's climatological monthly mean streamflow; b) Boxplot of Elbe's climatological monthly low streamflow (NM7Q); c) Boxplot of Elbe's climatological monthly high streamflow (MQ)*

2.4 Danube River

The Danube River basin is the second largest river basin in Europe, after the Volga River, covering an area of 801.463 km^2. Due to its large extension from west to east, and diverse topography (Figure 6a), the Danube River basin also shows large climatic differences. The upper regions in the west feature strong influence from the Atlantic climate with high precipitation, whereas the eastern regions are affected by continental climate with lower precipitation and typical cold winters.

a)

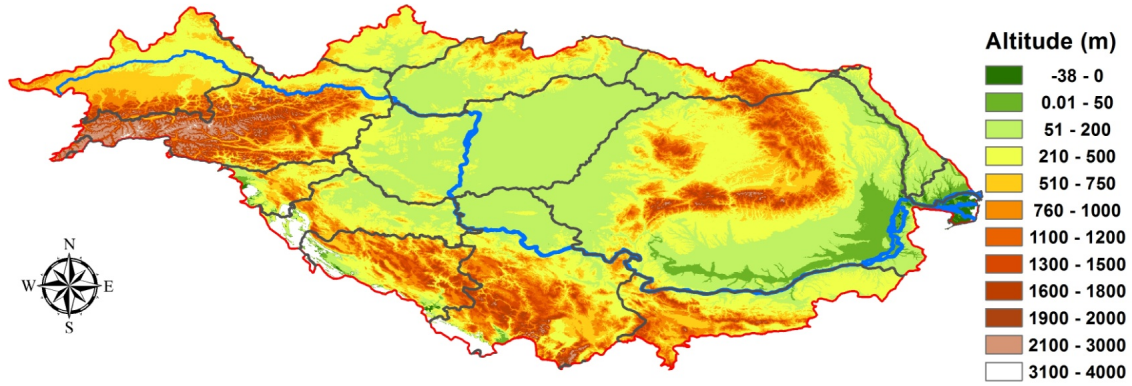

b)

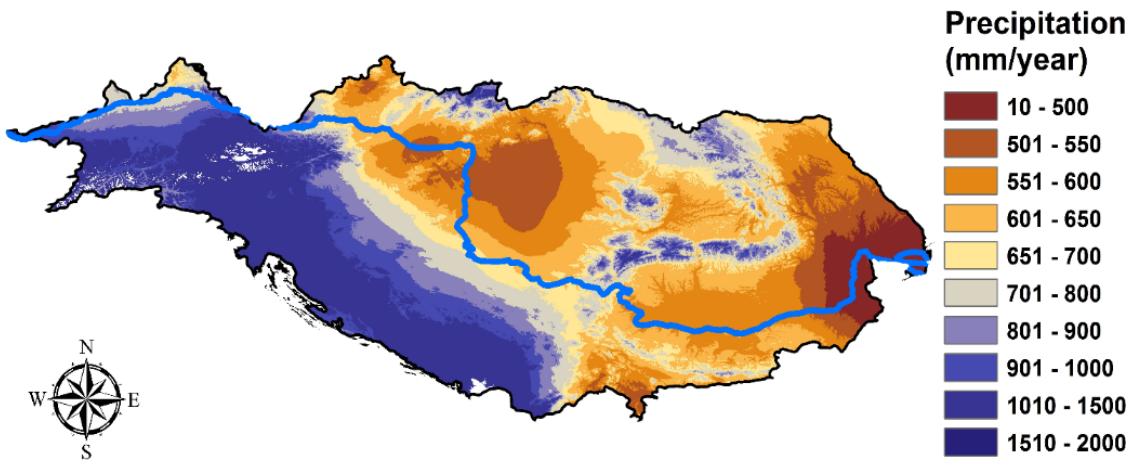

Fig. 6: a) *The topographic map of Danube catchment area;*
b) *Mean annual precipitation in the Danube basin (1961 – 2000)*

The precipitation ranges from < 500 mm/year in the areas located at lower altitudes up to > 2000 mm in the areas located at higher altitudes (Figure 6b). The maximum of the long-term mean precipitation is recorded in the western part of the Danube basin in mid-summer (July) and the minimum in spring (April) [*Brilly, 2010*]. The highest annual temperature average with values of +12° is recorded in the middle and the lower part of Danube basin, while the coldest regions are at the heights of the mountains (e.g. the Carpathians and the Alps) [*Brilly, 2010*]. The highest streamflow values are recorded from March to May (Figure 7) and the lowest ones are recorded from September to November (Figure 5).

a)

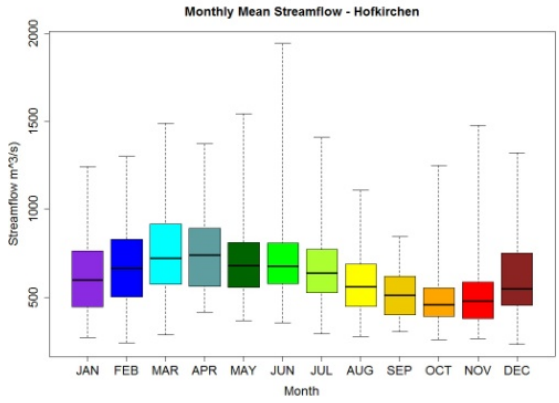

b)

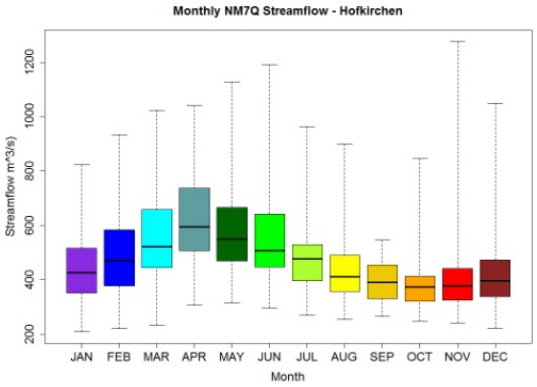

c)

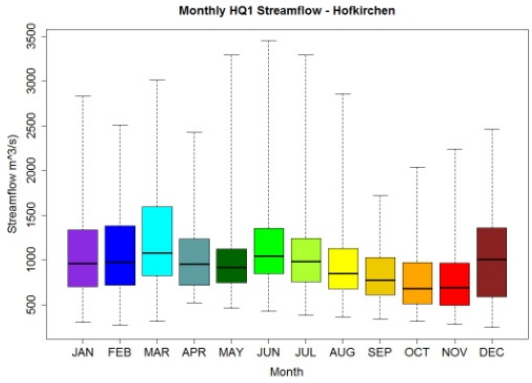

Fig. 7. *a) Boxplot of Danube's (Hofkirchen) climatological monthly mean streamflow; b) Boxplot of Danube's (Hofkirchen) climatological monthly low streamflow (NM7Q); c) Boxplot of Danube's (Hofkirchen) climatological monthly high streamflow (MQ).*

2.6 Data sets

The gridded precipitation (PP) and temperature (TT) data are extracted from the E-OBS-version8 (E-OBSv8) data set [*Haylock et al., 2008*]. These fields have a 0.25º x 0.25º spatial resolution and cover the period from January 1950 up to present. The Soil Moisture (SM), Geopotential Height at 700-mb (Z700), sea level pressure (SLP) and the Relative Humidity (RH) data sets are provided by the National Centre for Atmospheric Research (NCAR) and they cover the period from January 1948 to December 2013 [*Kalnay et al., 1996*]. The Volumetric Soil Moisture data is based on the NCEP/NCAR reanalysis product R-1 [*Kalnay et al., 1996; Kistler et al., 2001*]. The soil moisture quantity reported here is linearly interpolated to a depth of 10 cm. The units are volumetric water content.

To investigate the relationship of streamflow variability with global SST we use the Extended Reconstructed Sea Surface Temperature [ERSST.v3, *Smith et al., 2008*]. This data set covers the period January 1854 – December 2013.

The precipitation and temperature data, at country level and for each federal state, are extracted from the ftp server of the Deutscher Wetterdienst (ftp://ftp-cdc.dwd.de/pub/CDC/). These data sets are updated at the end of each month. For this

report, the following federal states have been used (Figure 8): Baden-Württenberg (Bad); Hessen (Hes); Nordrhein-Westfalen (Nhw); Rheinland-Pfalz (Rhp), Saarland (Sar), Niedersachsen (Nds), as well as the monthly average precipitation and mean temperature at country level (Ger).

Fig. 8: *The federal states of Germany*

3. METHODOLOGY

3.1 Stability Maps

The forecast scheme for the monthly/seasonal prediction of Rhine, Elbe and Danube streamflow and water levels using climate information (e.g. PP, TT, Z700 and SST) from previous months is based on a methodology similar to that used for seasonal prediction of Danube streamflow [*Rimbu et al., 2005*] and Elbe streamflow [*Ionita et al., 2008, 2015, Meissner et al., 2017*].
The basic idea of this procedure is to identify regions with stable teleconnections between the predictors and the predictand [*Lohmann et al., 2005; Rimbu et al., 2005*]. To obtain such stable teleconnections, we correlate the streamflow and water levels with global SST, TT, PP and Z700 from previous months in a moving window of 31 years. The correlation is considered to be stable for those grid-points where the streamflow/water levels and previous months SST, TT, PP and Z700 are significantly correlated at 90% level or 80% level for more than 80% of the 31-year windows (Figure 9).

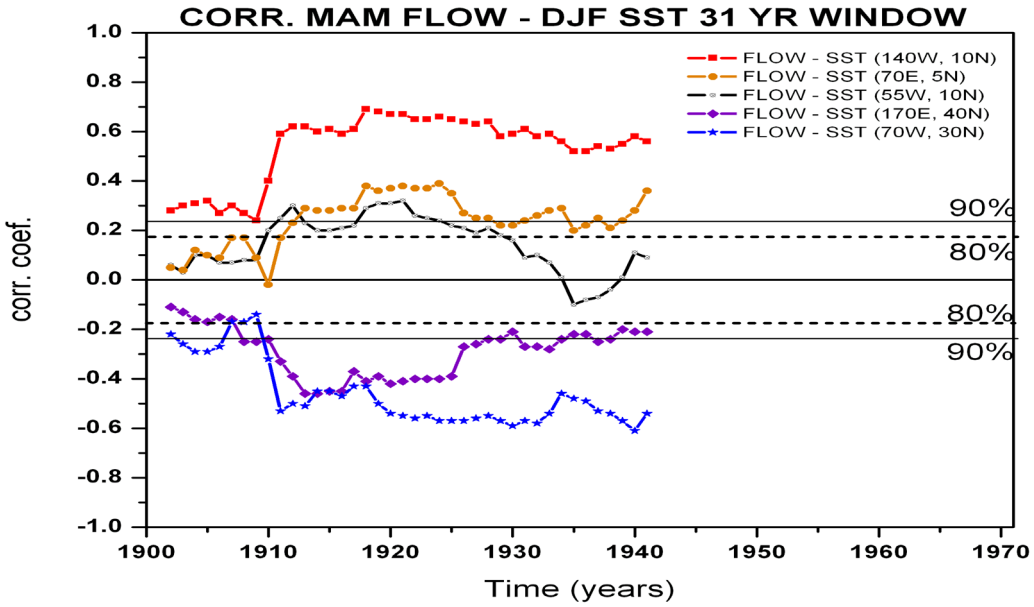

***Fig. 9**: Running correlation (31-year window) between spring flow and winter SST anomalies from the grid points indicated in the upper-right corner of the figure. The correlation is plotted at the beginning of each 31-year window. The first points represent the correlation between spring flow from 1902-1933 and SST from 1901/1902-1932/1933.*

The regions where correlation is positive and stable at 90% (80%) level will be represented as red (yellow) on a global map. The regions where correlation is negative and stable at 90% (80%) level will be represented as blue (green). Such maps will be referred in our study as stability correlation maps and their structures remain qualitatively unchanged if the significance levels that define the stability of the correlation vary within reasonable limits. The optimal model is established based on a multiple regression analysis of the stable predictors.

To better understand how the correlation stability maps are constructed, we analyze decadal variation of the correlation between spring Rhine streamflow and SST anomalies from several grid points (Figure 9). The spring streamflow and winter SST from (140.5°W, 10.5°N) grid point are positively correlated for all 31-year windows covering the period 1901-2002 and above the 90% significance level for more than 80% of the windows. The streamflow and SST from the grid point (70.5°E, 5.5°N) is positive and above 80% significance level for more than 80% of the windows (Figure 10). Therefore, these grid points are stable correlated with streamflow and are represented on the stability map of correlation as red and yellow respectively (Figure 11). The spring streamflow and SST from the grid-points (70.5°W, 30.5°N) and (170.5°E, 40.5°N) are negative and above 90% and 80% significance level, respectively, for more than 80% of the windows. Also, these grid points are stable correlated with streamflow and are represented on the stability correlation map as blue and green respectively (Figure 10).

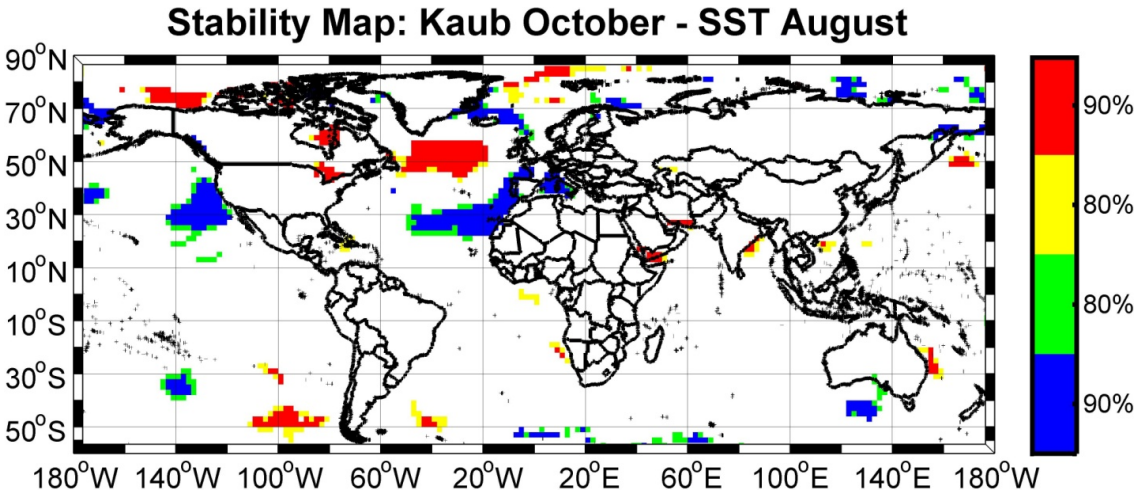

Fig. 10: *The stability map of the correlation between water levels at Kaub in October and previous August SST. The regions where the correlation is stable, positive and significant at 90% (80%) level for at least 80% of the windows are shaded red (yellow). The corresponding regions where the correlation is stable, but negative, are shaded blue (green).*

On contrary, the streamflow and SST from the grid point (55.5°W, 10.5°N) are significantly correlated for less than 80% windows and therefore the correlation is unstable according to our criteria. Such a grid point appears in white color on the stability map of correlation (Figure 11).

3.2 Multiple Linear Regression

In order to choose just the optimal predictors identified by the stability maps we have also adopted a different approach compared to previous studies *[Rimbu et al., 2005, Ionita et al., 2008]*. Previous studies used the first principal component based on all the stable indices as a potential predictor. However, the optimal predictors here are identified by employing stepwise multiple regression analysis to choose the optimal stable indices, which can be further used for the prediction of the monthly/seasonal streamflow. Although the method identifies multiple stable regions for each climate/oceanic parameters, after applying the stepwise multiple regression analysis the optimal model is based just on the most significant regions.

To forecast the monthly/seasonal streamflow we have used a multiple linear regression model. The regression equation is:

$$Y = \beta_0 + \beta_1 x_1 + \beta_2 x_2 + \cdots + \beta_n x_n + \varepsilon$$

Where Y represents the SSIE index, β_o, β_1, β_2,…β_n are constants determined by the least squares procedure, x_1, x_2,…x_n the predictors used (e.g. SLP, PP, TT, etc.) and ε the error. In stepwise regression, each predictor is prioritized taking into account its correlation coefficient with the predictand and its added to the model gradually. As the predictors are added, the F statistic is used to determine whether or not they are significant for the final regression equation (F statistics are set to 0.05 and 0.1, respectively). We choose stepwise regression because it prioritizes predictors based on the partial correlation and it is likely that high and significant correlations ill reflect underlying physical processes.

4. SKILL MEASURES

To better assess the skill of the streamflow prediction, different statistical measures have been employed: ***ME*** – Mean error, ***MA*** – Mean absolute error, ***MSE*** – Mean squared error, ***RMSE*** – Root mean squared error, ***NRMSE*** – Normalized root mean square error (-100% <= NRMS <= 100%), ***PBIAS*** – Percent bias, ***RSR*** – Ratio of RMSE (RSR = rms / sd (obs). (0 <= RSR <= + Inf)), ***rSD*** – Ratio of standard deviations (RSD = sd (sim) / sd (obs)), ***NSeff*** – Nush-Sutcliffe Efficiency ((-Inf <= NSeff <= 1), ***mNSeff*** - Nash-Sutcliffe Efficiency modified. SSNM = 1 - (sum (abs (obs - sim) ^ j) / sum (abs (obs - mean (obs)) ^ j), ***rNSeff*** - Relative Nash-Sutcliffe Efficiency, ***d*** – Index of Agreement, ***Rd*** – relative index of agreement. It varies between 0 and 1. A value of 1 indicates a perfect match, and 0 indicates no agreement at all, ***CP*** – persistence index***,*** R^2 – coefficient of determination and ***KGE -*** Kling-Gupta efficiency.

NSeff it's a metric to measure the ability of a model to predict the observed values. This index produces less than or equal results to 1, if the result is 1 the fit is perfect, if zero, error is of the same order of magnitude as the variance of the observed data so that the average of the observed data will have a capacity similar to the model predictor. Below zero values imply that the media has a higher predictive ability of the model [*Nash and Sutcliffe, 1970*].

d – Index of Agreement (0 <= d <= 1). The Index of Agreement (d) developed by *Willmott* [*1981*] as a standardized measure of the degree of model prediction errors and varies between 0 and 1. A value of 1 indicates a perfect match, and 0 indicates no agreement at all [*Willmott, 1981*]. The index of agreement is overly sensitive to extreme values due to the squared Differences [*Legates and McCabe, 1999*].

CP – persistence index (0 <= PI <= 1). The coefficient of persistence compares the predictions of the model with the predictions obtained by assuming that the process is a Wiener process (variance increasing linearly with time), in which case, the best estimate for the future is given by the latest measurement [*Kitadinis and Bras, 1980*]. Persistence model efficiency is a normalized model evaluation statistic that quantifies the relative magnitude of the residual variance (noise) to the variance of the errors obtained by the use of a single persistence model [*Moriasi et al., 2007*]. CP ranges from 0 to 1, with CP = 1 being the optimal value and it should be larger than 0 to indicate a minimally acceptable performance model.

R^2 – coefficient of determination. Gives the proportion of the variance of one variable that is predictable from the other variable.

KGE - Kling-Gupta efficiency (0 <= KGE <= 1). This goodness-of-fit measure was developed by *Gupta et al. [2009]* to provide a diagnostically interesting decomposition of the Nash-Sutcliffe efficiency which facilitates the analysis of the relative importance of its different components in the context of hydrological modeling. Kling-Gupta efficiencies ranges from -Inf to 1. Essentially, the closer to 1, the more accurate the model is.

5. RESULTS

The skill of a long-range forecast is associated with the predictors that represent the slow varying components of the climate system such as sea ice, snow cover, soil moisture and sea surface temperature (SST) [*Koster et al., 2010*]. Most of the streamflow predictors are based on meteorological parameters or SSTs [*Rimbu et al., 2005; Ionita et al., 2008, 2014; Gámiz-Fortis et al., 2010*]. The information related to the soil moisture has the potential to improve seasonal precipitation prediction [*Dirmeyer et al., 1999; Reichle and Koster, 2003*] whereas different studies suggest that it can also substantially improve streamflow prediction [*Berg et al., 2006; Koster et al., 2010*]. According to a number of observational-based studies, soil moisture memory may have a time scale of 1-3 months [*Vinnikov and Yeserkepova, 1991*], thus providing some indication of the conditions prior to the forecasted month or season. As a result, here we investigated a potential link between saturated, wet, cold springs and upcoming floods.

Since precipitation (PP) and temperature (TT) have significant influence on streamflows, we consider them, together with the geopotential height at 700-mb (Z700), Sea Level Pressure (SLP), soil moisture (SM), ground temperature in the upper 10 cm (TEMP10), air temperature (AIRTT), temperature at 850-mb level (TT850), zonal wind at 700-mb level (U700), meridional wind at 700-mb level (V700) and sea surface temperature (SST) as potential predictors for the water levels and streamflow. In order to identify possible links between these predictors and water levels and streamflow, stability correlation maps (see Methods for definition) are calculated between the monthly/seasonal water levels and streamflow time series on one hand and monthly PP, TT, TEMP10, SM, Z700, SLP, U700, V700, AIRTT, TT850 and SST on the other hand. The optimal predictors are defined as the average values over the stable regions for each gridded parameter (black squares in the stability maps).

The stability maps used for the prediction of the water levels at Kaub station for the month of November are shown in Figures 11 – 18. The forecasted and observed values of November water level at Kaub station are shown in Figure 19. The stability maps used for the prediction of the NM7Q at Kaub station for the month of November are shown in Figures 11 – 18. The forecasted and observed values of November NM7Q at Kaub station are shown in Figure 19. The stability maps used for the prediction of the water levels at Kaub station for the month of November are shown in Figures 20 – 24. The forecasted and observed values of November water level at Kaub station are shown in Figure 25. The stability maps used for the prediction of NM7Q at Neu Darchau station for the month of August are shown in Figures 26 – 35. The forecasted and observed values of August NM7Q at Neu Darchau station are shown in Figure 36. The stability maps used for the prediction of NM7Q at Hofkirchen station for the month of November are shown in Figures 37 – 42. The forecasted and observed values of November NM7Q at Hofkirchen station are shown in Figure 43.

5.1. Monthly prediction of water levels at Kaub station

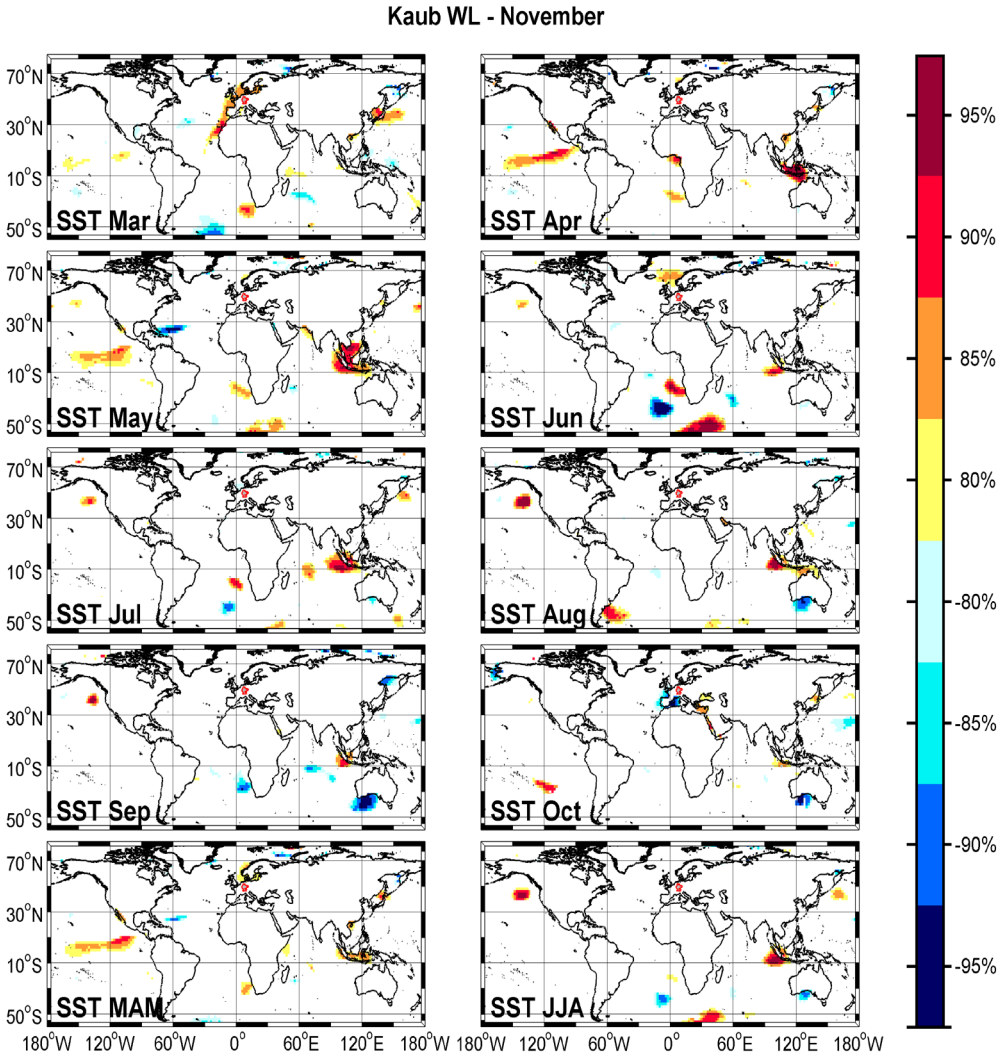

Fig. 11: *Stability maps of the correlation between November water levels at Kaub station and monthly SST with different lags a) March; b) April; c) May; d) June; e) July; f) August; g) September; h) October; i) March-April-May (MAM) and j) June-July-August (JJA). The regions where the correlation is stable, positive and significant at 95% (80%) level for at least 80% of the windows are shaded with red (yellow). The corresponding regions where the correlation is stable, but negative, are shaded with blue (light blue).*

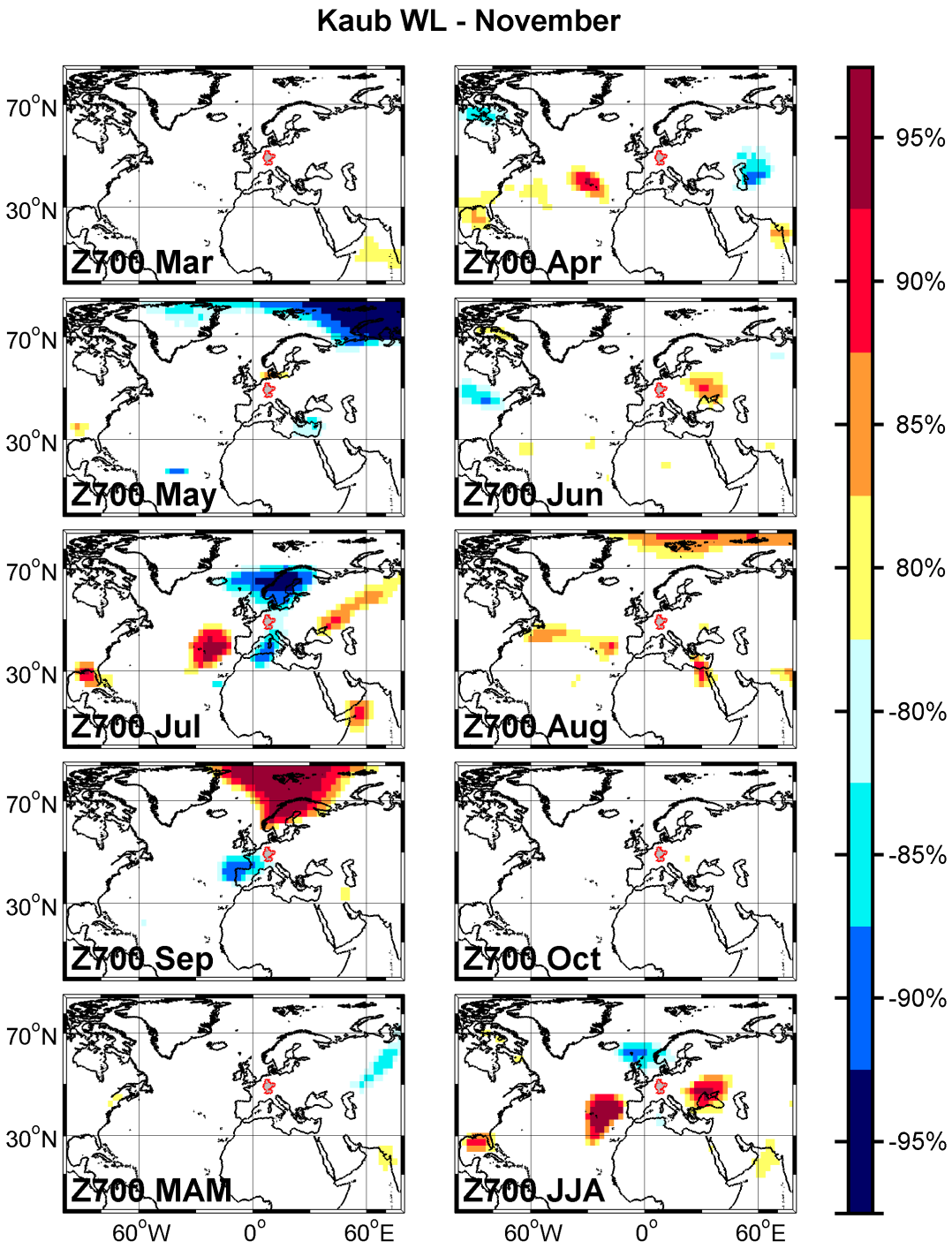

Fig. 12: *As in Figure 11, but for Z700*

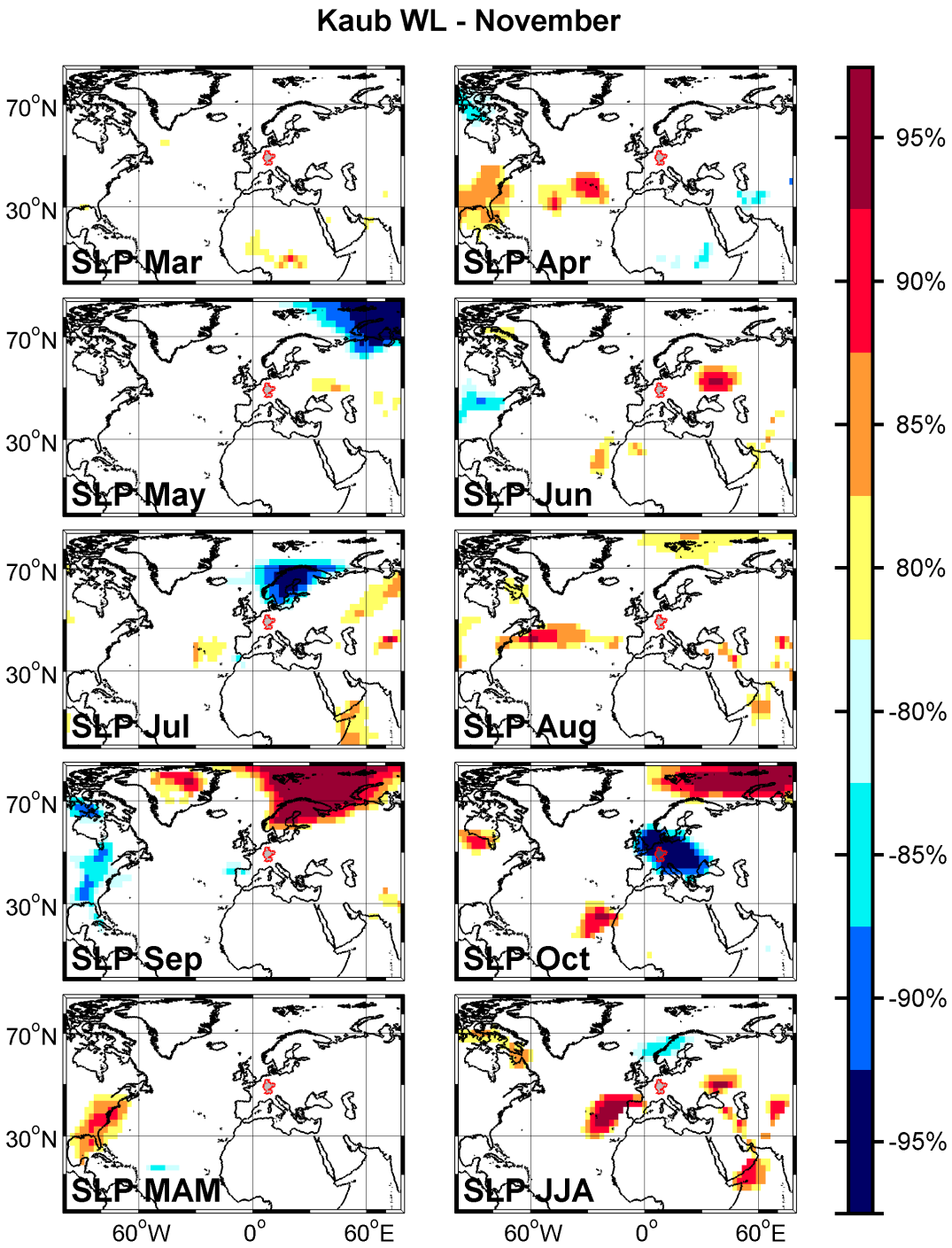

Fig. 13: *As in Figure 11, but for SLP*

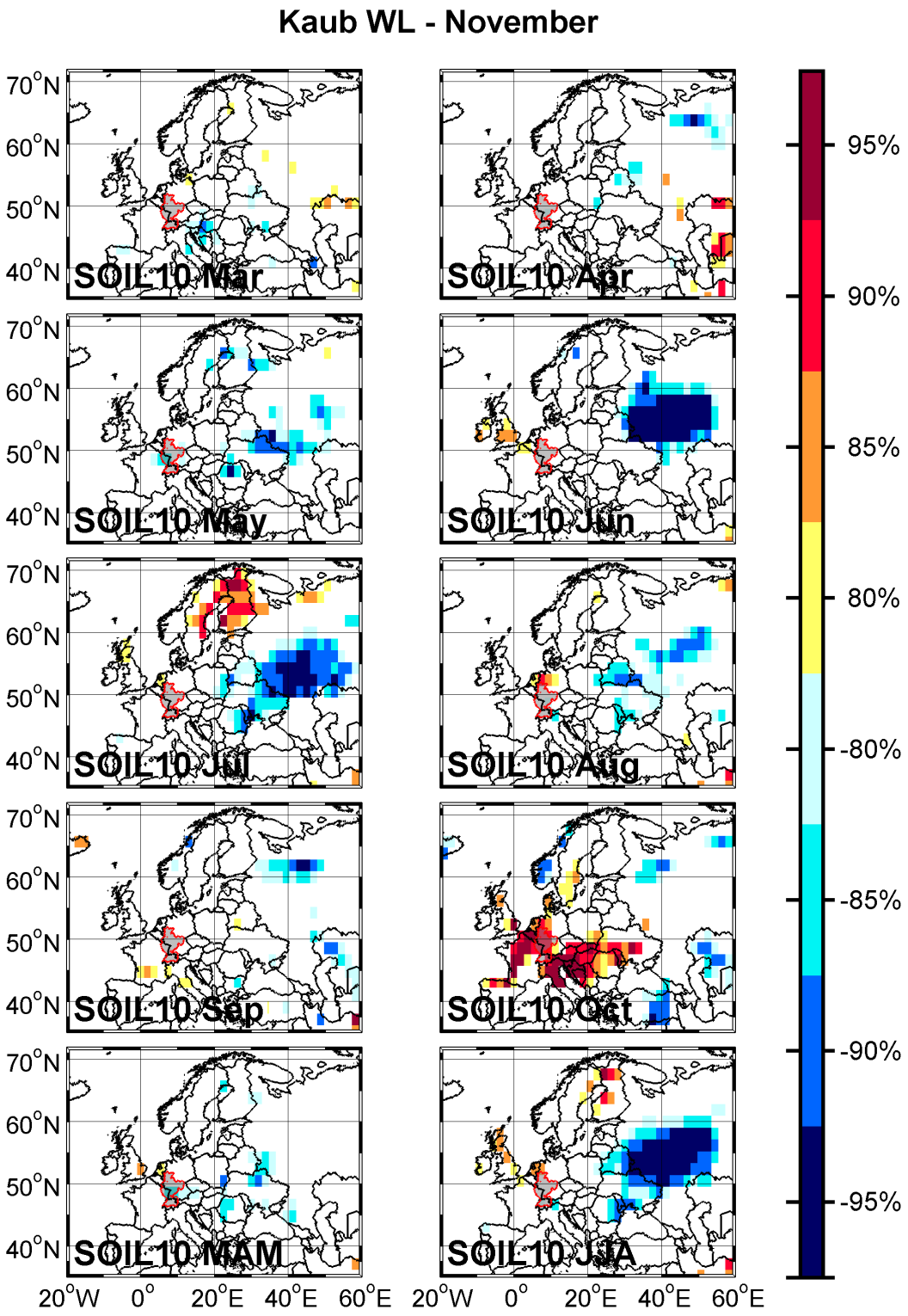

Fig. 14: *As in Figure 11, but for SOIL10*

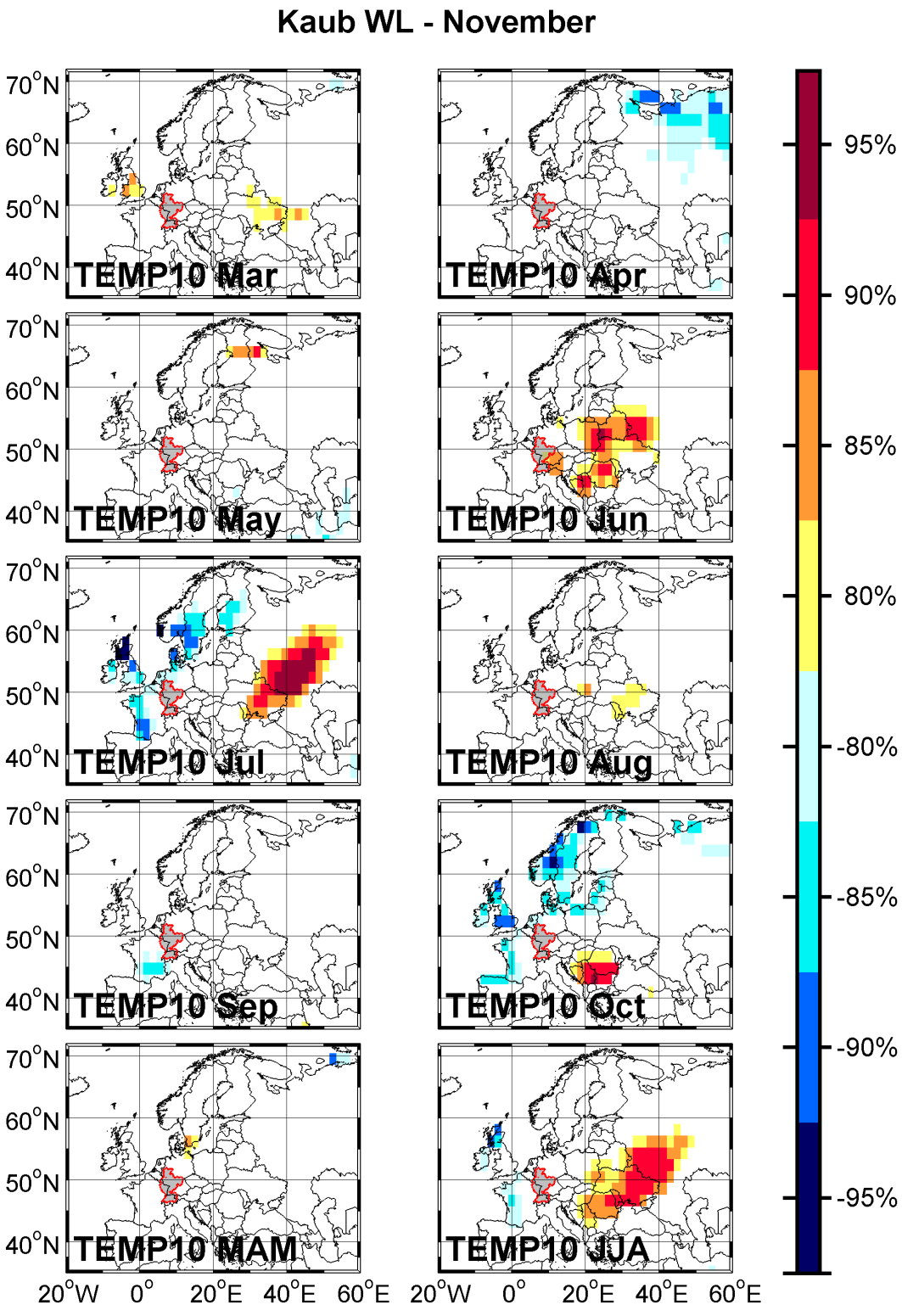

Fig. 15: *As in Figure 11, but for TEMP10*

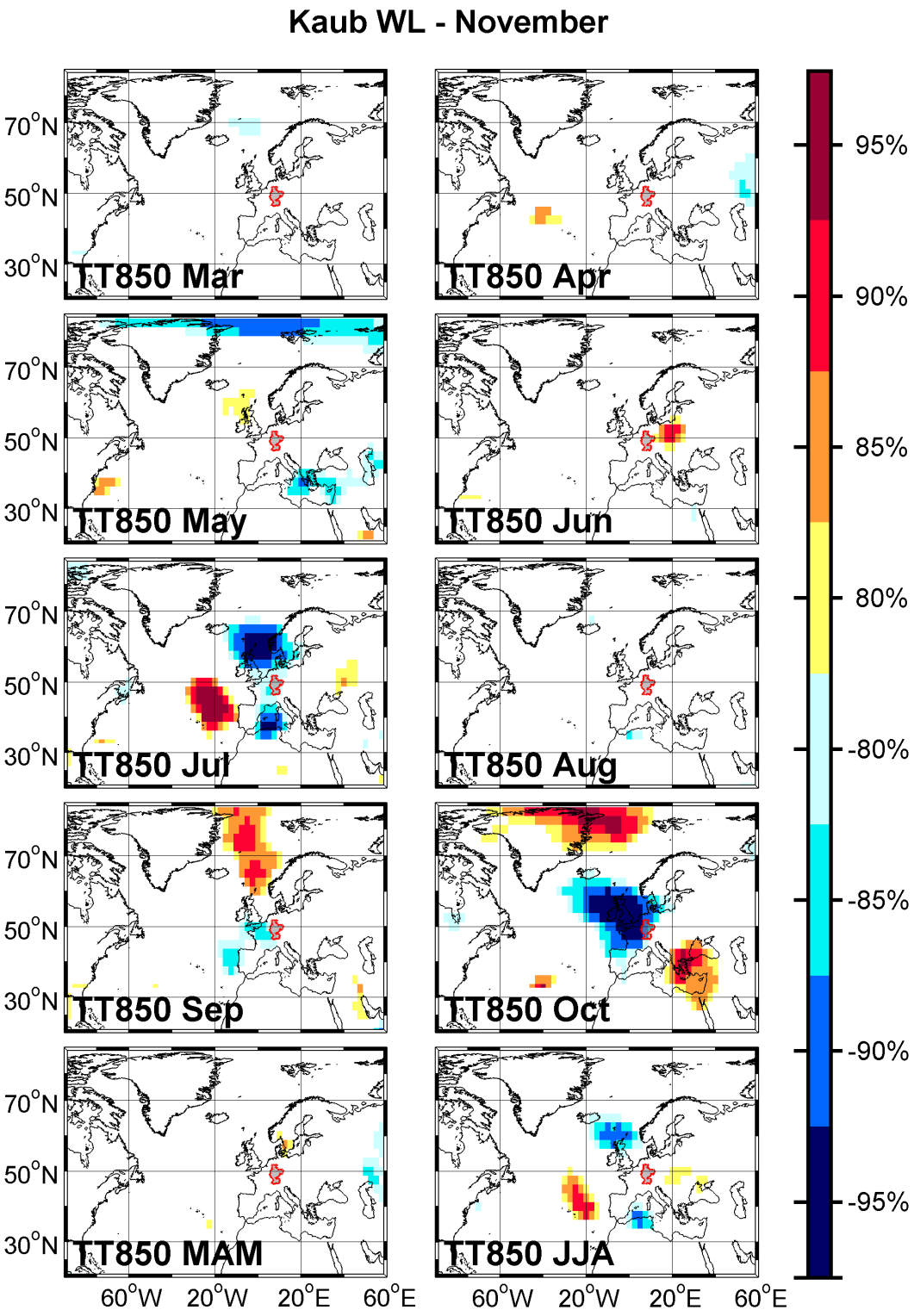

Fig. 16: *As in Figure 11, but for TT850*

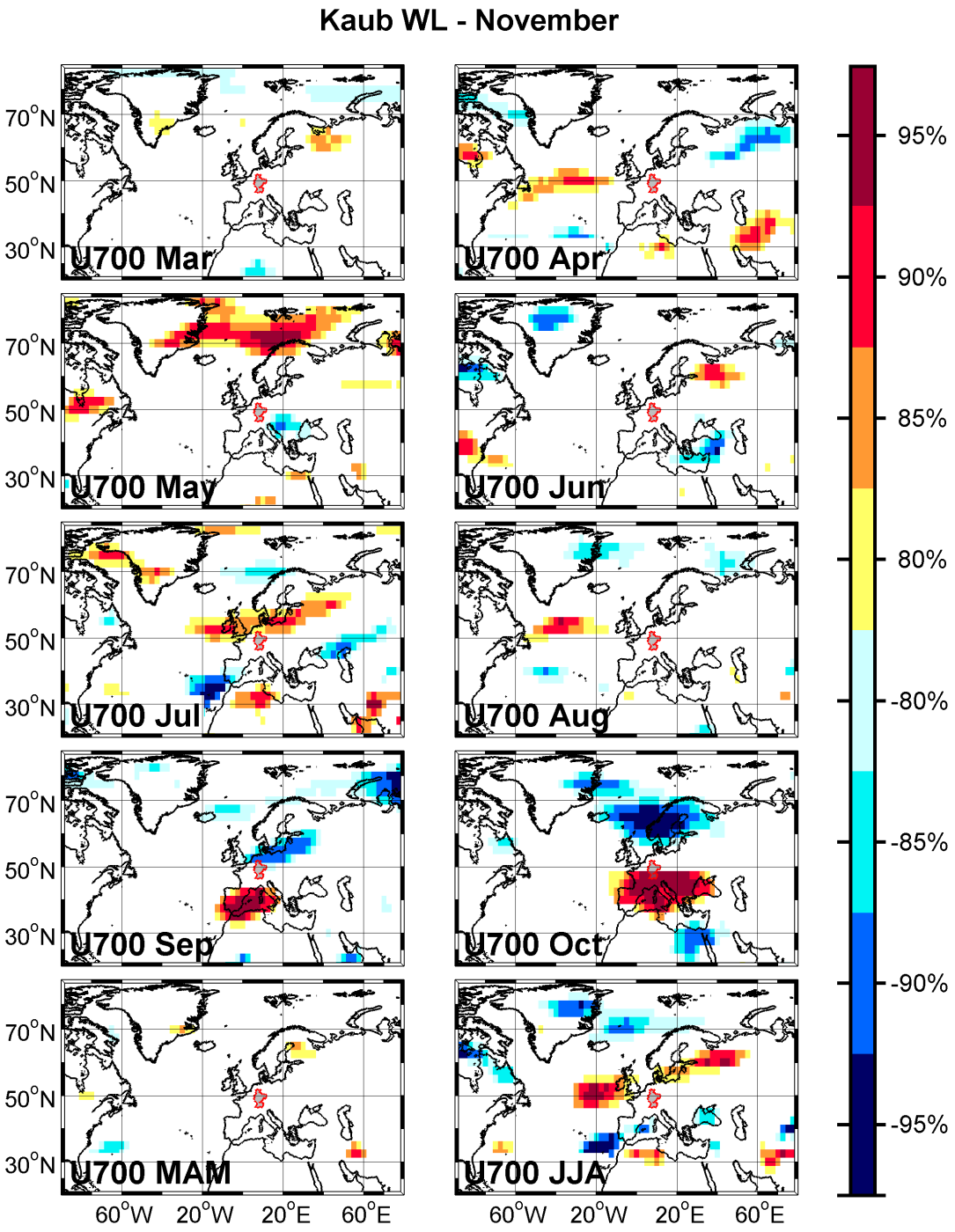

Fig. 17: *As in Figure 11, but for U700*

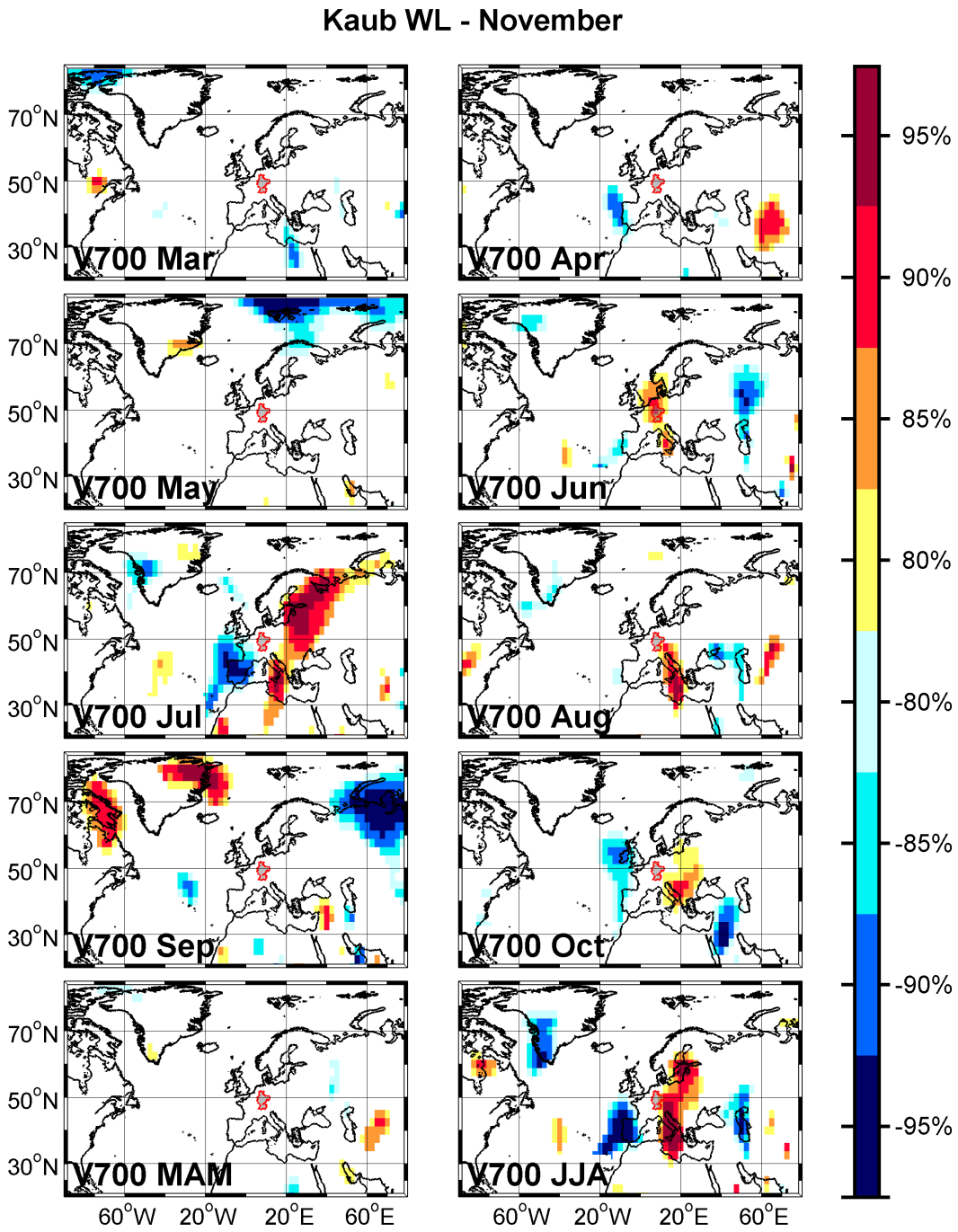

Fig. 18: *As in Figure 11, but for V700*

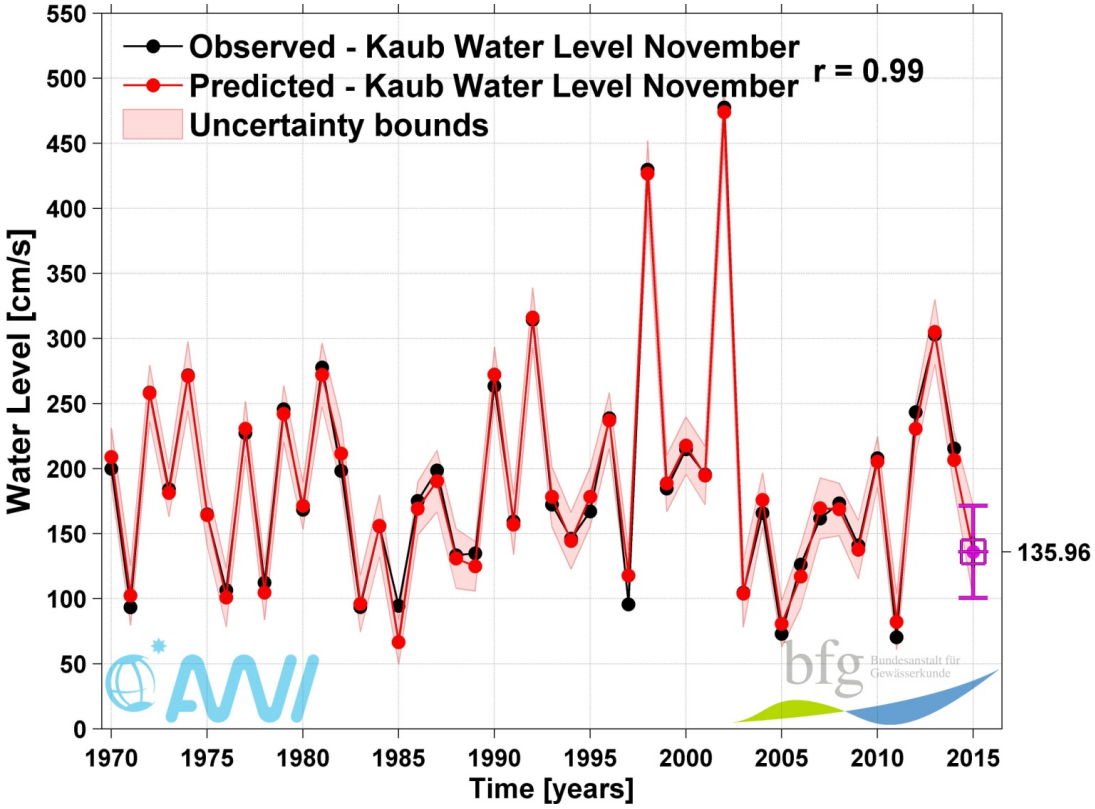

Fig. 19: *Comparison between the observed and predicted water level values for November at Kaub station: Observed (black) and Predicted (red) November water levels values for the period 1970-2015.*
The light red shaded area represents the 95% uncertainty bounds.

WL NOV = id1 + id2 + id3 + id4 + id5 + id6 + id7 + id8 + id9 + id10 + id11 + id12 + id13 + id14 + id15 + id16 + id17 + id18 + id19 + id20 + id21 + id22 + id23 + id24 + id25 + id26 + id27

id1=hesppoct; id2=soil10jun; id3=saarttsep; id4=u700oct1; id5=sstmay; id6=ndhppoct; id7=hesppsep; id8=soil10oct; id9=rheinppsep; id10=slpoct2; id11=bayttoct; id12=kauboct; id13=saarppsep; id14=kaubmqsep; id15=hesttoct; id16=kaubwloct; id17=slpoct1; id18=ndhttoct;
id19=v700jja; id20=badttoct; id21=z700jul; id22=tt850jul; id23=kaubsep; id24=gerppsep; id25=gerttsep; id26=bayppoct; id27=v700sep.

Statistics:

Residual standard error: 13.3 on 17 degrees of freedom
Multiple R-squared: 0.9903, Adjusted R-squared: 0.9749
F-statistic: 64.25 on 27 and 17 DF, p-value: 1.739e-12

5.2 Monthly prediction of NM7Q at Kaub station

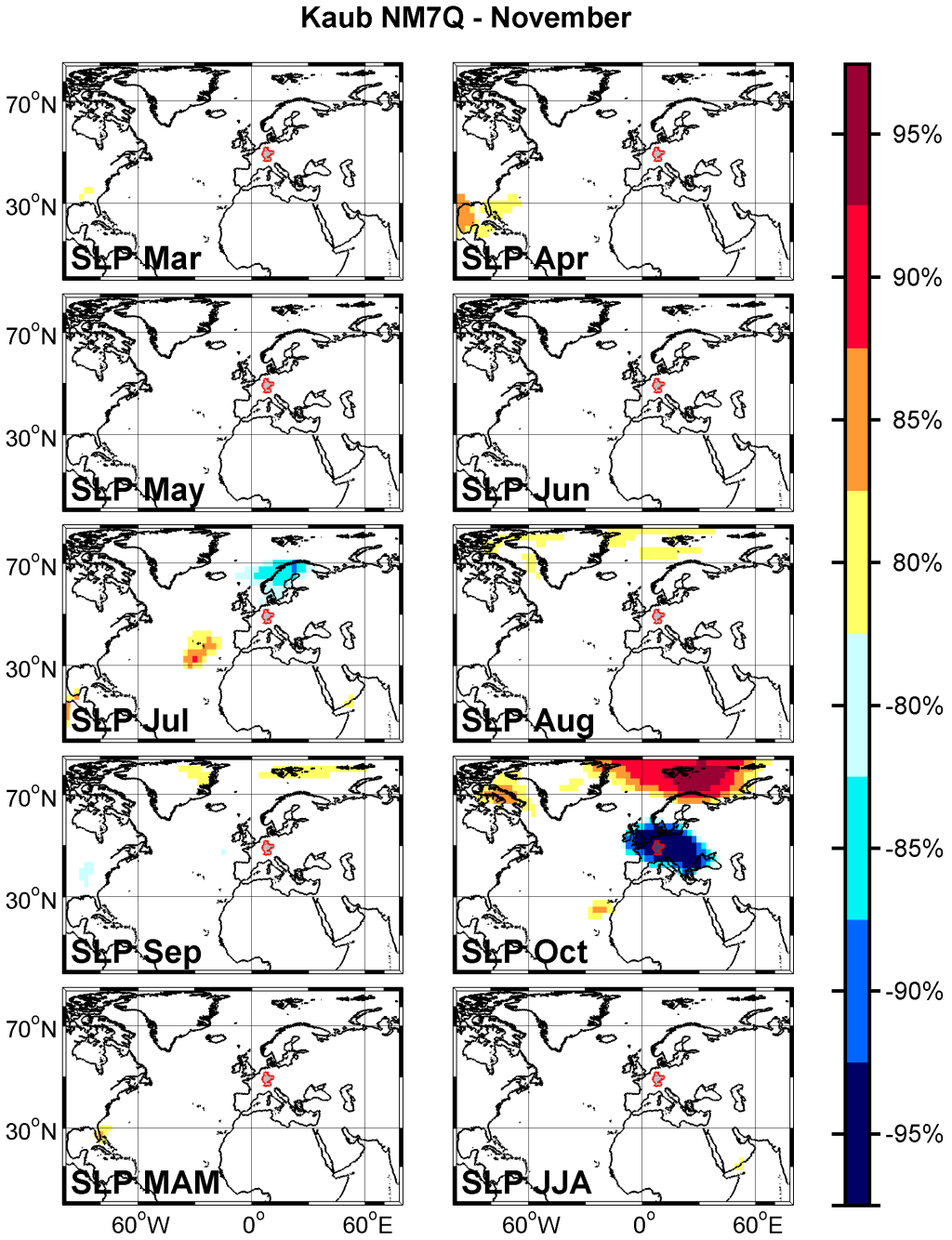

Fig. 20: *Stability maps of the correlation between November NM7Q at Kaub station and monthly SLP with different lags a) March; b) April; c) May; d) June; e) July; f) August; g) September; h) October; i) March-April-May (MAM) and j) June-July-August (JJA). The regions where the correlation is stable, positive and significant at 95% (80%) level for at least 80% of the windows are shaded with red (yellow). The corresponding regions where the correlation is stable, but negative, are shaded with blue (light blue).*

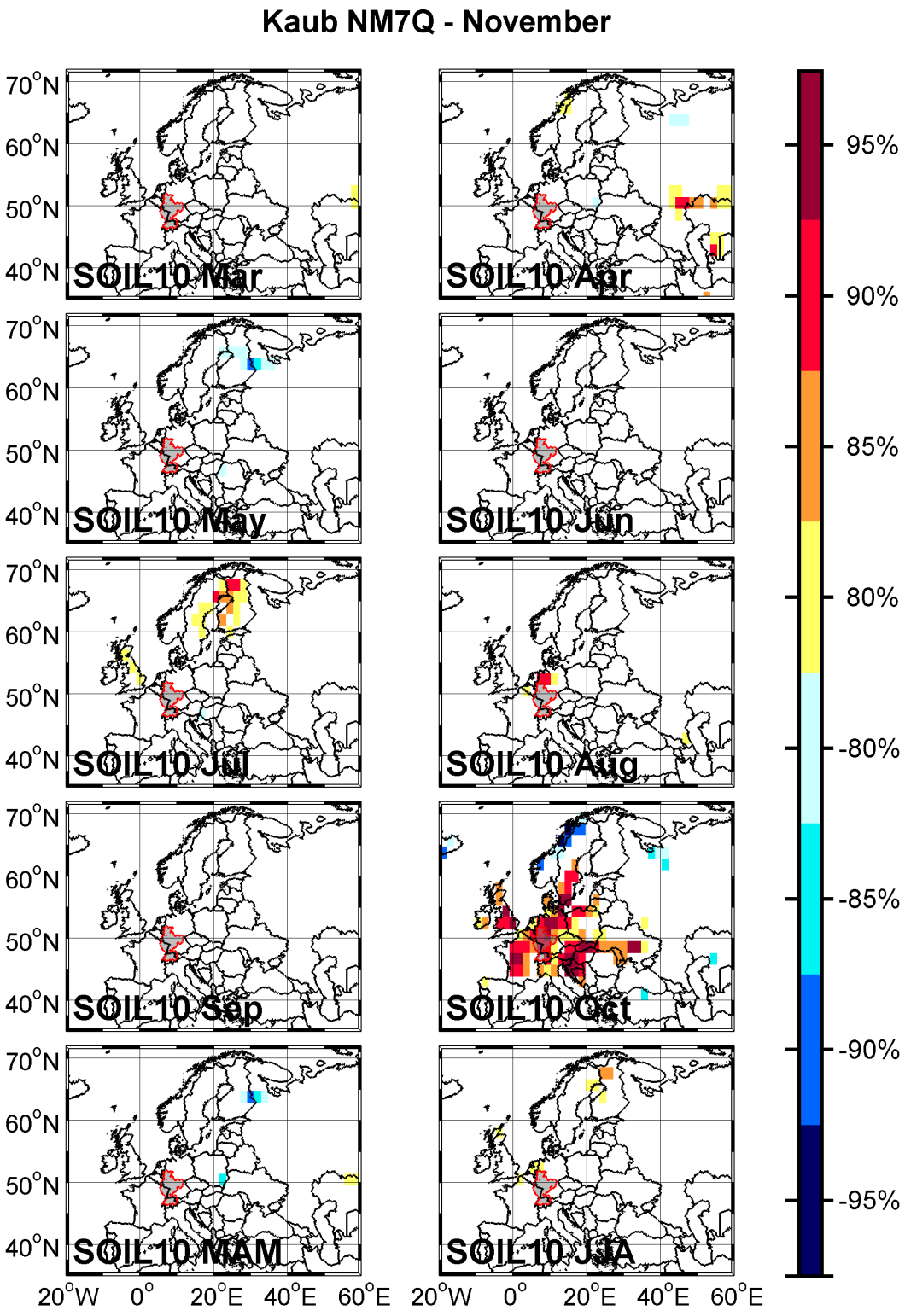

Fig. 21: *As in Figure 20, but for SOIL10*

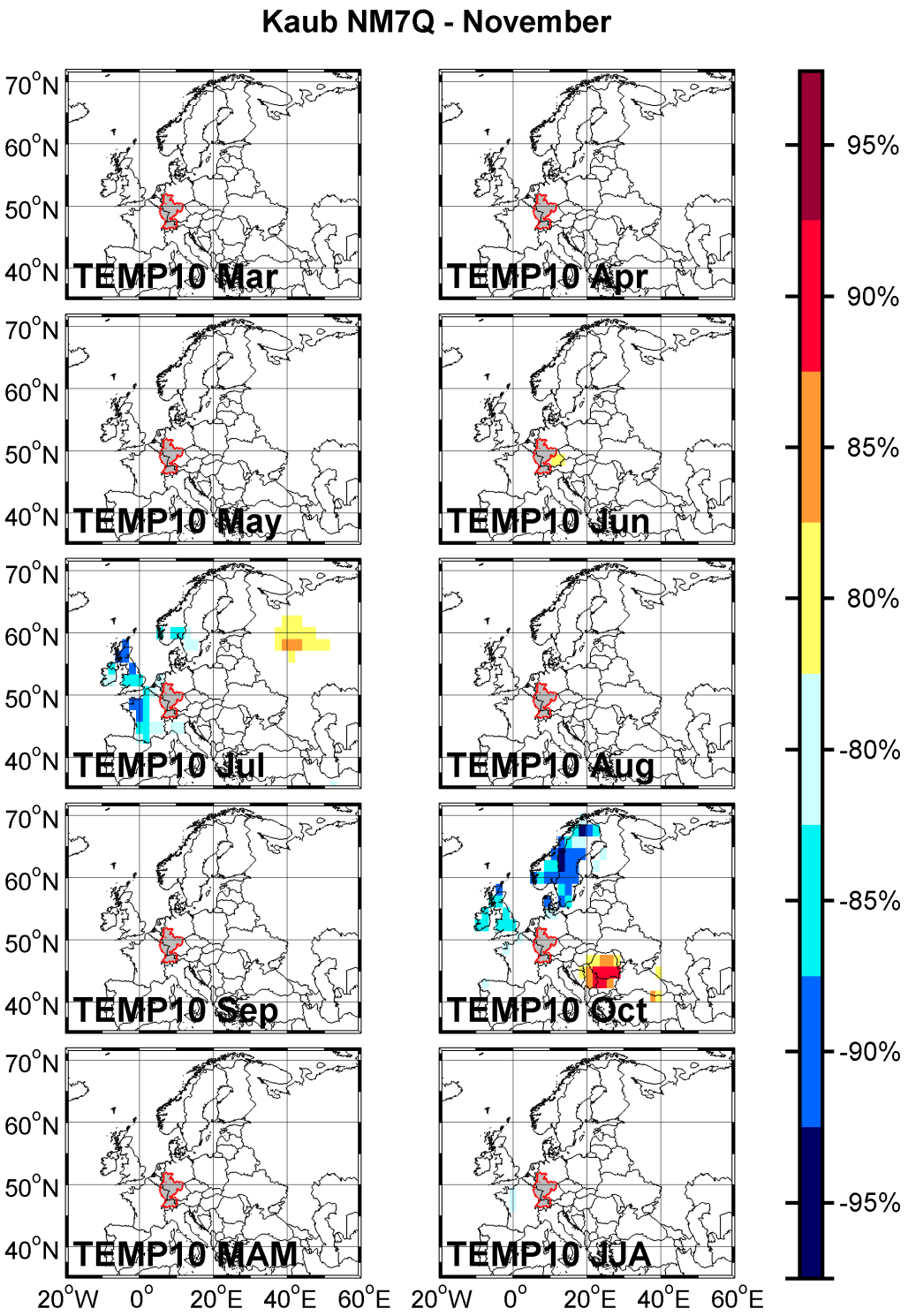

Fig. 22: *As in Figure 20, but for TEMP10*

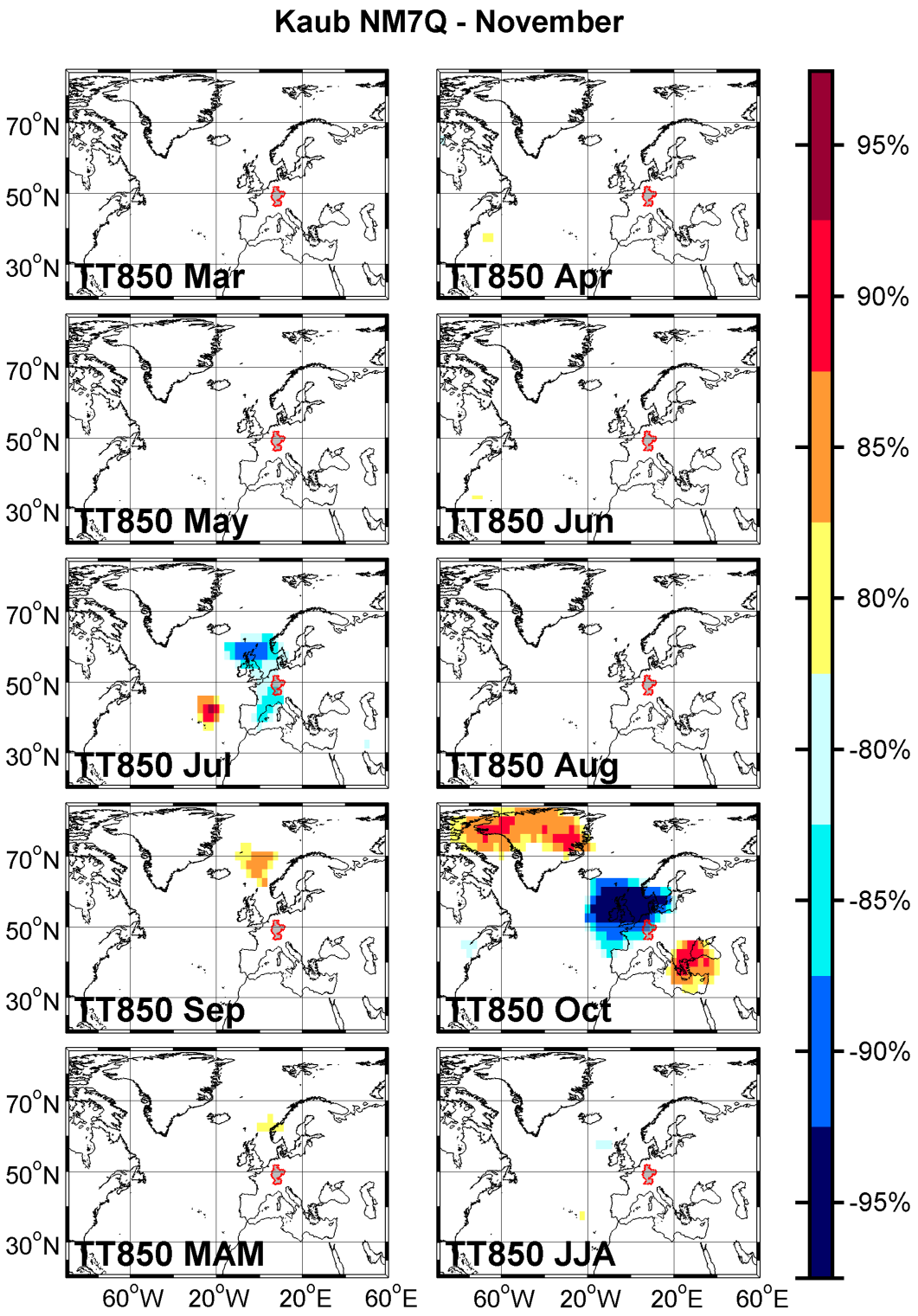

Fig. 23: *As in Figure 20, but for TT850*

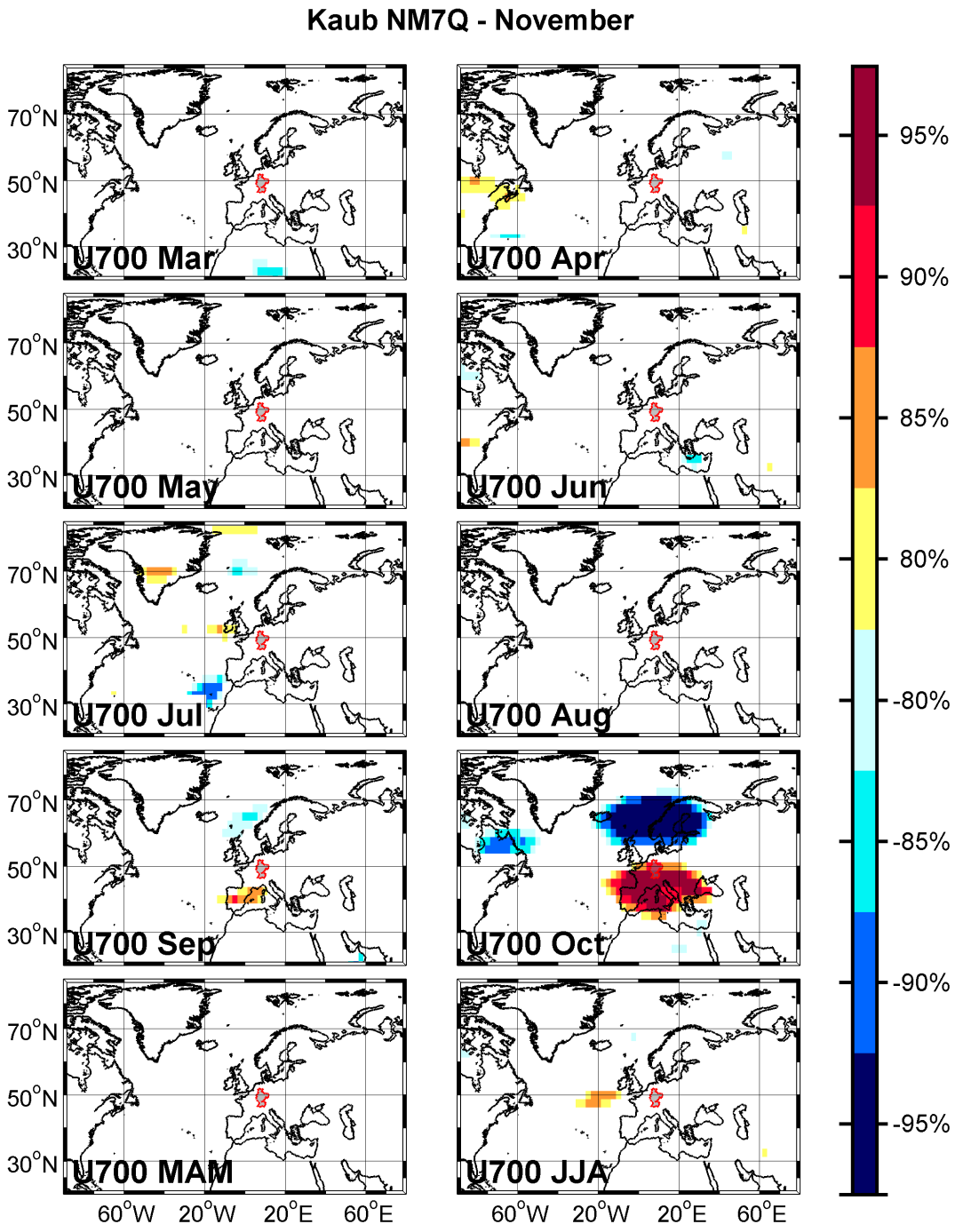

Fig. 24: *As in Figure 20, but for U700*

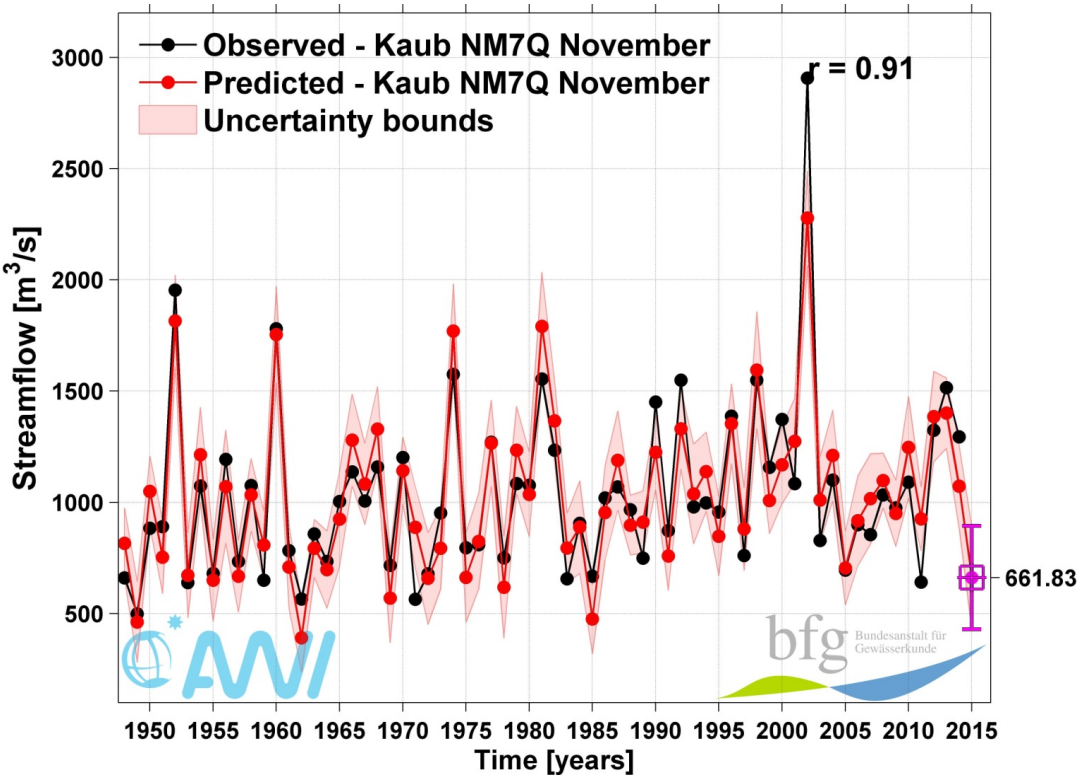

Fig. 25: *Comparison between the observed and predicted NM7Q values for November at Kaub station: Observed (black) and Predicted (red) November water levels values for the period 1948-2015. The light red shaded area represents the 95% uncertainty bounds.*

NM7Q NOV = id1 + id2 + id3 + id4 + id5 + id6 + id7 + id8 + id9 + id10 + id11 + id12 + id13 + id14 + id15 + id16 + id17

id1=badppoct; id2=u700oct1; id3=saarttsep; id4=kauboct; id5=ndhppaug; id6=gerttaug; id7=hesppoct; id8=rheinppsep; id9=bayppsep; id10=soil10oct; id11=kaubaug; id12=gerppjul;
id13=gerttoct; id14=saarppsep; id15=saarttoct; id16=gerppjun; id17=kaubjul.

Statistics:

Residual standard error: 180.8 on 49 degrees of freedom
Multiple R-squared: 0.8382, Adjusted R-squared: 0.782
F-statistic: 14.93 on 17 and 49 DF, p-value: 7.156e-14

5.3 Monthly prediction of NM7Q at Neu Darchau station

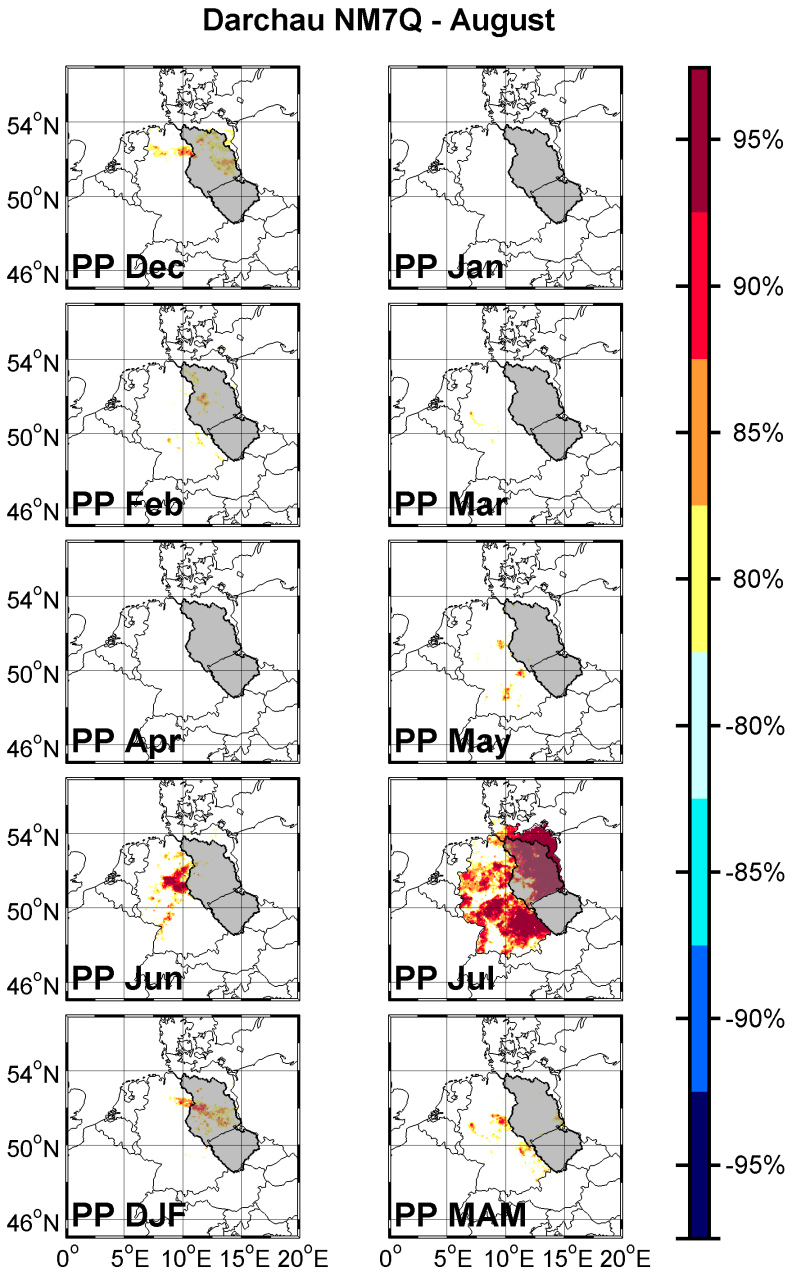

Fig. 26: *Stability maps of the correlation between August NM7Q at Neu Darchau station and monthly PP-DWD with different lags a) December; b) January; c) February; d) March; e) April; f) May; g) June; h) July; i) December-January-February (DJF) and j) March-April-May (MAM). The regions where the correlation is stable, positive and significant at 95% (80%) level for at least 80% of the windows are shaded with red (yellow). The corresponding regions where the correlation is stable, but negative, are shaded with blue (light blue).*

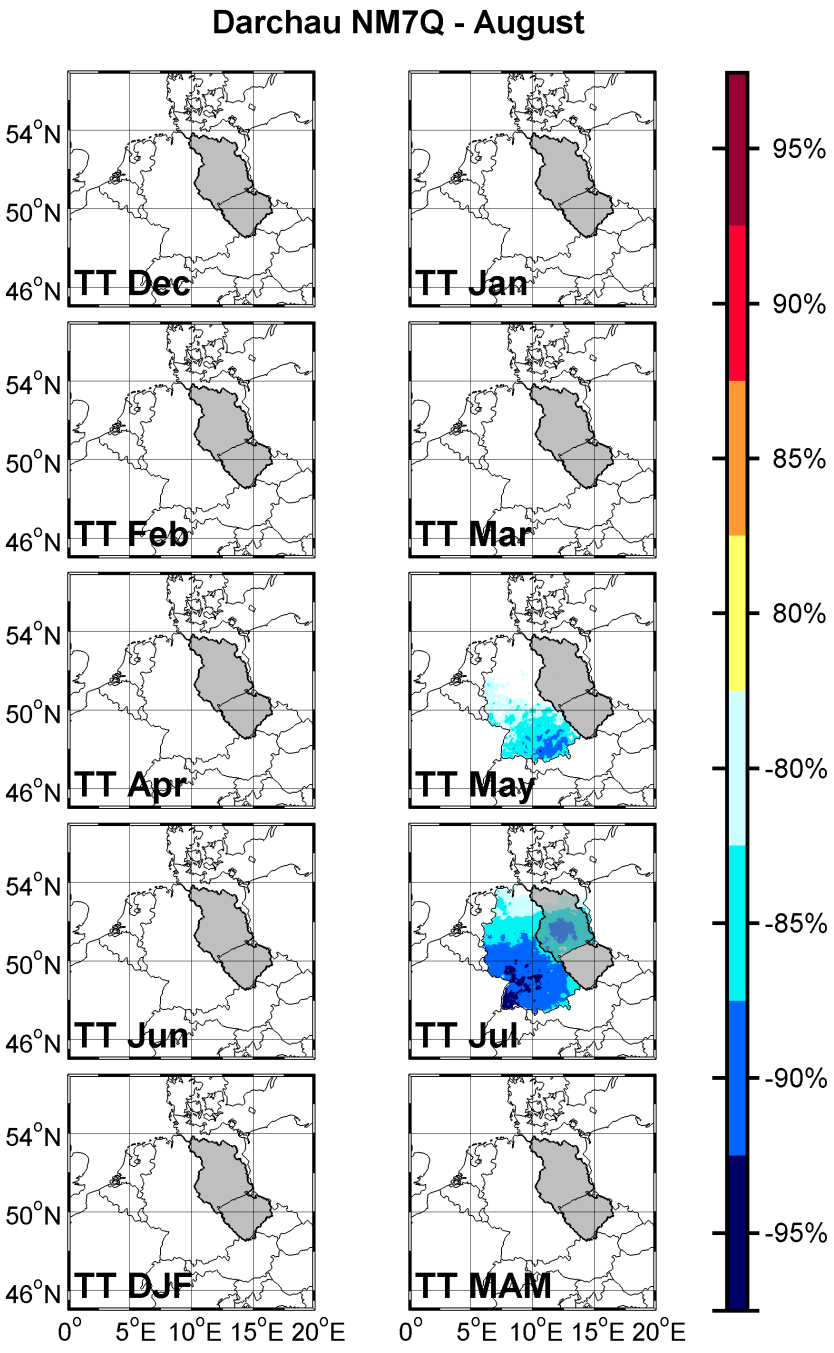

Fig. 27: As in Figure 26, but for TT – DWD

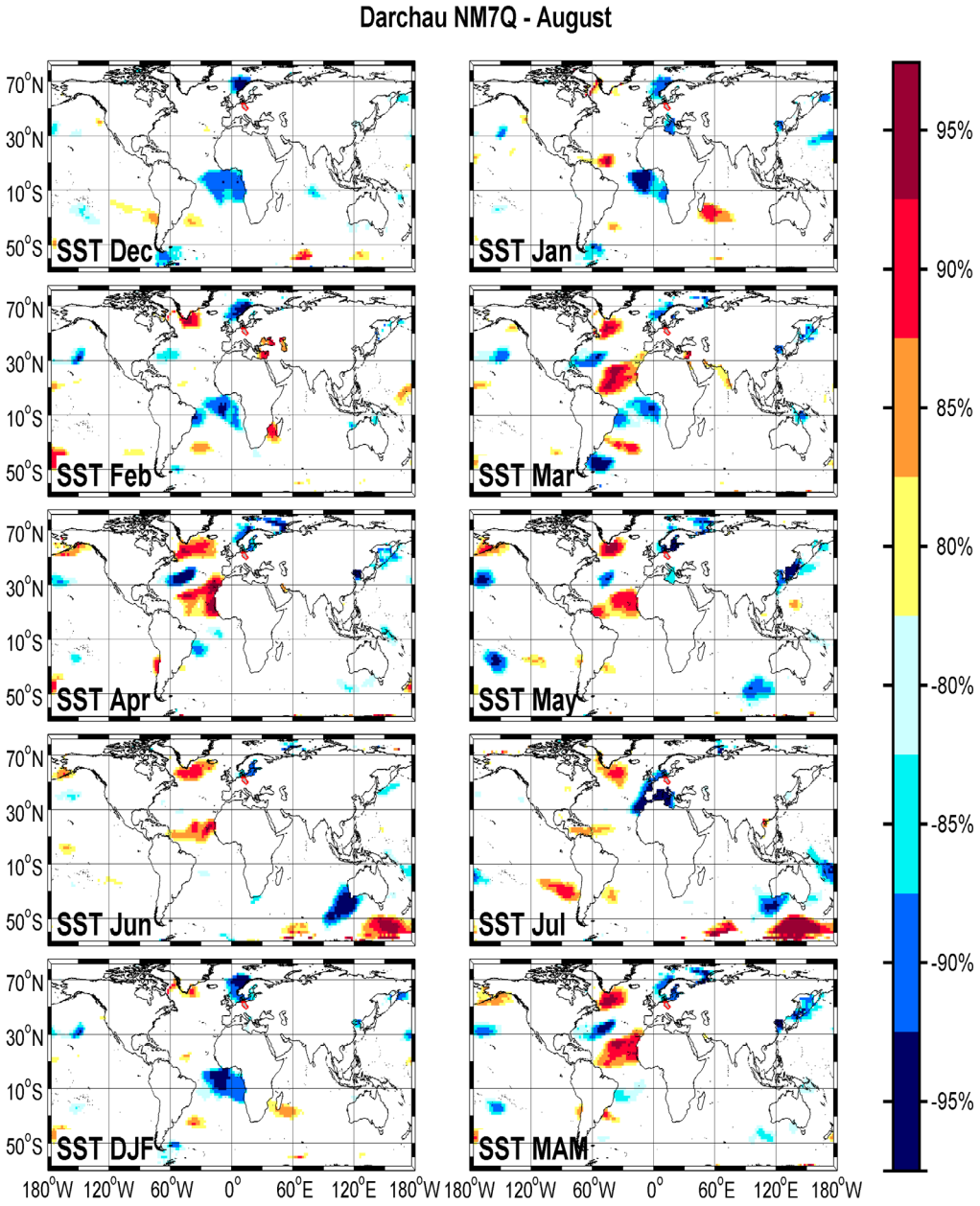

Fig. 28: As in Figure 26, but for SST

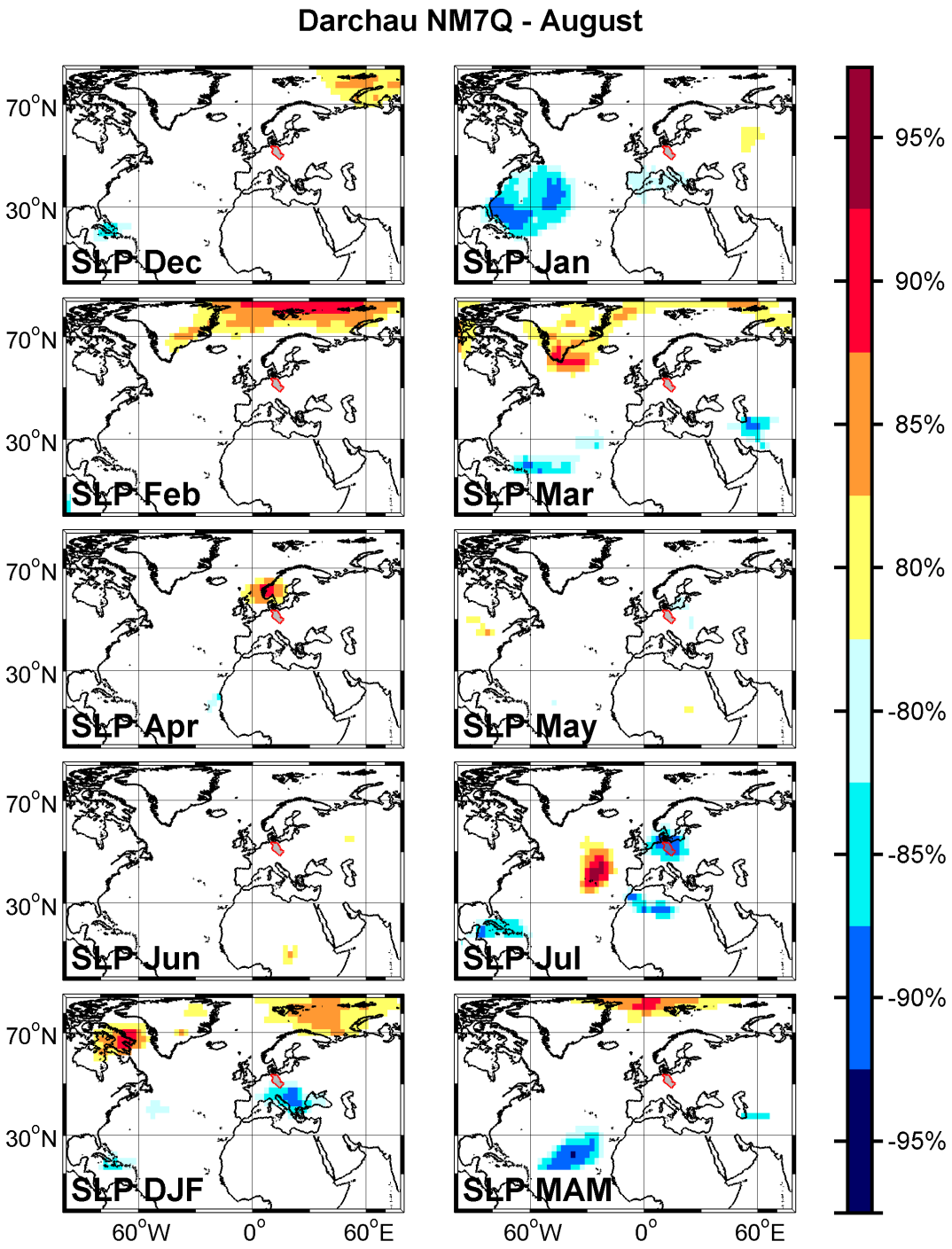

Fig. 29: *As in Figure 26, but for SLP*

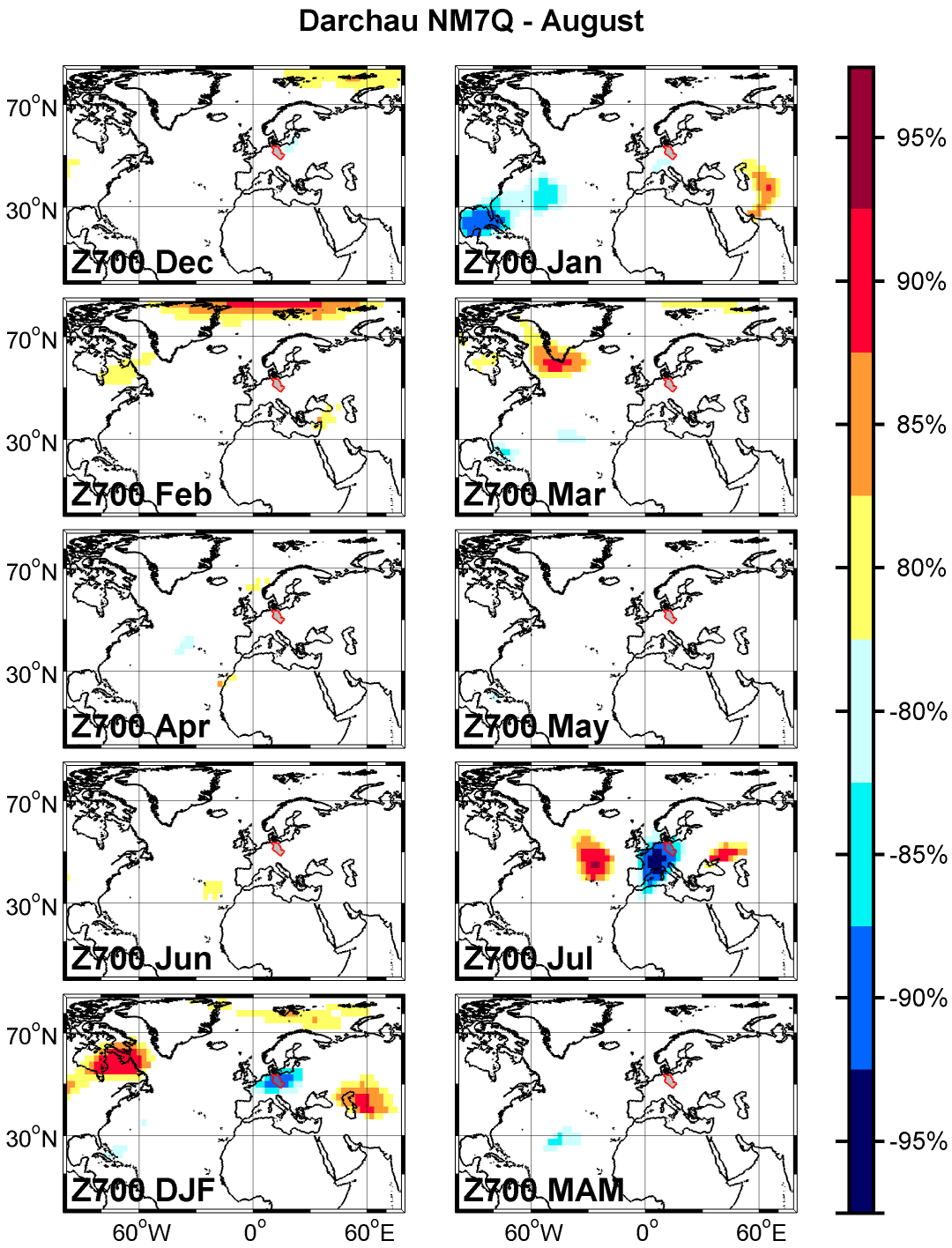

Fig. 30: *As in Figure 26, but for Z700*

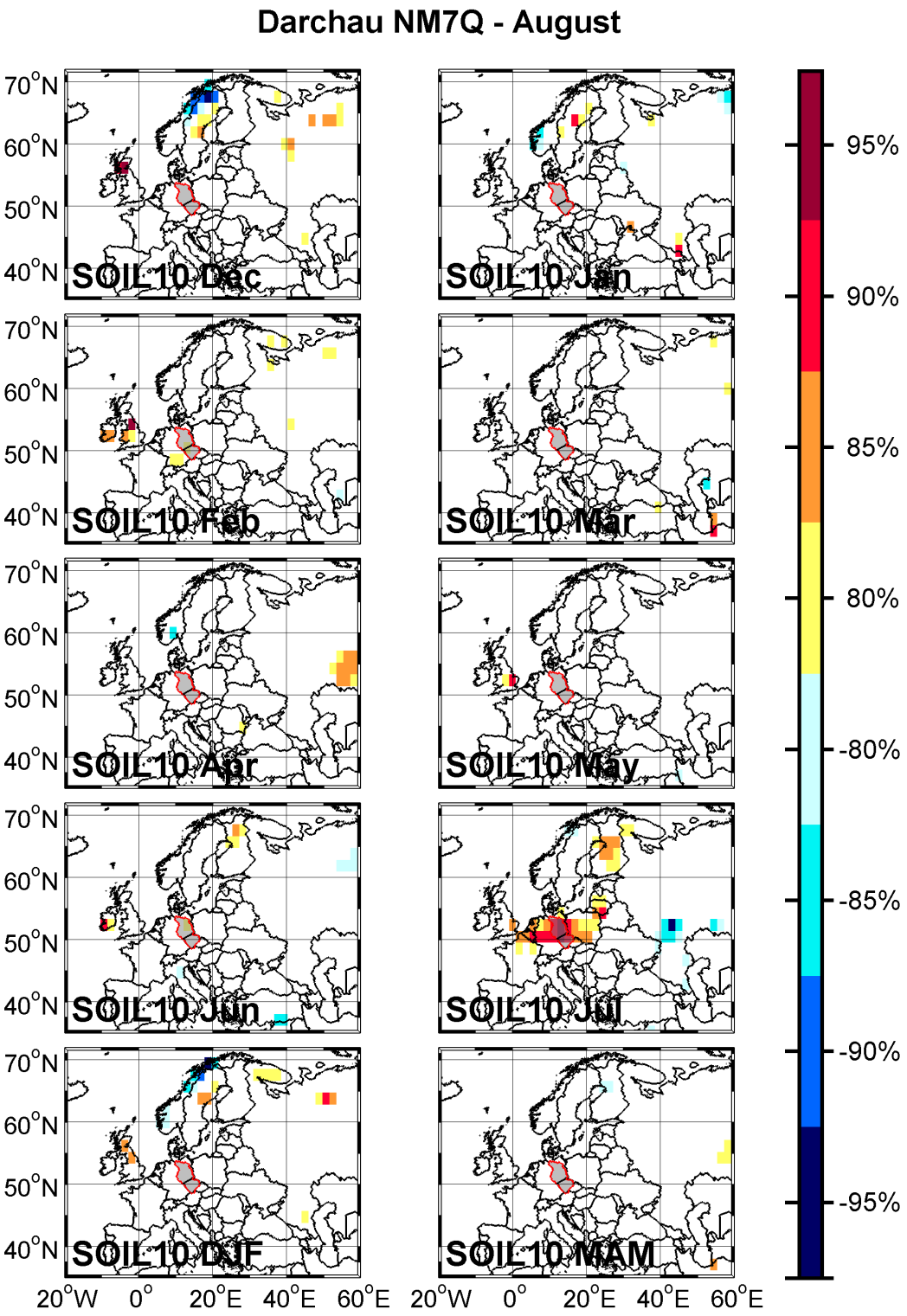

Fig. 31: *As in Figure 26, but for SOIl10*

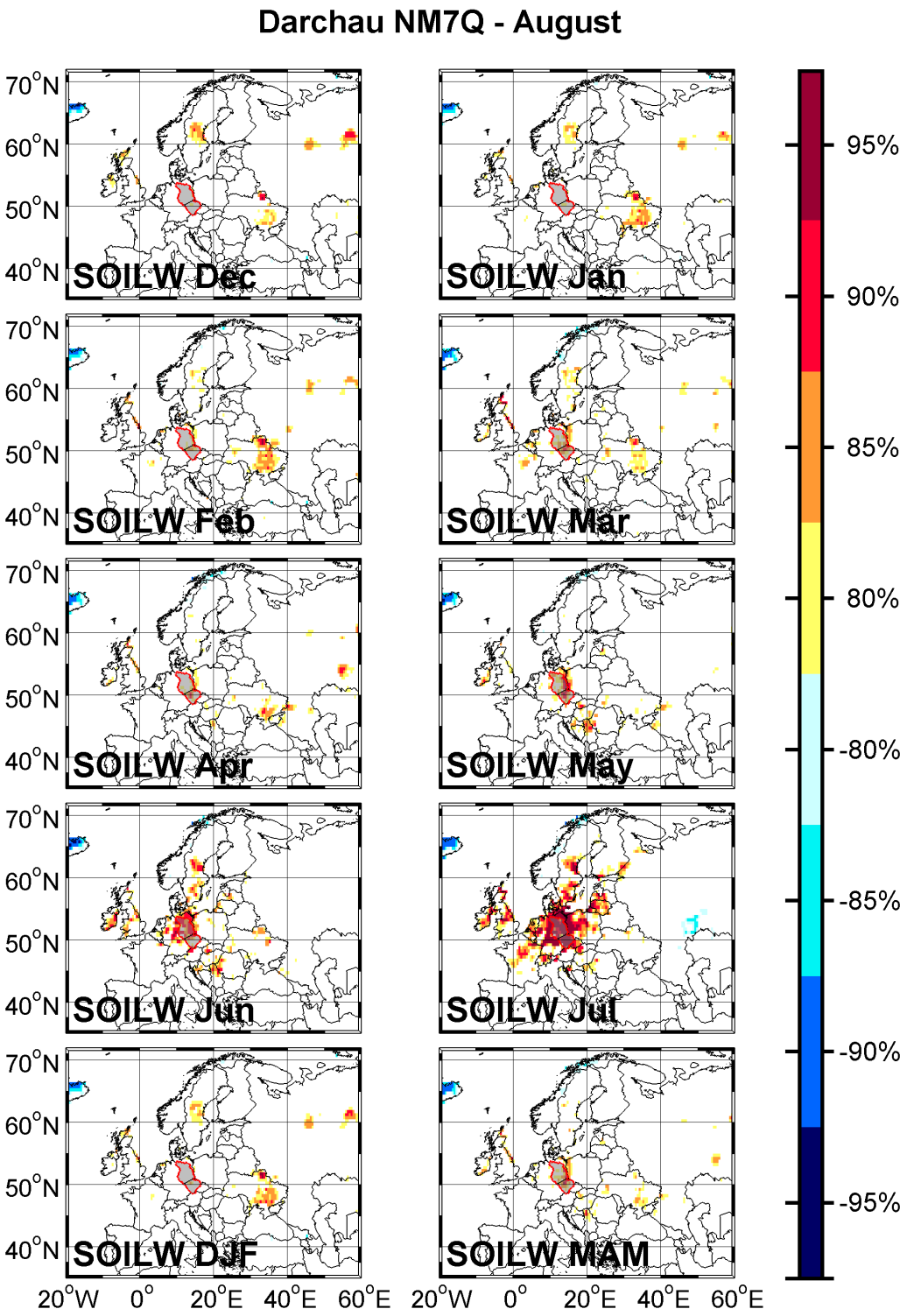

Fig. 32: *As in Figure 26, but for SOILW*

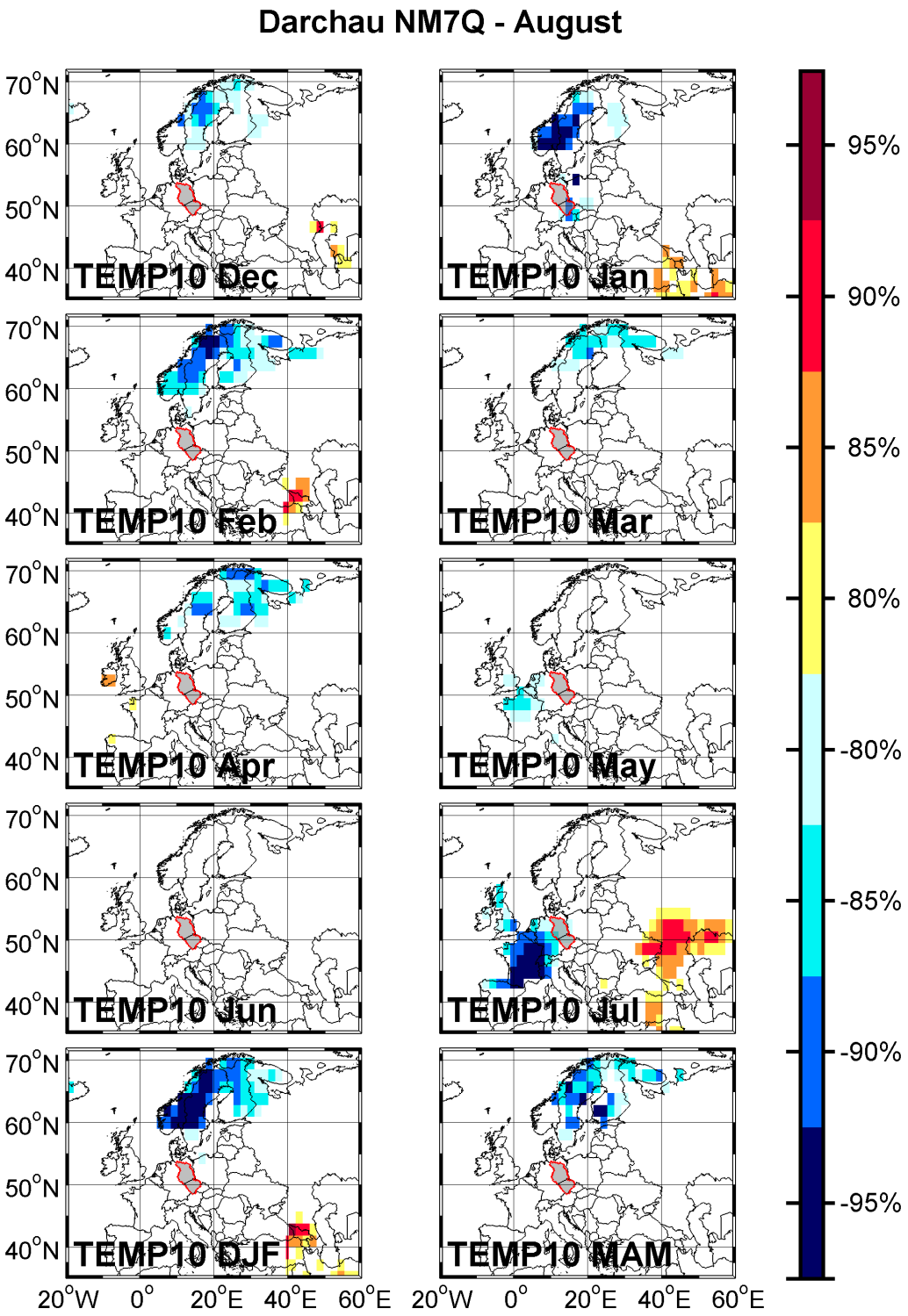

Fig. 33: *As in Figure 26, but for TEMP10*

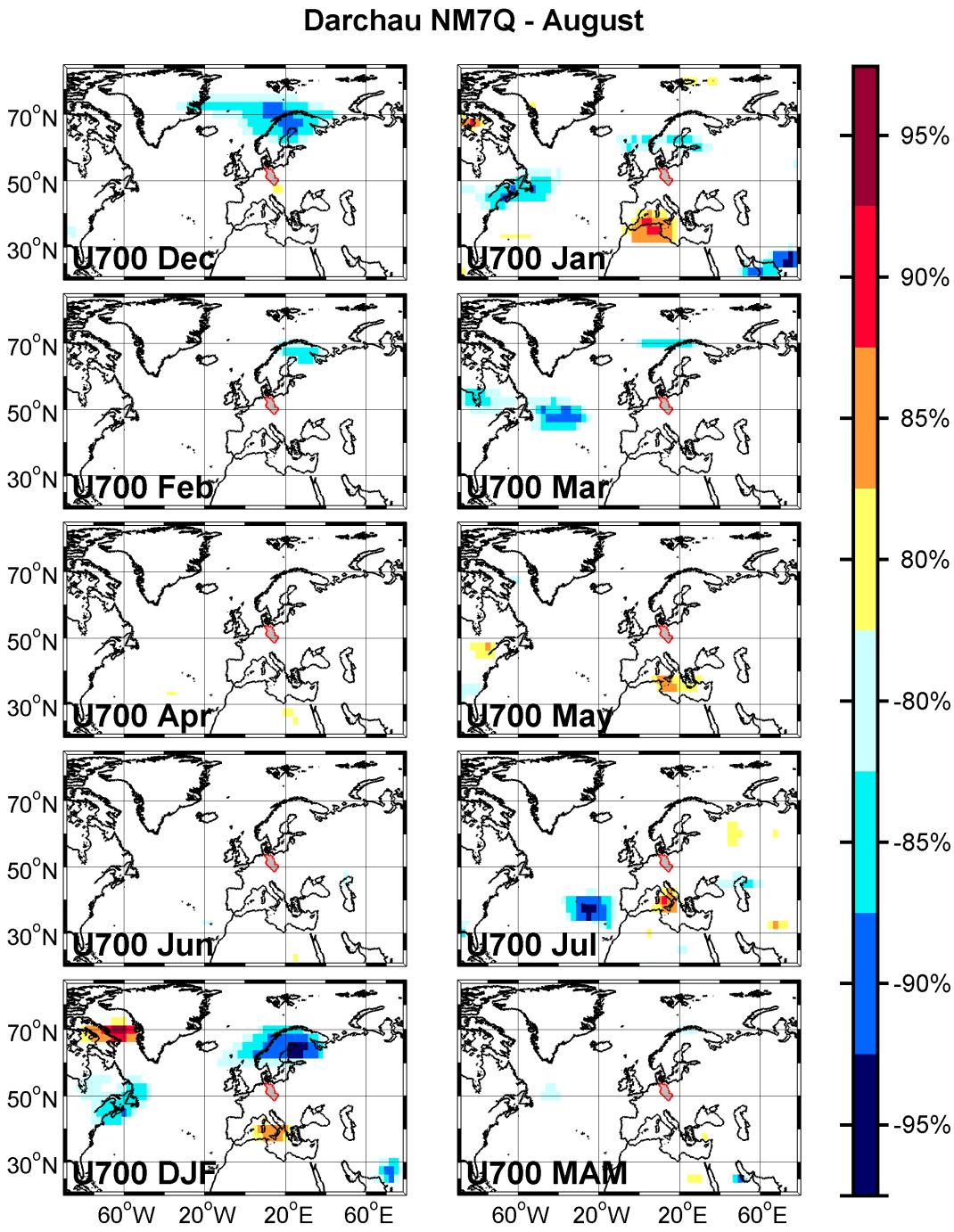

Fig. 34: *As in Figure 26, but for U700*

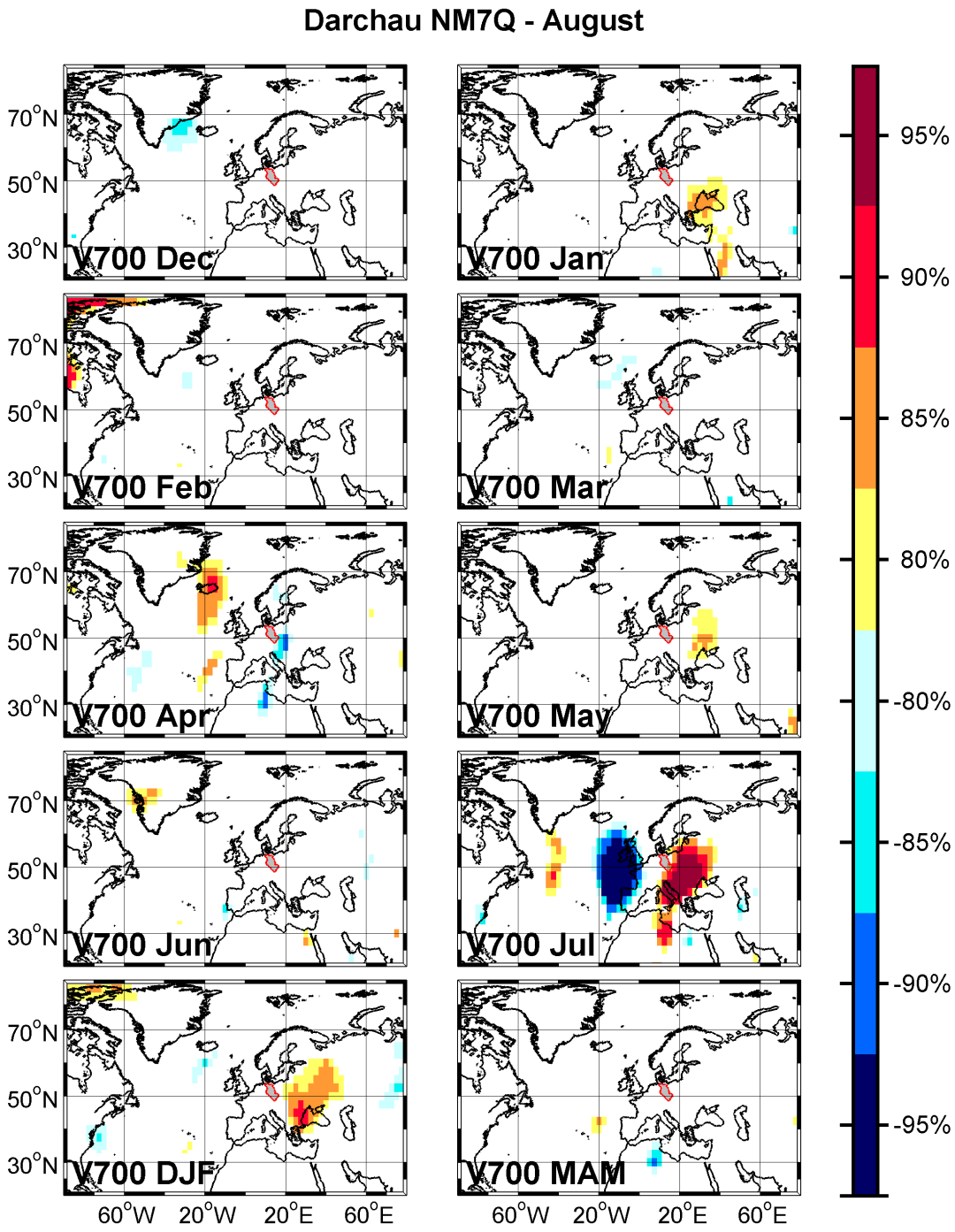

Fig. 35: *As in Figure 26, but for V700*

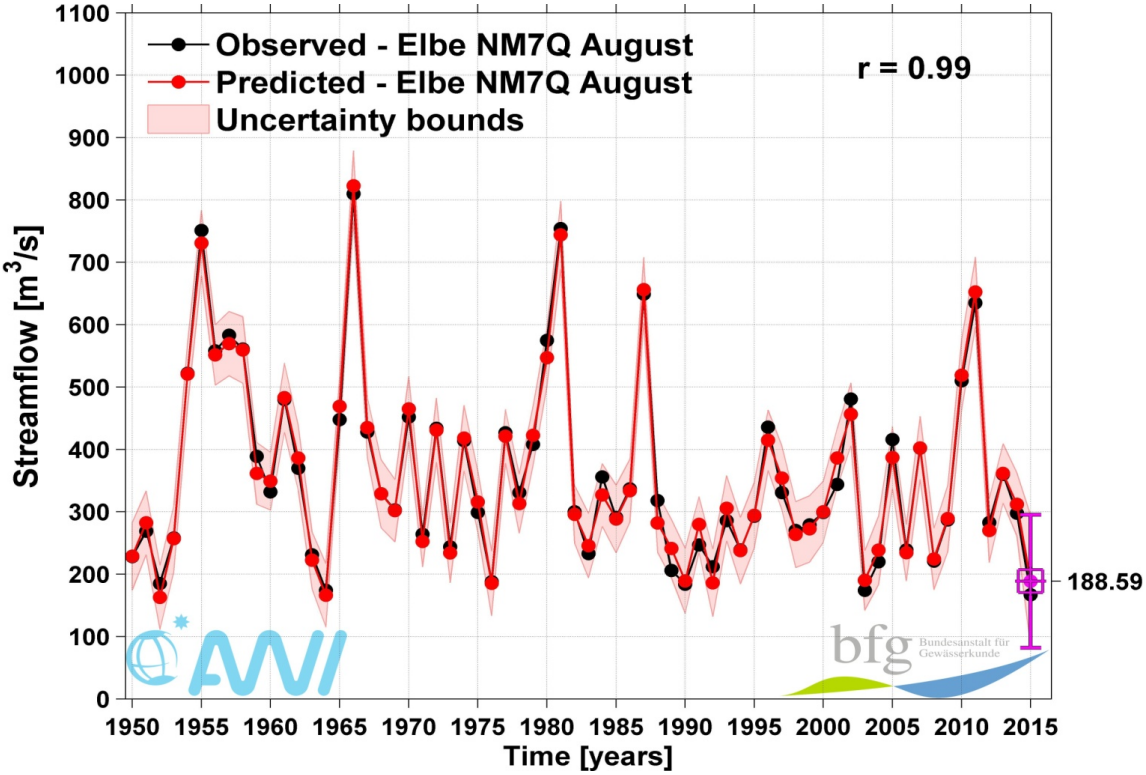

Fig. 36: *Comparison between the observed and predicted NM7Q values for August at Neu Darchau station: Observed (black) and Predicted (red) August water levels values for the period 1950-2015. The light red shaded area represents the 95% uncertainty bounds.*

NM7Q AUG = id1 + id2 + id3 + id4 + id5 + id6 + id7 + id8 + id9 + id10 + id11 + id12 + id13 + id14 + id15 + id16 + id17 + id18 + id19 + id20 + id21 + id22 + id23 + id24 + id25 + id26 + id27 + id28 + id29 +id30 + id31 + id32 + id33 + id34 + id35 + id36 + id37 + id38 + id39 + id40 + id41 + id42 + id43 + id44

id1=elbejul;id2=u700jul;id3=bayppjul;id4=soilwjun;id5=u700jan1;id6=ttmay;id7=v700jul2;id8=ndsppjul;id9=ppjul;
id10=hesppjul;id11=badppjun;id12=sstapr2;id13=sstjan;id14=ndsppjun;id15=tt10jul;id16=sstmay2;
id17=sstfeb;id18=slpmar1;id19=badttjul;id20=slpjul1;id21=saarttjul;id22=ndsttjun;id23=gerttjun;id24=z700jul1;
id25=v700jul1;id26=slpjul2;id27=hesppjun;id28=saarppjun;id29=sstapr1;id30=sstjun;id31=tt10feb;
id32=rheinppjun;id33=bayppjun;id34=sstmar2;id35=tt10jan;id36=slpfeb;id37=bayttjun;id38=saarttjun;
id39=sstmam2;id40=sstmam1;id41=badppjul;id42=sstmay1;id43=slpjan;id44=hesttjun.

Statistics:

Residual standard error: 29.24 on 20 degrees of freedom
Multiple R-squared: 0.9879, Adjusted R-squared: 0.9613
F-statistic: 37.11 on 44 and 20 DF,p-value: 2.367e-12

5.4 Monthly prediction of NM7Q at Hofkirchen station

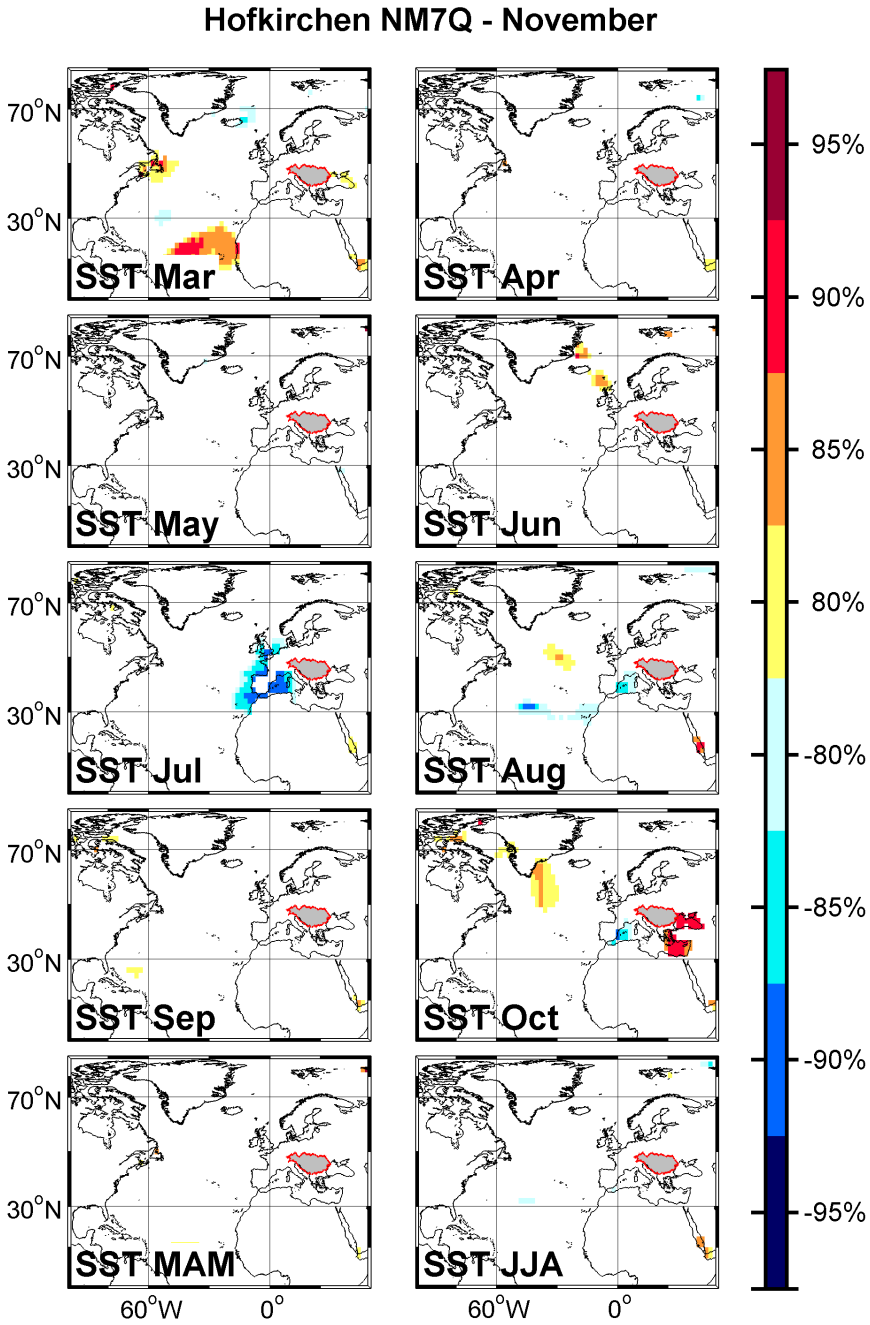

Fig. 37: *Stability maps of the correlation between November NM7Q at Hofkirchen station and monthly SST with different lags a) March; b) April; c) May; d) June; e) July; f) August; g) September; h) October; i) March-April-May (MAM) and j) June-July-August (JJA). The regions where the correlation is stable, positive and significant at 95% (80%) level for at least 80% of the windows are shaded with red (yellow). The corresponding regions where the correlation is stable, but negative, are shaded with blue (light blue).*

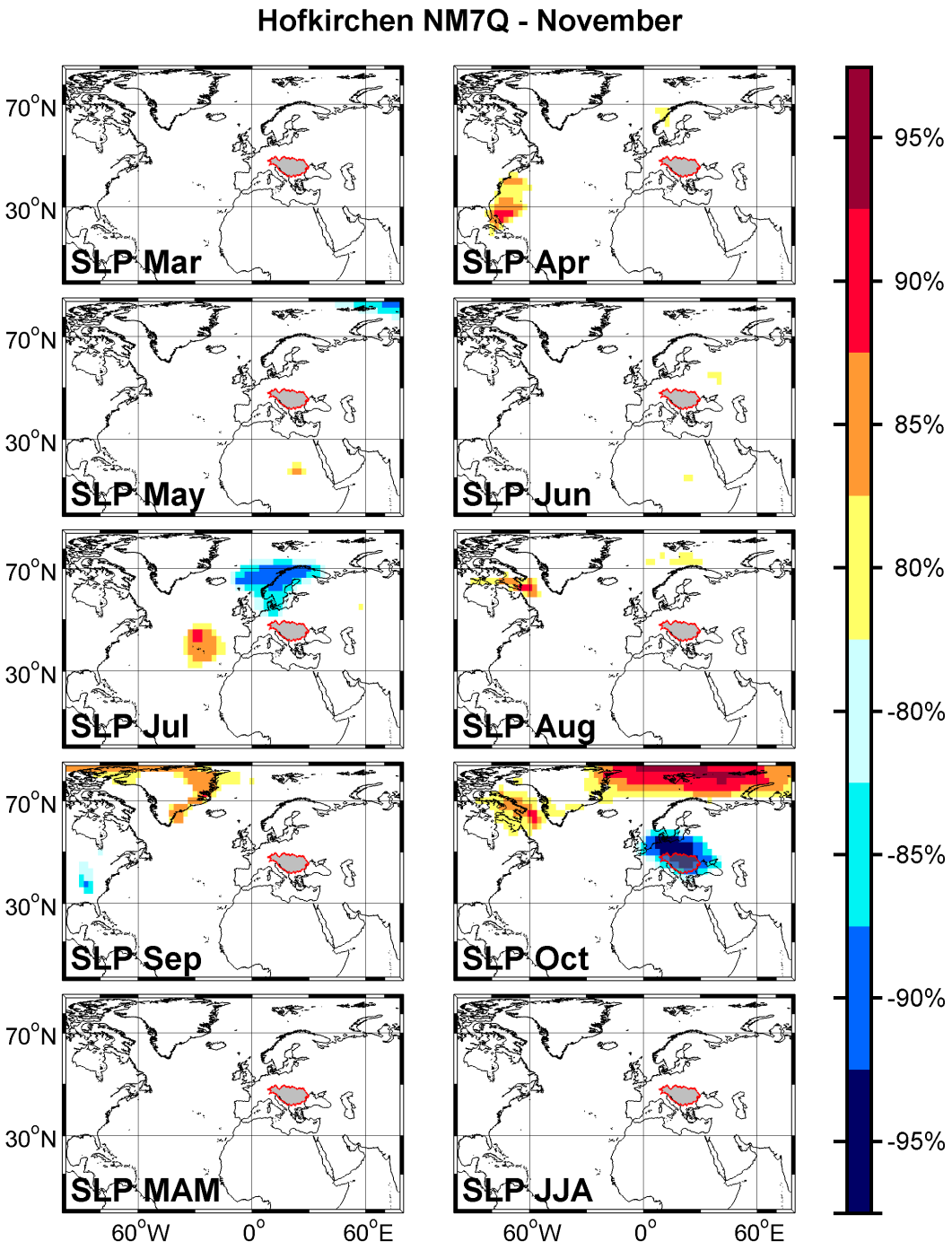

Fig. 38: *As in Figure 37, but for SLP*

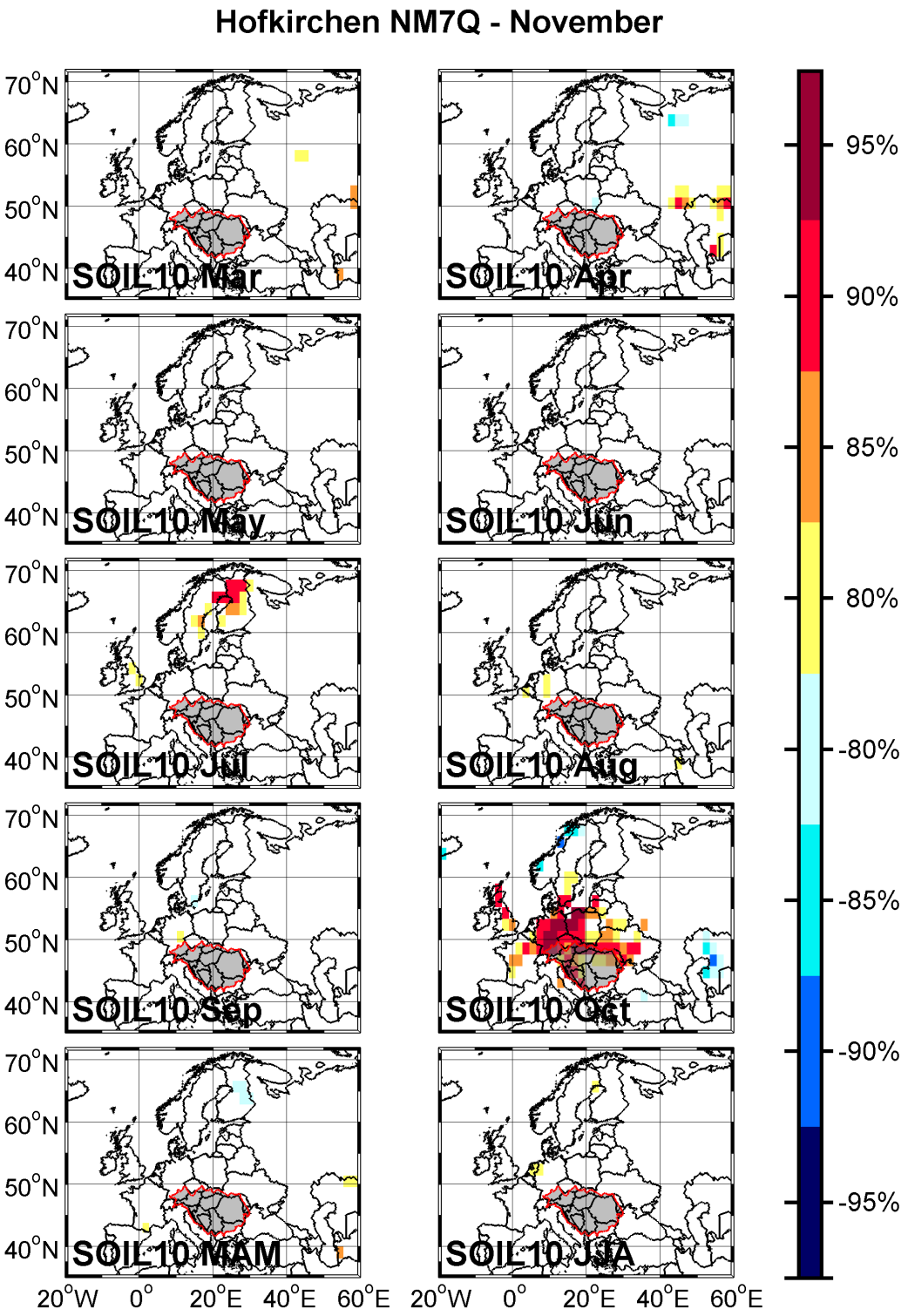

Fig. 39: *As in Figure 37, but for SOIL10*

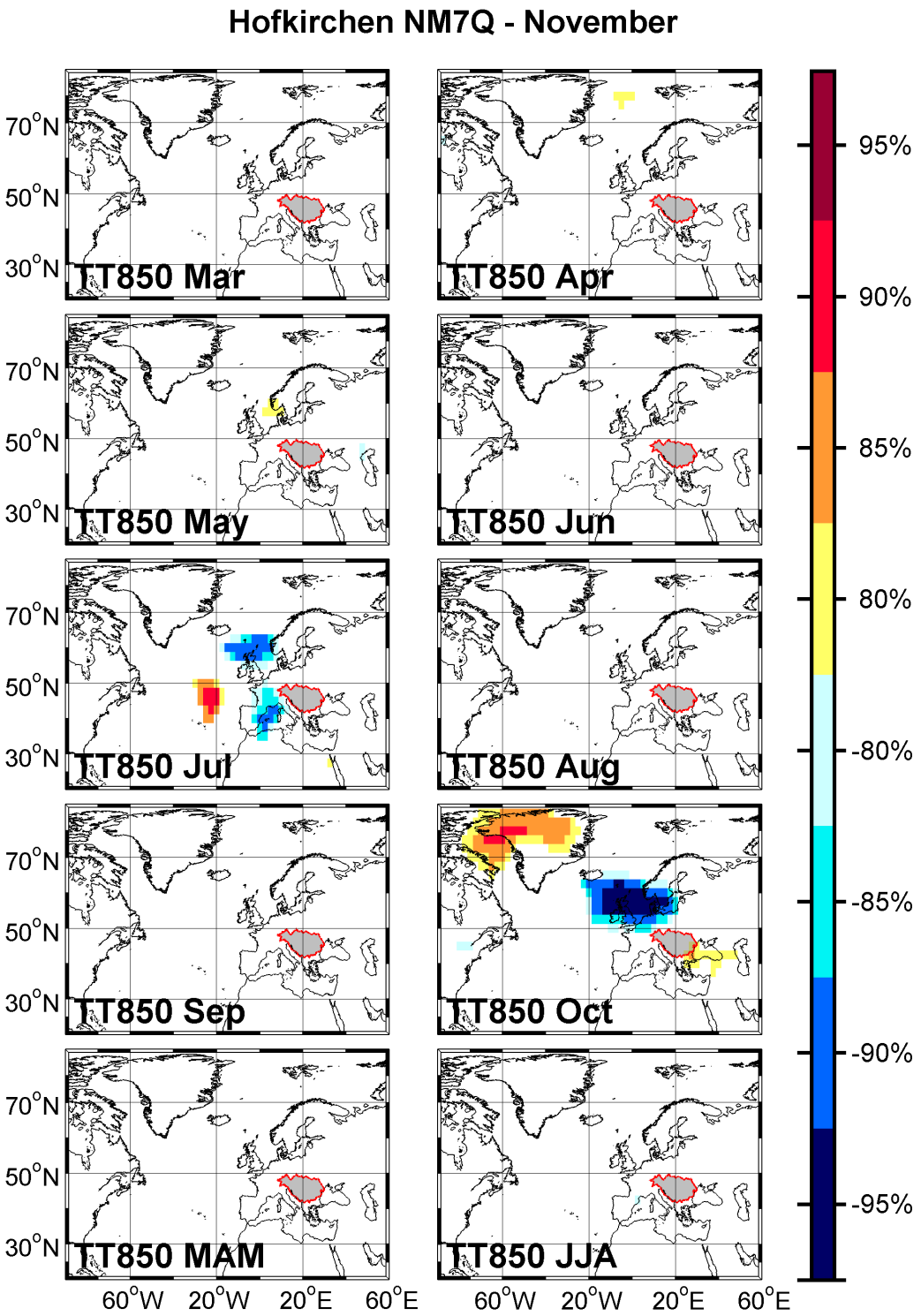

Fig. 40: *As in Figure 37, but for TT850*

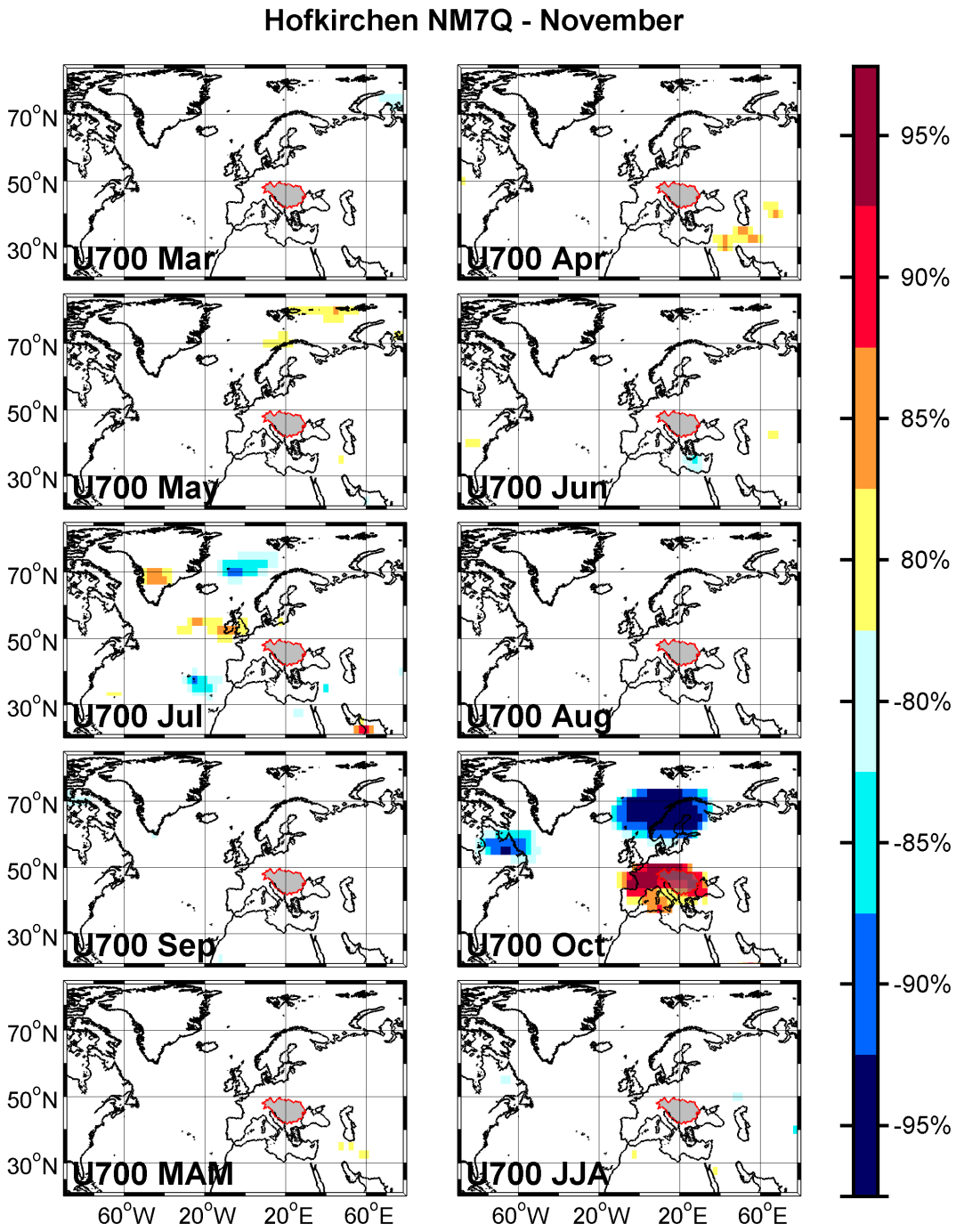

Fig. 41: *As in Figure 37, but for U700*

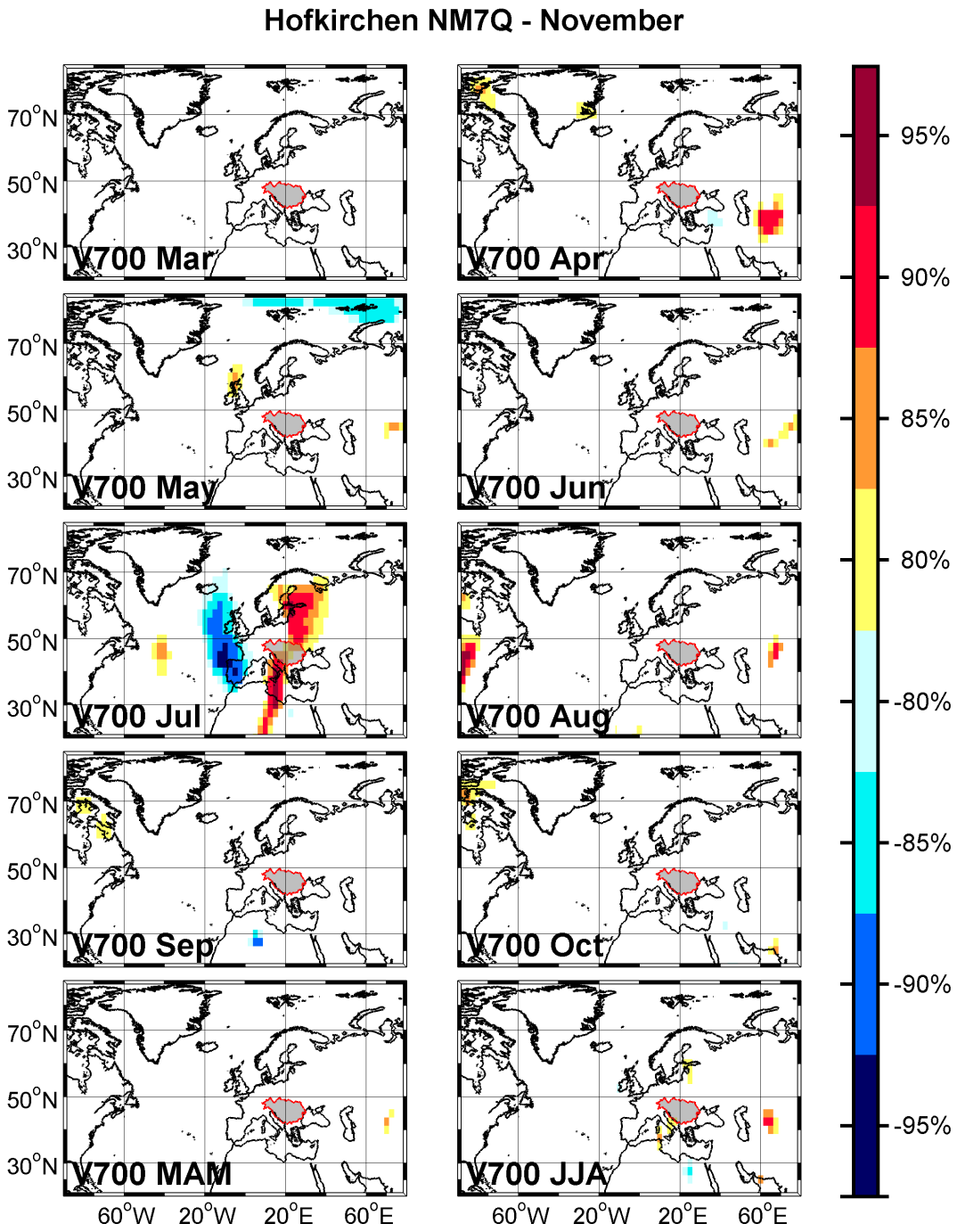

Fig. 42: *As in Figure 37, but for V700*

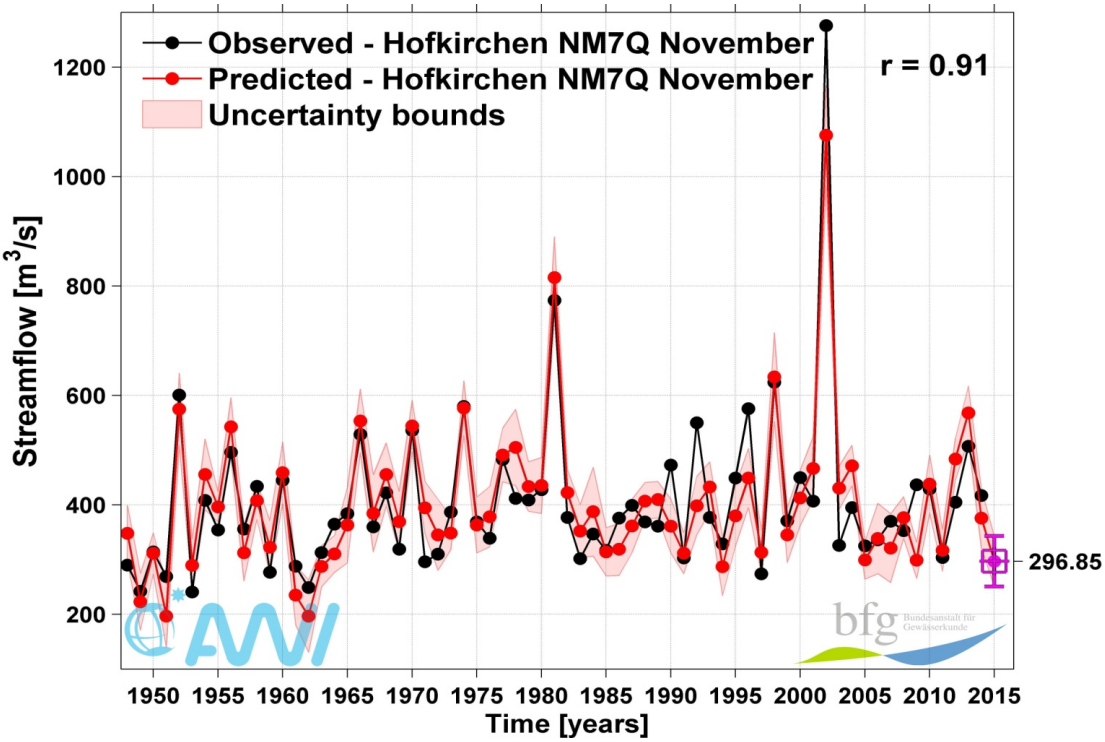

Fig. 43: *Comparison between the observed and predicted NM7Q values for November at Hofkirchen station: Observed (black) and Predicted (red) November water levels values for the period 1948-2015. The light red shaded area represents the 95% uncertainty bounds.*

NM7Q NOV = id1 + id2 + id3 + id4 + id5 + id6 + id7 + id8 + id9 + id10

id1=hofkirchenoct; id2=u700oct2; id3=saarppsep; id4=bayttsep; id5=gerttjul;
id6=gerppjun;
id7=slpoct2; id8=hofkirchensep; id9=hofkirchenmqsep; id10=rheinppsep.

Statistics:

Residual standard error: 65.13 on 56 degrees of freedom
Multiple R-squared: 0.8334, Adjusted R-squared: 0.8037
F-statistic: 28.02 on 10 and 56 DF, p-value: < 2.2e-16

6. CONCLUSIONS

The hydrological system acts as spatial and temporal integrator of precipitation (rain and snow), temperature, and related evapotranspiration over a specific region. Therefore, seasonal to decadal streamflow variability in many large river-basins can be controlled by corresponding changes in large scale atmospheric circulation patterns. The relationship between these climatic regimes and its hydrological response, through its streamflow, presents different grades of complexity according to the physical characteristics of the basin. Nevertheless, streamflow can be better related with important patterns of climate teleconnections than precipitation or temperature fields, since variations in precipitation are amplified in streamflow, and in general, it is easier to detect a change in discharge than directly in the basic climatic variables [*Dettinger and Diaz, 2000; Trigo et al., 2004*].

Water resources management is an important and delicate subject, especially for the regions characterized by intense irrigation, hydropower systems and navigational systems. The concern of the effect of climate variability and change on water resources makes management problems more challenging and water managers are looking for a way to improve their management decisions. A key element of the water management problem is to find out how much water will be available in the underlying water resources system during the following months, seasons and year.

Streamflow forecasting is challenging because of the complexity of the hydrologic system. Improving the quality of streamflow forecasting has always been an important task for researchers and hydrologic forecasters. Therefore, the motivation of this report relies on the necessity to improve the understanding of the large-scale climate variability that drives the streamflow variability for the main German rivers, which becomes the basis for developing streamflow forecast at scales that are of paramount importance for population and natural environment. The report presented herein focuses on streamflow forecasting on monthly and seasonal time scales for the Rhine River, Elbe River and Danube River, respectively. The streamflow predictability, based on a statistical multimodel approach that uses as predictors such as precipitation, temperature, soil moisture, geopotential height at 700-mb, mean sea level pressure, zonal and meridional wind, ground temperature and sea surface temperature from the previous months has been investigated. Overall, our analysis reveals the existence of a valuable predictability of the water levels and streamflow at monthly and seasonal time scales, a result that may be useful to water resources management. Although the analysis is restricted to particular gauging stations, the conceptual basis and lessons learned could be transferable to other catchment areas, which might lie under different climatological and/or hydrological background.

The advantages of this methodology, compared to other prediction products available for Europe [*Alifieri et al., 2013*] or globally [*Werner et al., 2013; Candogan-Youssed et al., 2013*] are: a) it is inexpensive in terms of computational and human resources; b) it does not require the use of a hydrological model, which is mostly not freely available and has high computational costs and c) it does not require the access to operational ensemble forecast data, like most of the available flood prediction products do. Therefore, using a simple and computationally inexpensive statistical model one can anticipate to a certain degree extreme upcoming floods/low levels, based on the antecedent climate conditions over specific regions. Finally, since the concept can be used as an early warning system for floods/low levels, the potential societal benefits in terms of limiting life and monetary loss are enormous. Moreover, a skillful prediction based on stable teleconnections could provide guidance for water management in the different catchment area with consequences for economy, agriculture and hydroelectricity.

Evaluation of the statistical model at Kaub station (Rhine):

- For all the months/seasons and variables (NM7Q and MQ) the Nash-Sutcliffe efficiency (NSE), the index of agreement (d) and the Kling-Gupta efficiency (KGE), at Kaub station, were skillful (i.e. above zero) with a maximum value of 0.98 (almost perfect forecast) for NM7Q for the month of July. Moreover, the percentage of "hits" for July NM7Q (when the observed streamflow falls in the limits of the predicted streamflow) reached 100% (Table 1, Figure 44).
- For **NM7Q** (Figure 44, Table 1 and Table 2), at ***Kaub*** station, the **months with the highest predictive skill**, based on the percentage of hits/miss, NSE, d and KGE, are: **July, January, March and February**. The **months with the lowest predictive** skill are: **August and October**. Nevertheless, even for these two months NSE and KGE have values above 0.70. The index of agreement is above 0.90 for all the months.
- For **MQ** (Figure 45, Table 3 and Table 4), at ***Kaub*** station, the **months with the highest predictive skill**, based on the percentage of hits/miss, NSE, d and KGE, are: **January, March, April, May, October and November**. For these months, NSE and KGE have values above 0.84 and the index of agreement is above 0.92. The **months with the lowest predictive** skill are: **February, June and July**. As in the case of NM7Q, even for these three months NSE and KGE have values above 0.74. The index of agreement is above 0.92 for all the analyzed months.
- At seasonal time scale (Figure 46, Table 5 and Table 6), for ***Kaub*** station, **the season with the highest predictive skill is spring (MAM)** (NSE = 0.89, d = 0.97 and KGE = 0.92), while the season with the lowest predictive skill is SON (NSE = 0.74, d = 0.92 and KGE = 0.80). Nevertheless, the differences between the predictive skill at seasonal time scale are relatively small.
- Overall, the predictive skill at Kaub station is very good, with small exceptions in summer months for MQ. The smaller skill during the summer months might be due to the influence of convective precipitation, which is not taken into account in the forecast model, and the tendency to a higher variability of the streamflow during these months.

Evaluation of the statistical model at Neu Darchau station (Elbe):

- For all the months/seasons and variables (NM7Q and MQ), the Nash-Sutcliffe efficiency (NSE), the index of agreement (d) and the Kling-Gupta efficiency (KGE), at Neu Darchau station, were skillful (i.e. above zero) with a maximum value of 0.99 for NSE and KDE (almost perfect forecast) and a maximum value of 1 (perfect forecast) for the index of agreement for August NM7Q. Moreover, the percentage of "hits" for August NM7Q (when the observed streamflow falls in the limits of the predicted streamflow) reached 100% (Table 7, Figure 47).
- For **NM7Q** (Figure 47, Table 7 and Table 8), at ***Neu Darchau*** station, the **months with the highest predictive skill**, based on the percentage of hits/miss, NSE, d and KGE, are: **August, September and October**. The **months with the lowest predictive** skill are: **February, April and June**. Nevertheless, even for these three months NSE and KGE have values above 0.72. The index of agreement is above 0.90 for all the months.
- For **MQ** (Figure 48, Table 9 and Table 10), at ***Neu Darchau*** station, the **months with the highest predictive skill**, based on the percentage of hits/miss, NSE, d and KGE, are: **March, May and October**. For these months NSE and KDE have values above 0.89 and the index of agreement is above

0.96. The **months with the lowest predictive** skill are: **June, July and August**. As in the case of NM7Q, even for these three months NSE and KGE have values above 0.678. The index of agreement is above 0.89 for all the months.

- At seasonal time scale (Figure 49, Table 11 and Table 12), for ***Neu Darchau*** station, **the season with the highest predictive skill are winter (DJF) and spring (MAM)** (NSE = 0.87/0.86, d = 0.96/0.96 and KGE = 0.91/0.90), while the season with the lowest predictive skill is summer (JJA) (NSE = 0.69, d = 0.90 and KGE = 0.76). Nevertheless, the differences between the predictive skills at seasonal time scale are relatively small as in the case of Kaub station.

- Overall, the predictive skill at ***Neu Darchau*** station is also very good, with small exceptions in summer months for MQ like in the case of Kaub station. The same issues (convective precipitation and/or higher variability of the summer mean streamflow) could be the cause for the smaller predictive skill during the summer months. Moreover, NM7Q has an overall better forecast skill when compared with MQ, at monthly time scale.

Evaluation of the statistical model at Hofkirchen station (Danube):

- For all the months/seasons and variables (NM7Q and MQ), the Nash-Sutcliffe efficiency (NSE), the index of agreement (d) and the Kling-Gupta efficiency (KGE), at Hofkirchen station, were skillful (i.e. above zero) with a maximum value of 0.87 for NSE, 0.90 for KGE and a maximum value of 0.96 for the index of agreement for August NM7Q. Moreover, the percentage of "hits" for August NM7Q (when the observed streamflow falls in the limits of the predicted streamflow) reached 84% (Table 13, Figure 50).

- For **NM7Q** (Figure 51, Table 13 and Table 14), at ***Hofkirchen*** station, the **months with the highest predictive skill**, based on the percentage of hits/miss, NSE, d and KGE, are: **January, May, June August and November**. The **months with the lowest predictive** skill are: **March and July**. The index of agreement is above 0.85 for all the analyzed months.

- For **MQ** (Figure 52, Table 15 and Table 16), at ***Hofkirchen*** station, the **months with the highest predictive skill**, based on the percentage of hits/miss, NSE, d and KGE, are: **March, April, October and November**. For these months NSE and KGE have values above 0.84 and the index of agreement is above 0.94. The **months with the lowest predictive** skill are: **February, June and July**. As in the case of NM7Q, even for these three months NSE and KGE have values above 0.63. The index of agreement is above 0.87 for all the months.
- At seasonal time scale (Figure 53, Table 17 and Table 18), for ***Hofkirchen*** station, **the season with the highest predictive skill is spring (MAM)** (NSE = 0.80, d = 0.94 and KGE = 0.85), while **the season with the lowest predictive skill is autumn (SON)** (NSE = 0.64, d = 0.88 and KGE = 0.73). Nevertheless, the differences between the predictive skills at seasonal time scale are relatively small as in the case of Kaub and Neu Darchau stations.

- Overall, the predictive skill at ***Hofkirchen*** station is also very good, with small exceptions in summer months for MQ like in the case of Kaub and Neu Darchau stations. The same issues (convective precipitation and/or higher variability of the summer mean streamflow) could be the cause for the smaller predictive skill during the summer months. Moreover, NM7Q has an overall better forecast skill when compared with MQ, at monthly time scale, a feature that is found for all the analyzed stations.

The main conclusion of this report can be summarized as follows:

- The role of the climatic and oceanic factors played in forecasting the monthly/seasonal streamflow is very significant.
- The climatic/oceanic predictors differ from one month to another and from one station to another.
- The lagged relationship between the monthly/seasonal streamflow and the climatic/oceanic variables varied from 6 months (SST, Air temperature) up to 1 month (local precipitation and temperature, soil moisture).
- The persistence plays also an important role in the skill of the forecast.
- The most reliable predictors are: sea surface temperature, sea level pressure, geopotential height at 700-mb, air temperature, precipitation, soil moisture, zonal and meridional wind at 700-mb.
- The forecast performances of the stability maps and the multiple linear regression models for forecasting the monthly and seasonal streamflow over Germany, as represented by three major rivers (Rhine, Elbe and Danube) by using hydrologic (persistence), atmospheric and oceanic predictors are very good.
- The study reported herein concentrated on forecasting at monthly and seasonal time scales. It may be worth expanding the initial efforts to forecast at longer time scales such as half-yearly and yearly.
- The forecast skill for Kaub station and Neu Darchau station is very good, especially for NM7Q. The overall forecast skill for Hofkirchen station is weaker both at monthly as well as seasonal time scales, when compared to then one for Kaub and Neu Darchau.
- **The forecast skill for NM7Q is, in general, higher when compared to MQ for all analyzed stations and this aspect should be taken into account especially when forecast products are issued for inland waterway transport.**
- There is no real predictive skill for the monthly precipitation totals and mean temperature, aggregated over each of the catchment area**.**
- Due to the existences of dams and human influence, the predictive skill for the Weser river is reduced or not valid from a statistical point of view.

Possible improvements:

- Include observed/measured soil moisture data (if available).
- Include snow cover and sea ice extent (when and where available) to improve the potential predictability, especially for the winter and spring months.
- Apply the same methodology to test the potential predictability of meteorological and hydrological drought related indices [e.g. Standardized Precipitation Index (SPI), Standardized Precipitation Evapotranspiration Index (SPEI), and Standardized Streamflow Index (SSI)].
- Test the methodology for seasonal/annual streamflow minima and for smaller catchments areas.

7. REFERENCES

Alfieri, L., Burek, P., Dutra, E., Krzeminski, B., Muraro, D., Thielen, J., and Pappenberger, F. (2013), GloFAS – global ensemble streamflow forecasting and flood early warning, Hydrol. *Earth Syst. Sci.,* 17, 1161-1175, doi:10.5194/hess-17-1161-2013.

Arnell, N.W., Krasovskaia, I., and Gottschalk, L. (1993), River flow regimes in Europe. In: *Flow Regimes from International Experimental and Network Data (FRIEND), vol. 1. Hydrological Studies*, Gustard A (ed.). Institute of Hydrology: Wallingford, Oxfordshire, UK, 112-121.

Barnston, A. G., and R. E. Livezey, 1987: Classification, seasonality and persistence of low-frequency atmospheric circulation patterns. *Mon. Wea. Rev.*, **115**, 1083-1126.

Barnston, A.G., C. F. Ropelewski, 1992: Prediction of ENSO episodes using canonical correlation analysis. J. Climate, 5, 1316-1345.

Barnston, A.G., M. Chelliah and S.B. Goldenberg, 1997: Documentation of a highly ENSO-related SST region in the equatorial Pacific. Atmosphere-Ocean, 35, 367-383.

Berg, A.A. and Mulroy, K.A. (2006), Streamflow predictability in the Saskatchewan/Nelson River basin given macroscale estimates of the initial soil moisture status. *Hydrol. Sci. 51*, 642–654.

Branković, C., Palmer, T.N., and Ferranti, L. (1994), Predictability of seasonal atmospheric variation. *J. Climate,* 7, 217–237.

Brilly M. (2010), Hydrological Processes of the Danube River Basin. Springer: New York.

Candogan-Yossef, N., Winsemius, H., Weerts, A., van Beek R., and Bierkens, M.F.P. (2013), Skill of a global seasonal streamflow forecasting system, relative roles of initial conditions and meteorological forcing. *Water Resources Research 49*, doi:10.1002/wrcr.20350.

Colman, A. (1997), Prediction of summer Central England Temperature from preceding North Atlantic winter sea surface temperature. *Intl. J. Climatol.,* 17, 1285–1300.

Colman, A. and Davey, M. (1999) Prediction of summer temperature, precipitation and pressure in Europe from preceding winter North Atlantic Ocean temperature. *Intl. J. Climatol.*, 19, 513–536.

Croley, T.E. II. (2003), Great Lakes climate change hydrologic impact assessment I.J.C. Lake Ontario-St. Lawrence River Regulation Study. NOAA Technical Memorandum GLERL, 126, 77 pp.

Cullen, H.M., Kaplan, A., Arkin, P., and DeMenocal, P.B. (2002), Impact of the North Atlantic Oscillation on Middle Eastern climate and streamflow. *Clim. Change*, 55, 315–338.

Dettinger, M.D. and Diaz, H.F. 2000. Global characteristics of streamflow seasonality. *J. Hydrometeor., 1, 289–310.*

Dirmeyer, P.A. and Brubaker, K.L. (1999), Contrasting evaporative moisture sources during the drought of 1988 and the flood of 1993*, J. Geophys. Res.,* 104*(*D16*),* 19383–19397.

Gámiz-Fortis, S.R., Esteban-Parra, M.J., Trigo, R.M., and Castro-Díez, Y. (2010), Potential predictability of an Iberian river flow based on its relationship with previous winter global SST. *J. Hydrol*., 385, 14–149.

Grantz, K., Rajagopalan, B., Clark, M., and Zagona, E. (2005), A technique for incorporating large-scale climate information in basin-scale ensemble streamflow forecasts, *Water Resour. Res*., 41, W10410, doi:10.1029/2004WR003467.

Gupta, H.V., Kling, H.,H., Yilmaz, K.K., and Martinez, G.F. (2009), Decomposition of the mean squared error and NSE performance criteria: Implications for improving hydrological modelling. *J. Hydrol.*, 377(1-2), 80-91. doi:10.1016/j.jhydrol.2009.08.003.

Havinga, H. and Smits, A.J.M. (2000), River management along the Rhine: a retrospective view. In: Smits, A.J.M., Nienhuis, P.H., Leuven, R.S.E.W. (eds). *New Approaches to River Management*, Backhuys Publisher, Leiden, pp. 15–32.

Haylock, M.R., Hofstra, N., Klein Tank, A.M.G., Klok, E.J., Jones, P.D., and New, M.A. (2008), European daily high-resolution gridded dataset of surface temperature and precipitation. *J. Geophys. Res*. (Atmospheres), 113, D20119.

Ionita, M., Lohmann, G., and Rimbu, N. (2008), Prediction of Elbe discharge based on stable teleconnections with winter global temperature and precipitation. *J. Climate*, 21, 6215-6226.

Ionita, M., Dima, M., Lohmann, G., Scholz, P., and Rimbu, N. (2014), Predicting the June 2013 European Flooding based on Precipitation, Soil Moisture and Sea Level Pressure. *J. Hydrometeorology*, in press, doi: http://dx.doi.org/10.1175/JHM-D-14-0156.1.

Ionita, M., Lohmann, G., Rimbu, N., Chelcea, S.: Interannual Variability of Rhine River Streamflow and Its Relationship with Large-Scale Anomaly Patterns in Spring and Autumn. J. Hydrometeorol. 13, 172–188, 2012.

Ionita, M., Boroneant, C., and Chelcea, S.: Seasonal modes of dryness and wetness variability over Europe and their connections with large scale atmospheric circulation and global sea surface temperature. Climate Dynamics, online first, DOI: 10.1007/s00382-015-2508-2, 2015.

Ionita, M., Lohmann, G., Rimbu, N., Chelcea, S., and Dima. M.: Interannual to decadal summer drought variability over Europe and its relationship to global sea surface temperature. Climate Dynamics, 38: 363-377. DOI: 10.1007/s00382-011-1028-y, 2011.

Kalnay et al. (1996), The NCEP/NCAR 40-year reanalysis project, *Bull. Amer. Meteor. Soc*., 77, 437-470.

Kiladis, G.N. and Diaz, H.F. (1989), Global climatic anomalies associated with extremes in the Southern Oscillation. *J. Climate,* 2, 1069–1090.

Kistler, R. et al. (2001), The NCEP–NCAR 50–Year Reanalysis: Monthly Means CD–ROM and Documentation. *Bull. Amer. Meteor. Soc*., 82, 247–267.

Kitanidis, P.K. and Bras, R.L. (1980), Real-time forecasting with a conceptual hydrologic model. 2. Applications and results. *Water Resources Research*, 16(6), 1034-1044.

Koster, R.D., Mahanama, S.P.P., Livneh, B., Lettenmaier, D.P., and Reichle, R.H. (2010), Skill in streamflow forecasts derived from large-scale estimates of soil moisture and snow. Nature Geoscience, 3, 613-616.

Legates, D.R. and McCabe Jr., G.J. (1999), Evaluating the use of "goodness-of-fit" measures in hydrologic and hydroclimatic model validation, *Water Resour. Res*., 35, 1, 233–241.

Lloyd-Hughes, B. and Saunders, M.A. (2002), Seasonal prediction of European spring precipitation from ENSO and local sea surface temperatures. *Intl. J. Climatol*., 22, 1–14.

Lohmann, G., Rimbu, N., and Dima, M. (2005), Where can the Arctic Oscillation be reconstructed? Towards a reconstruction of climate modes based on stable teleconnections. *Clim. Past Disc*., 1, 17–56.

McCabe, G.J. and Dettinger, M.D. (2002), Primary modes and predictability of year-to-year snowpack variation in the Western United States from teleconnections with Pacific Ocean Climate. *J. Hydrometeor.*, 3, 13-25.

Meißner, D., Klein, B., and Ionita, M. (2017), Development of a monthly to seasonal forecast framework tailored to inland waterway transport in Central Europe, *Hydrol. Earth Syst. Sci. Discuss*., 2017, 1-31, doi:10.5194/hess-2017-293.

Moriasi, D. N. et al. (2007), Model Evaluation Guidelines for Systematic Quantification of Accuracy in Watershed Simulations. *Transactions of the ASABE*, 50(3), 885-900.

Nash, J. E. and Sutcliffe, J. V. (1970), River flow forecasting through conceptual models, Part I - A discussion of principles, *J. Hydrol.*, 10, 282–290.

Pinter, N., Van der Ploeg, R.R., Schweigert, P., and Hoefer, G. (2006), Flood magnification on the River Rhine. Hydrological Processes 20, 147–164.

Reichle, R.H., Koster, R.D., De Lannoy, G.J.M., Forman, B.A., Liu, Q., Mahanama, S., and Toure, A. (2011), Assessment and Enhancement of MERRA Land Surface Hydrology Estimates**.** *J. Climate*, 24, 6322-6338, doi:http://dx.doi.org/10.1175/JCLI-D-10-05033.1.

Rimbu, N., Dima, M., Lohmann, G., and Stefan, S. (2004), Impacts on the North Atlantic Oscillation and the El Niño-Southern Oscillation on Danube river flow variability. *Geophys. Res. Lett.*, 31, L23203, doi:10.1029/2004GL020559.

Rimbu, N., Dima, M., Lohmann, G., and Musat, I. (2005), Seasonal prediction of Danube flow variability based on stable teleconnection with sea surface temperature. *Geophys. Res. Lett.*, 32, L21704, doi:10.1029/2005GL024241.

Smith, T.M., Reynolds, R.W., Peterson, T.C., and Lawrimore, J. (2008), Improvements NOAAs Historical Merged Land–Ocean Temp Analysis (1880–2006). *Journal of Climate*, 21, 2283–2296.

Souza, F. and Lall, U. (2003), Seasonal to interannual ensemble streamflow forecasts for Ceara, Brazil: applications of a multivariate, semiparametric algorithm. *Water Resour. Res.,* 39, 1–13.

Trigo, R.M., Pozo-Vázquez, D., Osborn, T.J., Castro-Diez, Y., Gamiz-Fortis, S., and Esteban-Parra, M.J. (2004), North Atlantic Oscillation influence on precipitation, river flow and water resources in the Iberian Peninsula. *Int. J. Climatol*., 24, 925–944.

Van Oldenborgh, G.J., Burgers, G., and Klein Tank, A. (2000), On the El Niño teleconnection to spring precipitation in Europe. *Int. J. Climatol*., 20, 565–574.

Vinnikov, K. Y. and Yeserkepova, I. B. (1991), Soil moisture—empirical data and model results. *J. Climate* 4, 66–79.

Werner, M., Schellekens, J., Gijsbers, P., van Dijk, M., van den Akker, O., and Heynert, K. (2013), The Delft-FEWS flow forecasting system. *Environmental Modelling & Software*, 40, 65-77.

Wilby, R.L. (2001). Downscaling summer rainfall in the UK from North Atlantic Ocean temperatures. *Hydrology and Earth Systems Sciences,* 5, 245–257.

Willmot, C. J. (1981), On the validation of models, *Physical Geography*, 2,184–194.

Wood, A.W., Maurer, E.P., Kumar, A., and Lettenmaier, D.P. (2002), Long-range experimental hydrologic forecasting for the eastern United States. *Journal of Geophysical Research*, 107, (D20), 4429, doi:10.1029/2001JD000659.

Wood, A. W., Kumar, A., and Lettenmaier, D.P. (2005), A retrospective assessment of National Centers for Environmental Prediction climate model-based ensemble hydrologic forecasting in the western United States. *Journal of Geophysical Research*, 110, D04105, doi:10.1029/2004JD004508.

8. Acknowledgements

Part of this work has been conducted within the Helmholtz Portfolio Initiative „Earth System Knowledge Platform“ (ESKP). The financial support by the ESKP@AWI strategy is gratefully acknowledged.

9. Appendix 1

Abbreviations list

NAO = North Atlantic Oscillation

ENSO = El Niño – Southern Oscillation

NCEP = National Center for Environmental Prediction

NCAR = National Center for Atmospheric Research

VIC = Variable Infiltration Capacity Macroscale Hydrologic Model

DWD = Deutscher Wetterdienst

SLP = Sea Level Pressure

Z700 = Geopotential Height at 700-mb level

U700 = Zonal wind at 700-mb level

V700 = Meridional wind at 700-mb level

SOIL10 = Soil Moisture in the upper 10cm

TEMP10 = Ground Temperature in the upper 10cm

AIRTT = Air Temperature from NCEP data

TT = Air Temperature from DWD data

PP = Precipitation from DWD data

SOILW = Volumetric Soil Moisture

SST = Sea Surface Temperature

bad = Baden-Württemberg

bay = Bayern

ber = Berlin

brand = Brandenburg

ger = Germany

hes = Hessen

meck = Mecklenburg-Vorpommern

nds = Niedersachsen

rhein = Rheinland-Pfalz

saar = Saarland

sach = Sachsen

thur = Thüringen

schw = Schleswig-Holstein

ndh = Nordhein-Westfalen

10. Appendix 2

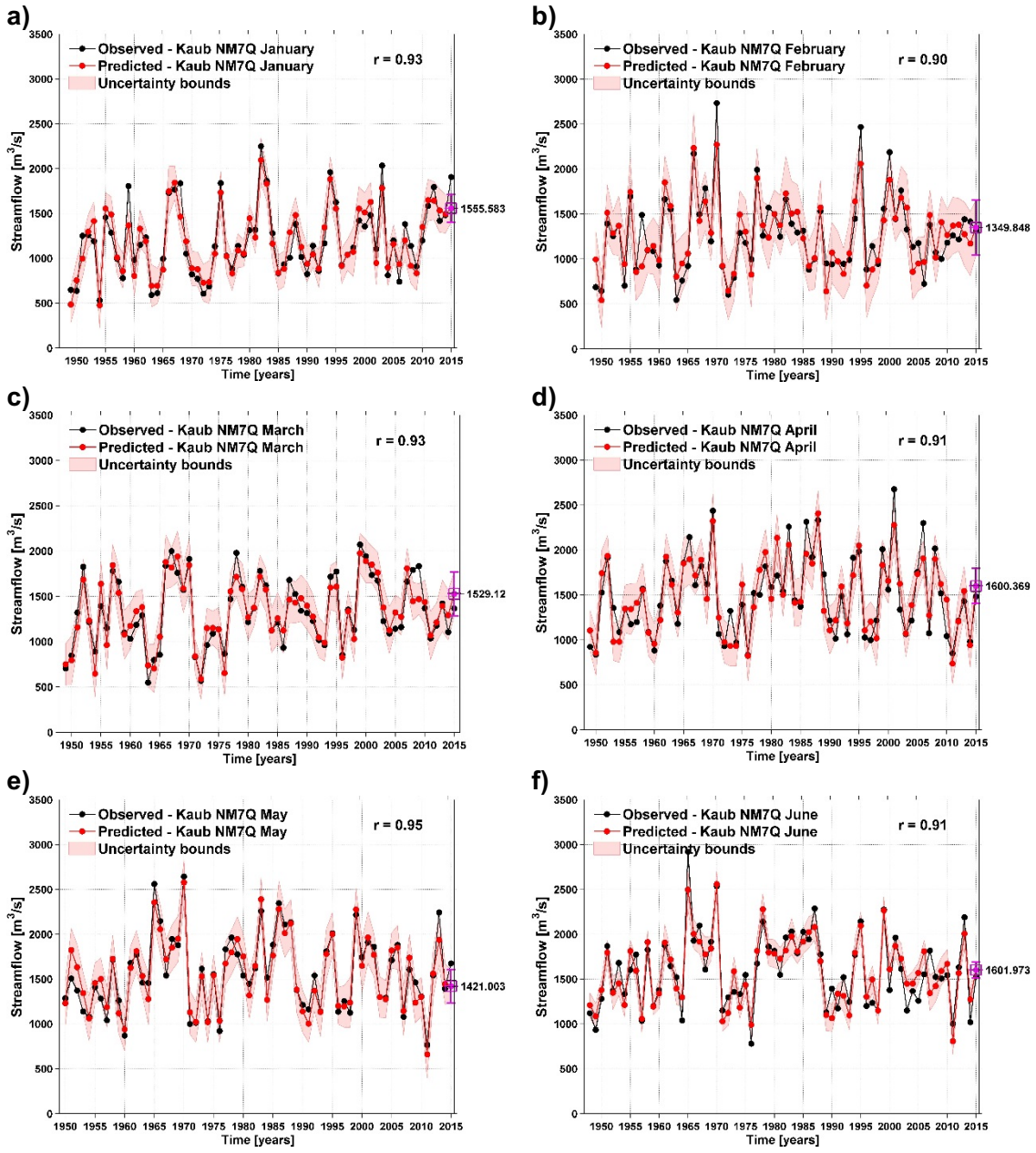

Fig. 44a: *Comparison between the observed and predicted monthly (January – June) NM7Q at Kaub station: Observed (black) and Predicted (red) values for the period 1948-2015. The light red shaded area represents the 95% uncertainty bounds.*

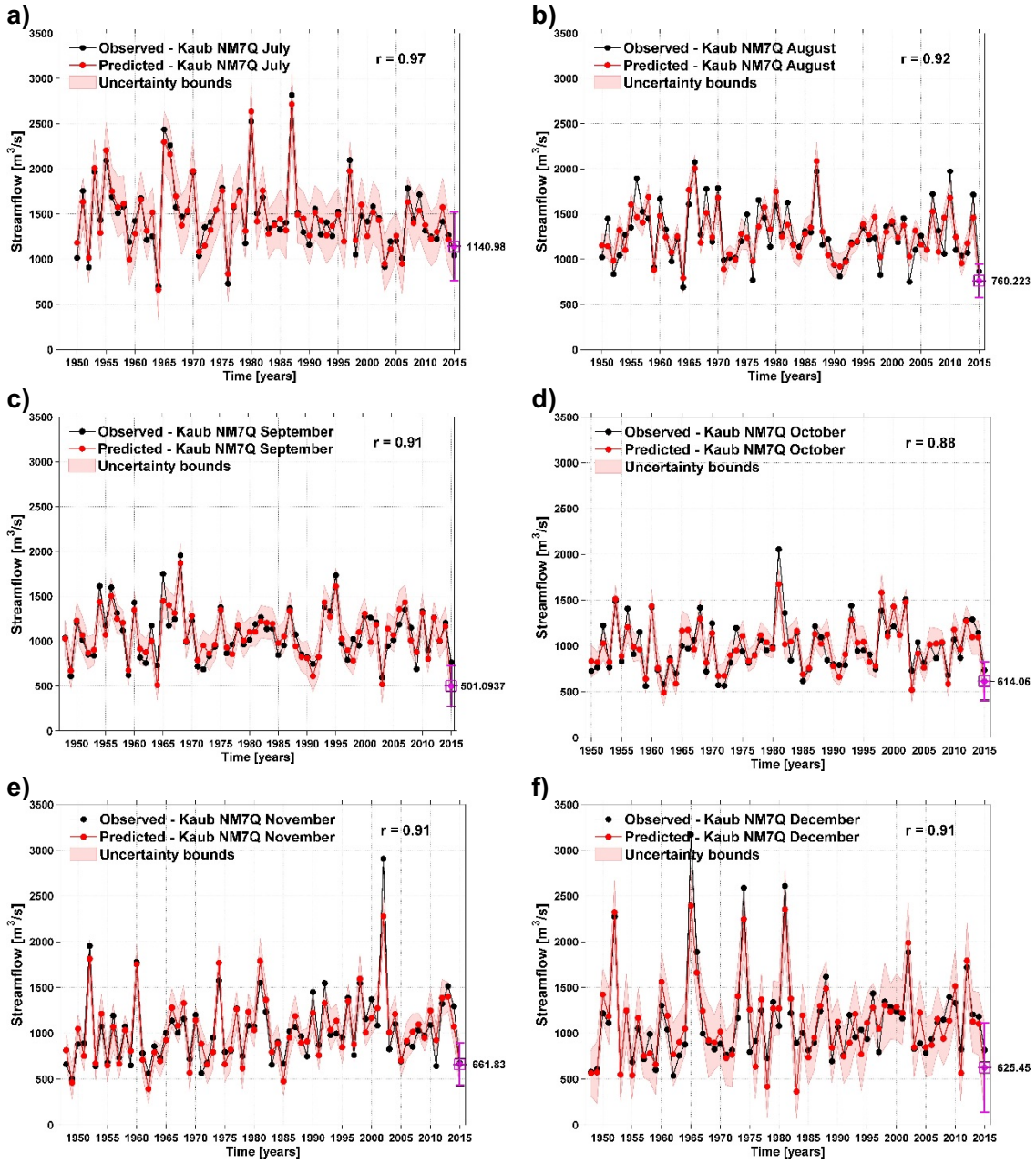

Fig. 44b: *Comparison between the observed and predicted monthly (July – December) NM7Q at Kaub station: Observed (black) and Predicted (red) values for the period 1948-2015. The light red shaded area represents the 95% uncertainty bounds.*

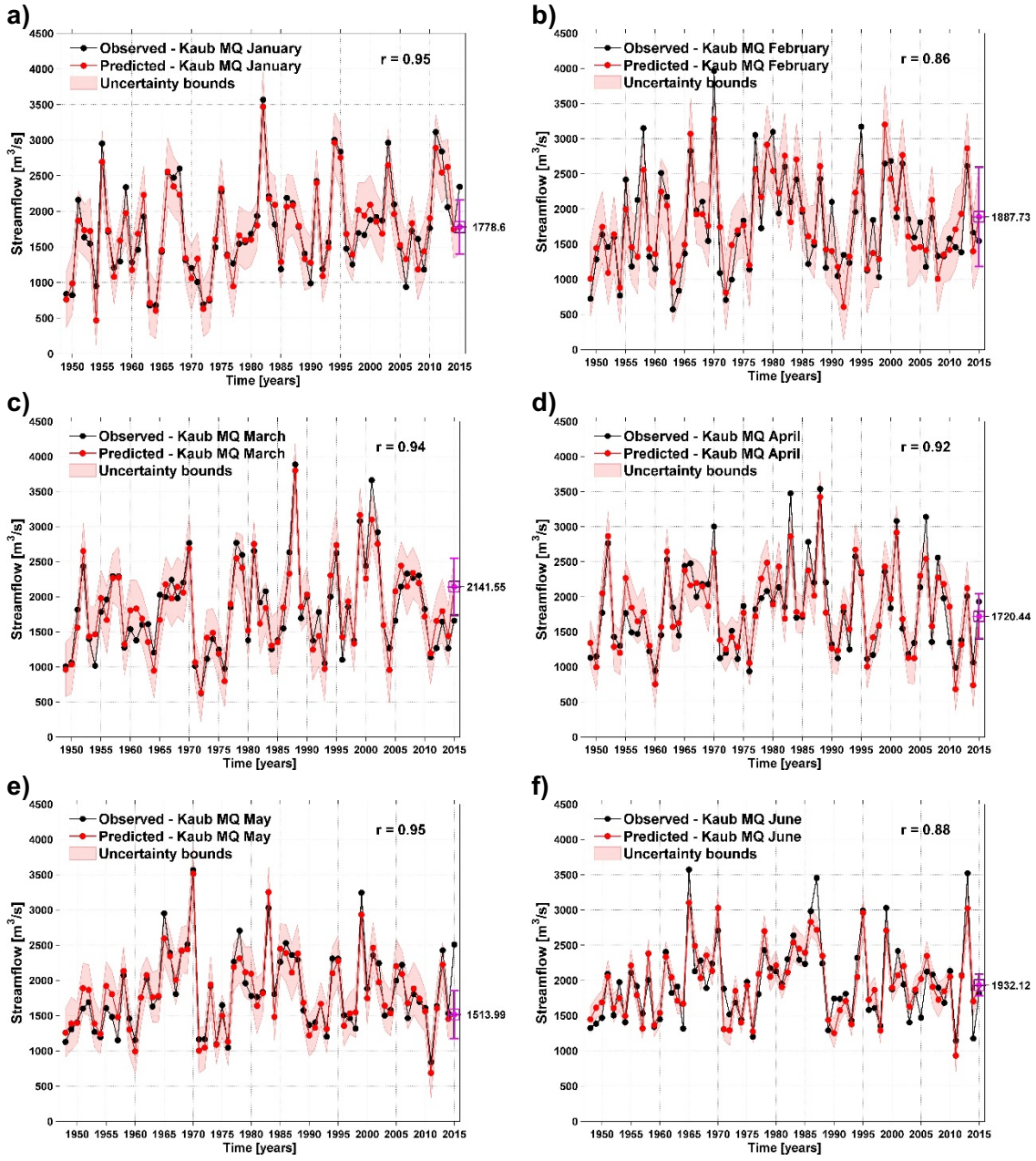

Fig. 45a: *Comparison between the observed and predicted monthly (January – June) MQ at Kaub station: Observed (black) and Predicted (red) values for the period 1948-2015. The light red shaded area represents the 95% uncertainty bounds.*

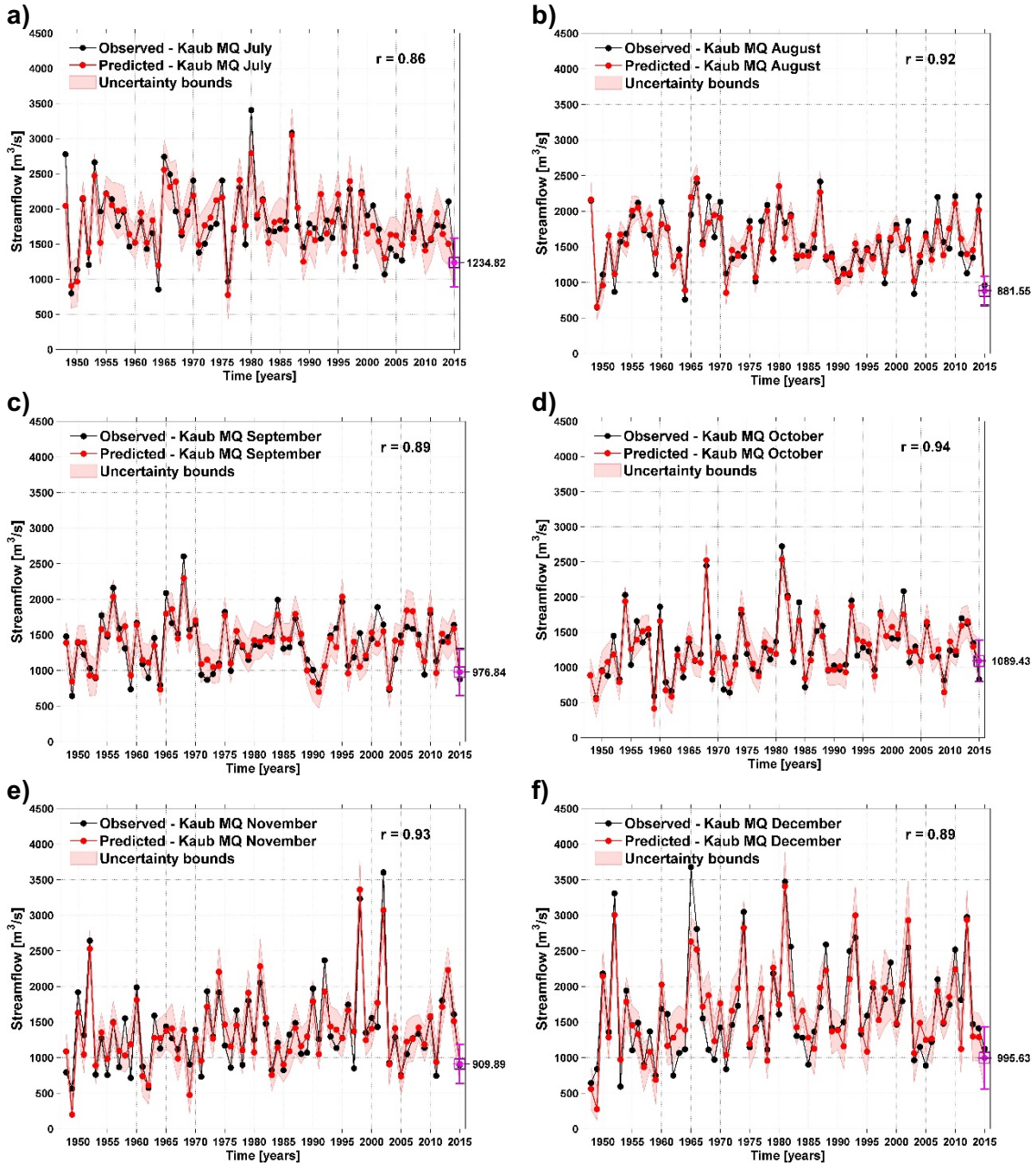

Fig. 45b: *Comparison between the observed and predicted monthly (July – December) MQ at Kaub station: Observed (black) and Predicted (red) values for the period 1948-2015. The light red shaded area represents the 95% uncertainty bounds.*

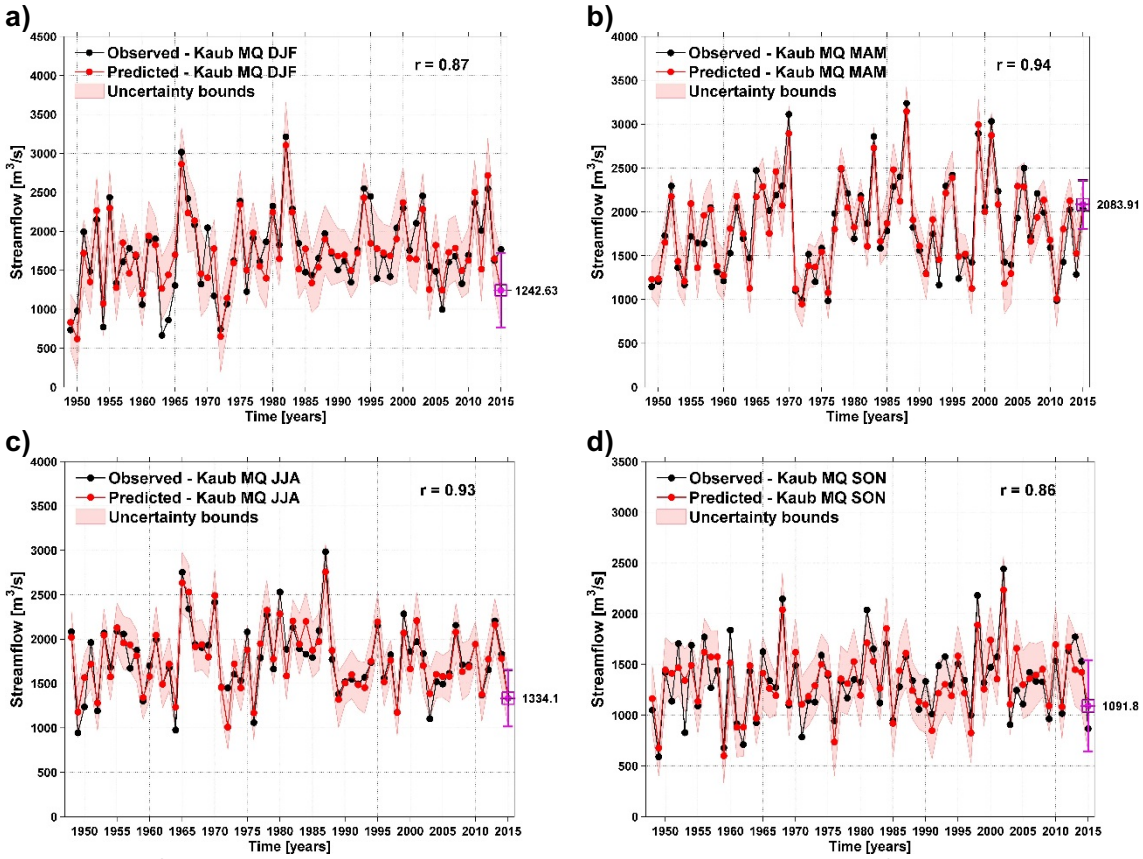

Fig. 46: *Comparison between the observed and predicted seasonal MQ at Kaub station: Observed (black) and Predicted (red) values for the period 1948-2015. The light red shaded area represents the 95% uncertainty bounds.*

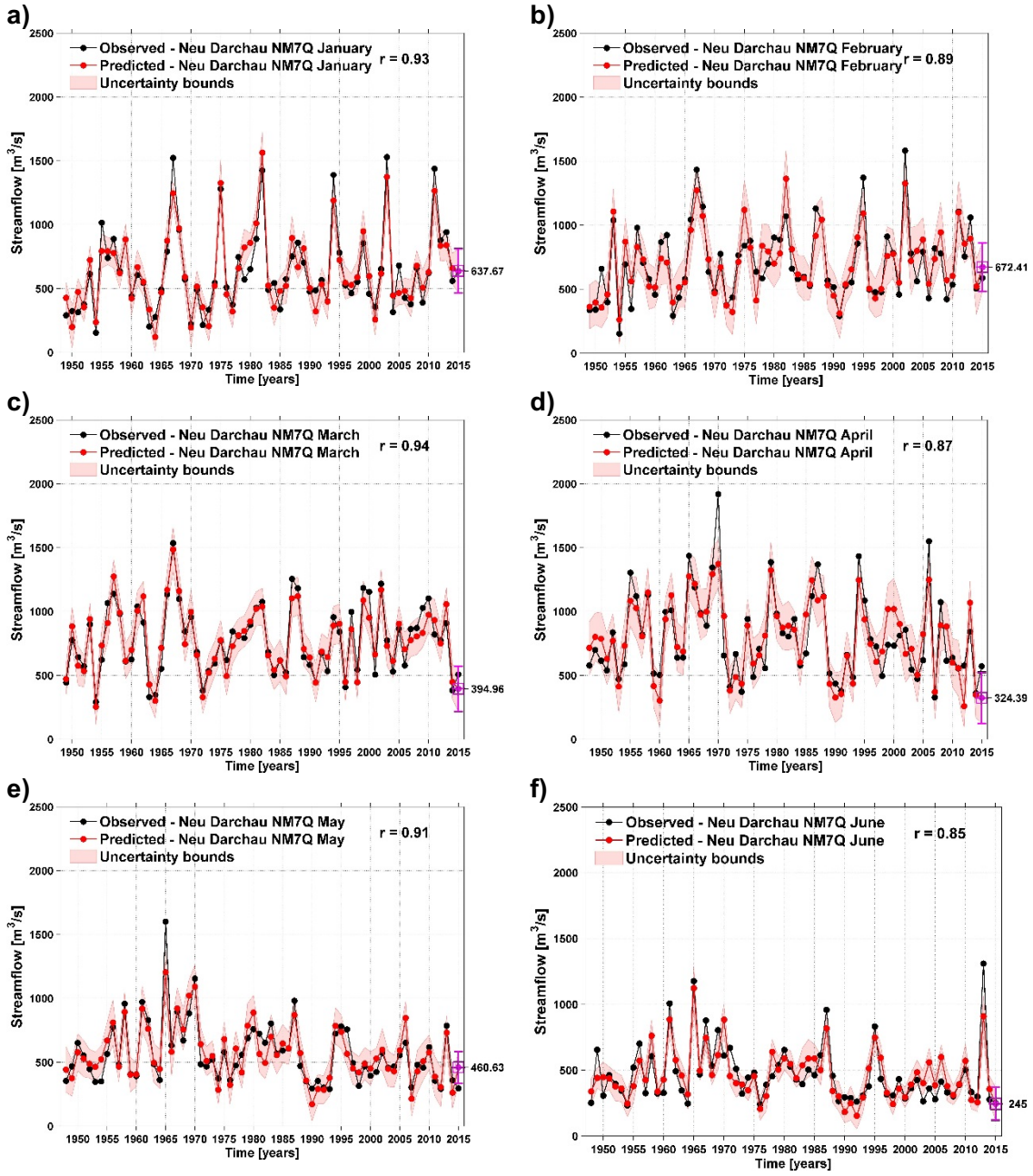

Fig. 47a: *Comparison between the observed and predicted monthly (January – June) NM7Q at Neu Darchau station: Observed (black) and Predicted (red) values for the period 1948-2015. The light red shaded area represents the 95% uncertainty bounds.*

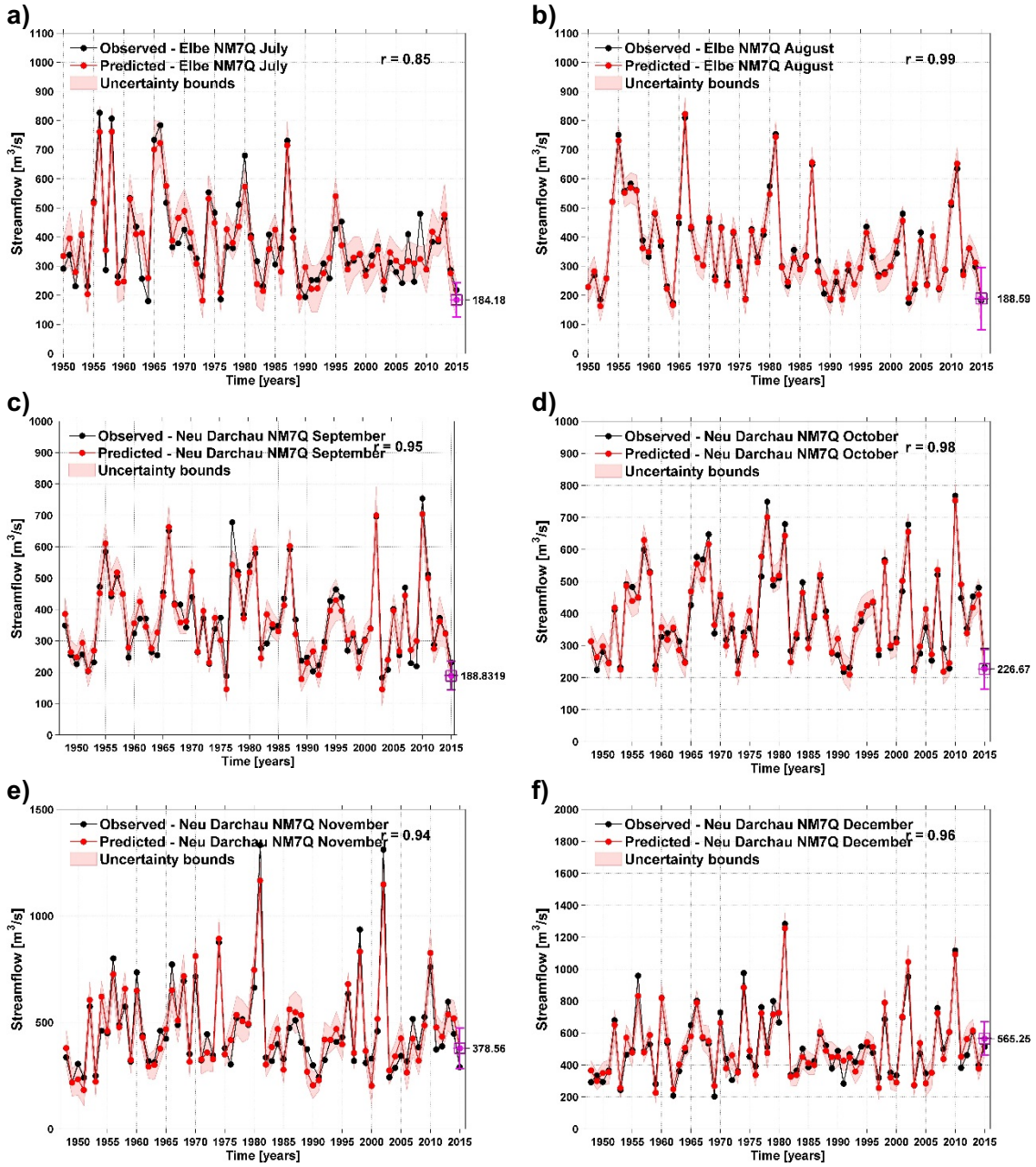

Fig. 47b: *Comparison between the observed and predicted monthly (July – December) NM7Q at Neu Darchau station: Observed (black) and Predicted (red) values for the period 1948-2015. The light red shaded area represents the 95% uncertainty bounds.*

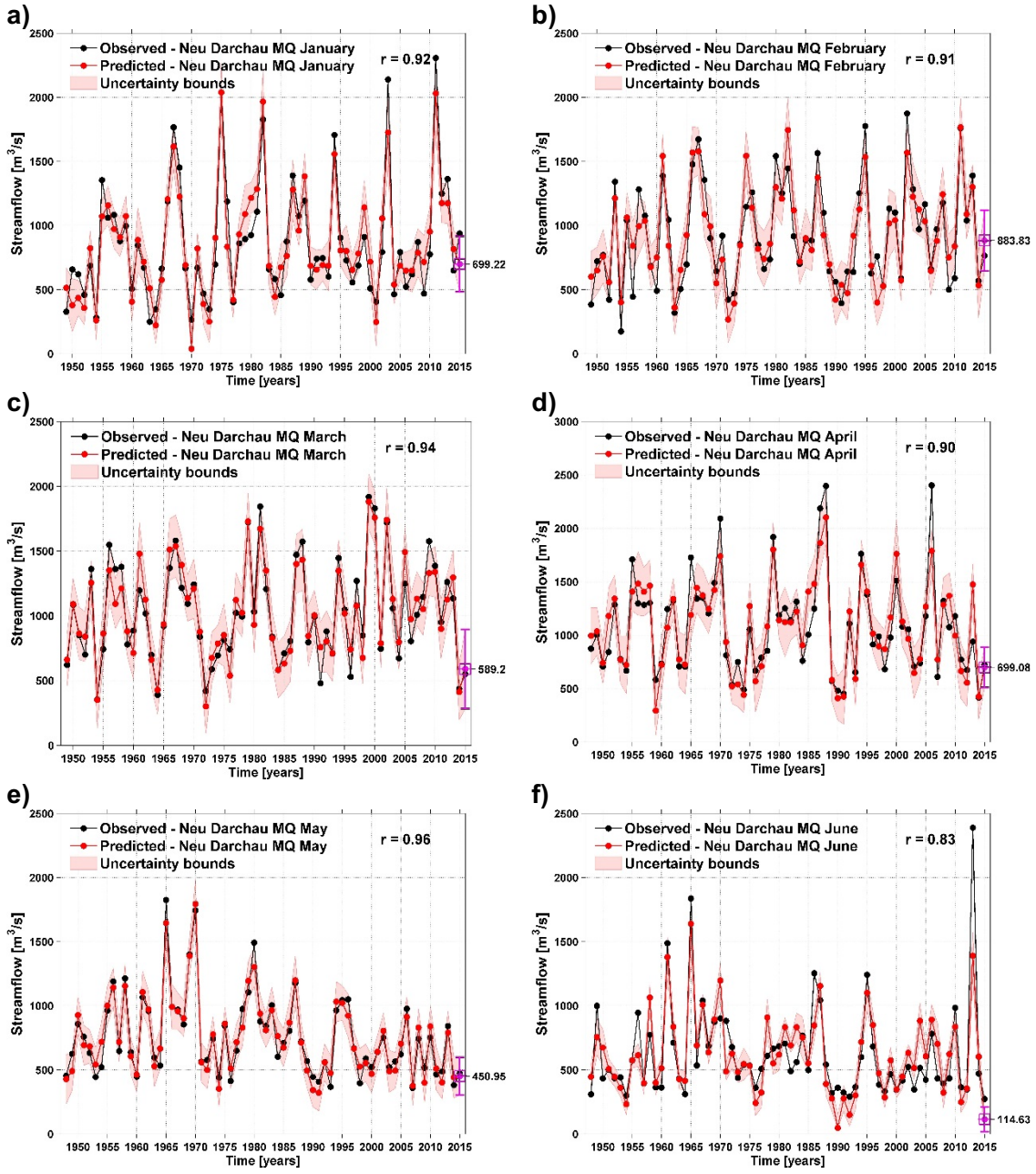

Fig. 48a: *Comparison between the observed and predicted monthly (January – June) MQ at Neu Darchau station: Observed (black) and Predicted (red) values for the period 1948-2015. The light red shaded area represents the 95% uncertainty bounds.*

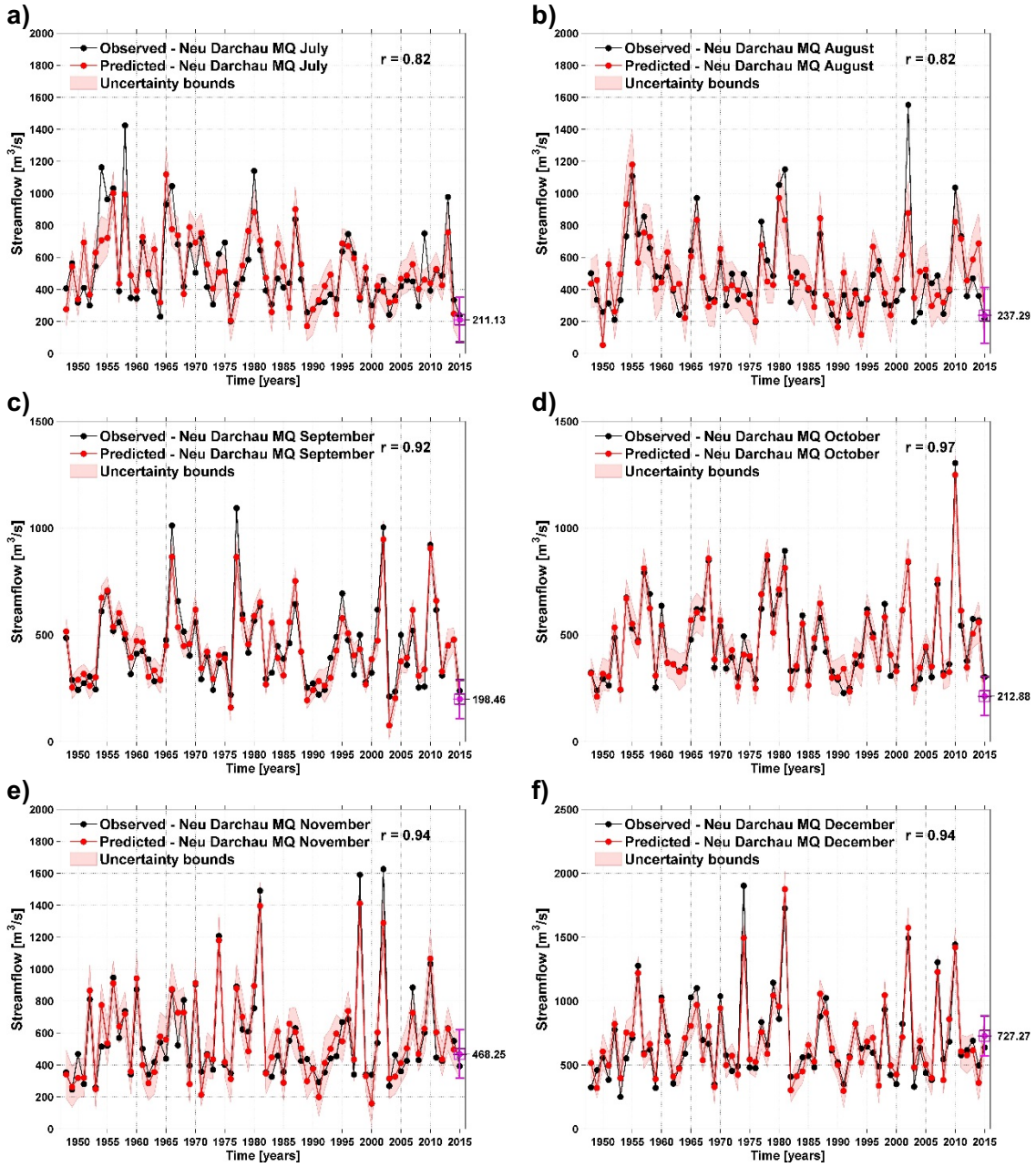

Fig. 48b: *Comparison between the observed and predicted monthly (July – December) MQ at Neu Darchau station: Observed (black) and Predicted (red) values for the period 1948-2015. The light red shaded area represents the 95% uncertainty bounds.*

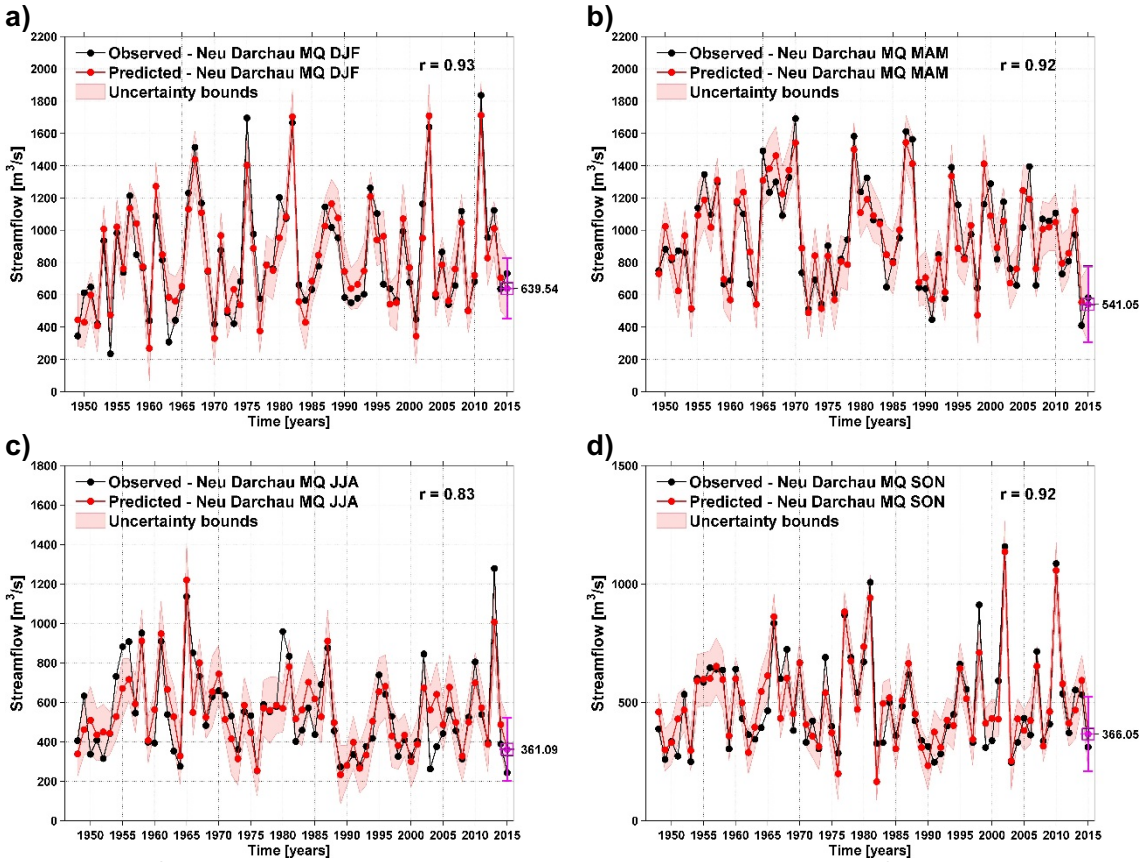

Fig. 49: *Comparison between the observed and predicted seasonal MQ at Neu Darchau station: Observed (black) and Predicted (red) values for the period 1948-2015. The light red shaded area represents the 95% uncertainty bounds.*

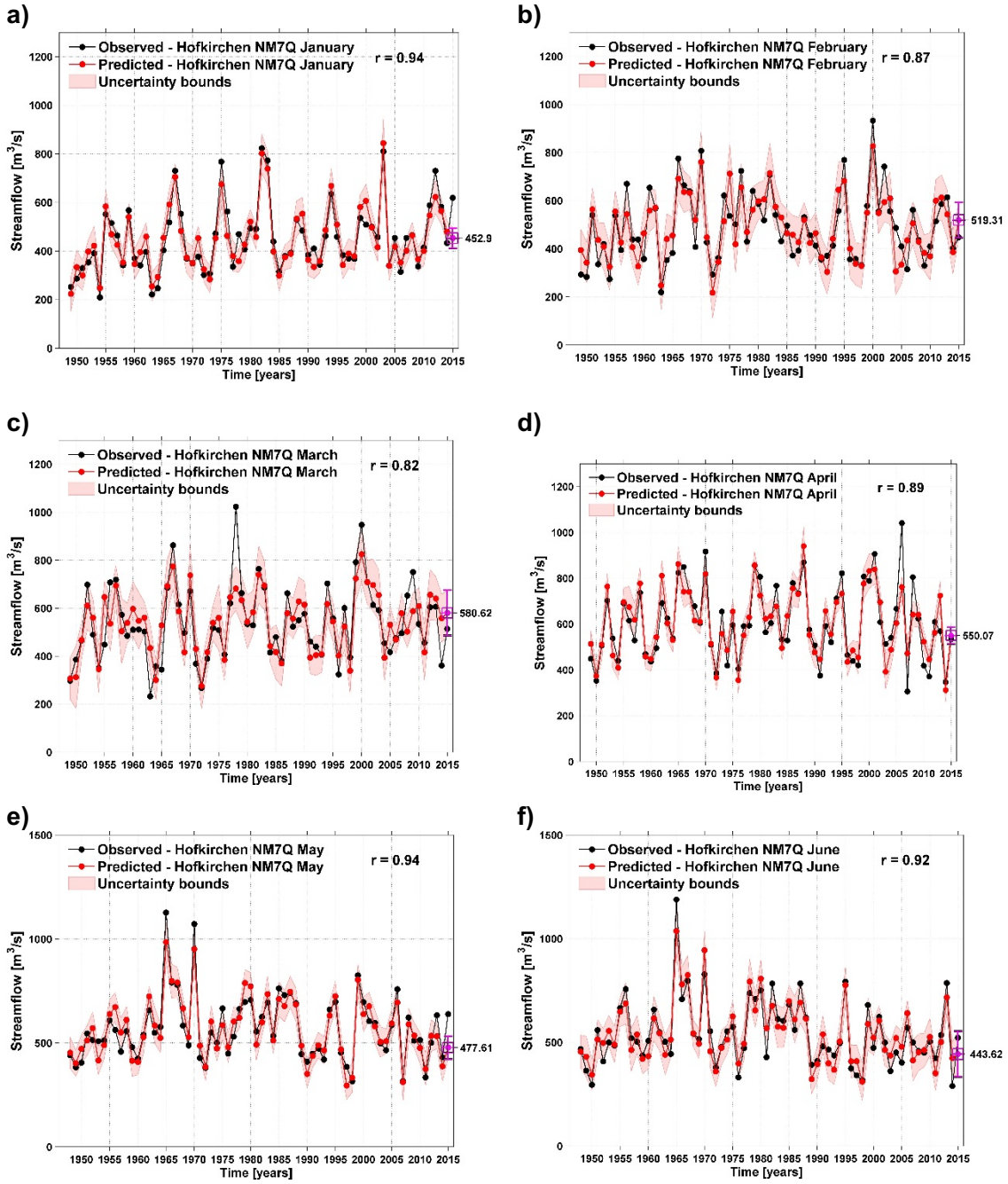

Fig. 50a: *Comparison between the observed and predicted monthly (January – June) NM7Q at Hofkirchen station: Observed (black) and Predicted (red) values for the period 1948-2015. The light red shaded area represents the 95% uncertainty bounds.*

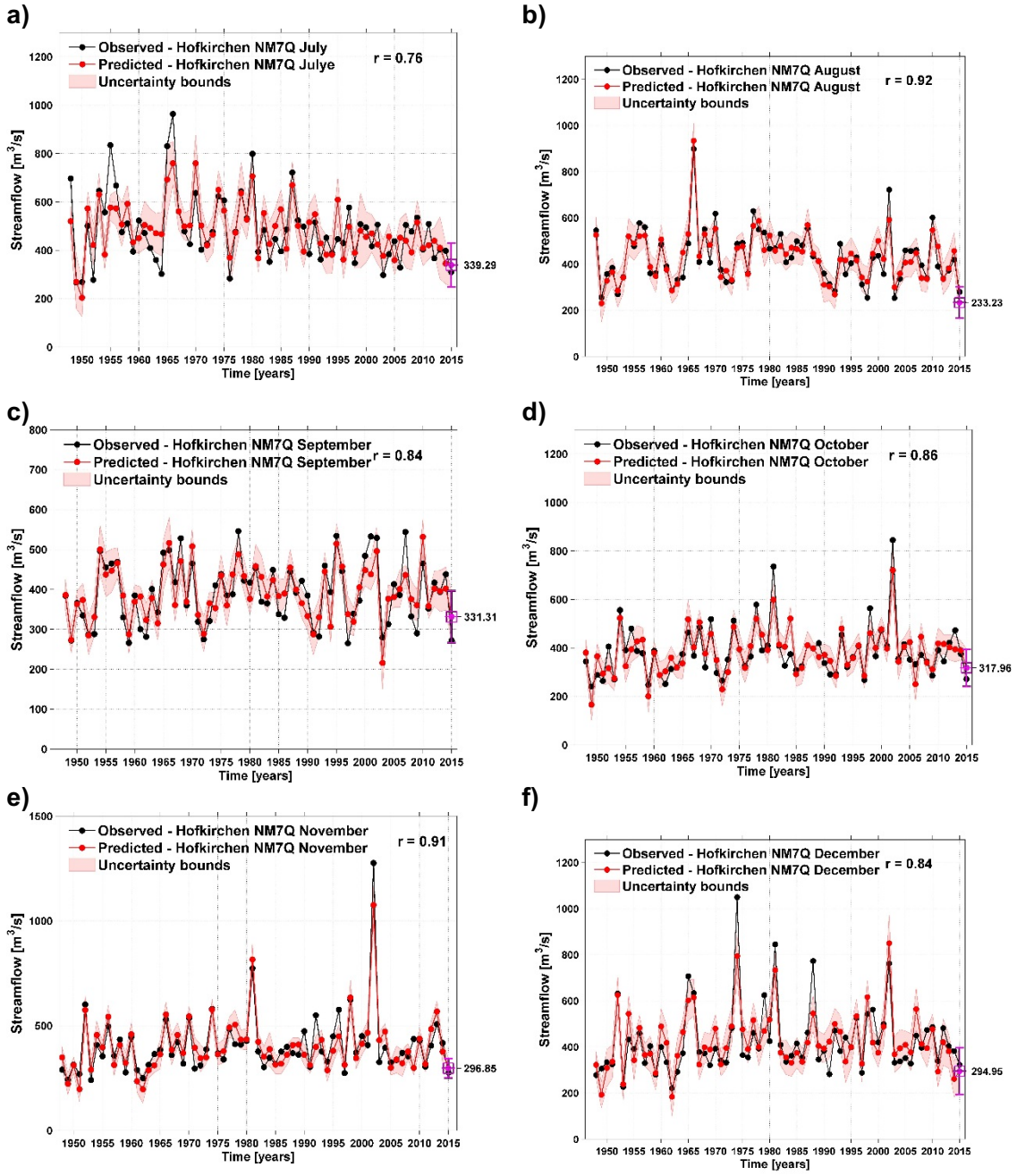

Fig. 50b: *Comparison between the observed and predicted monthly (July – December) NM7Q at Hofkirchen station: Observed (black) and Predicted (red) values for the period 1948-2015. The light red shaded area represents the 95% uncertainty bounds.*

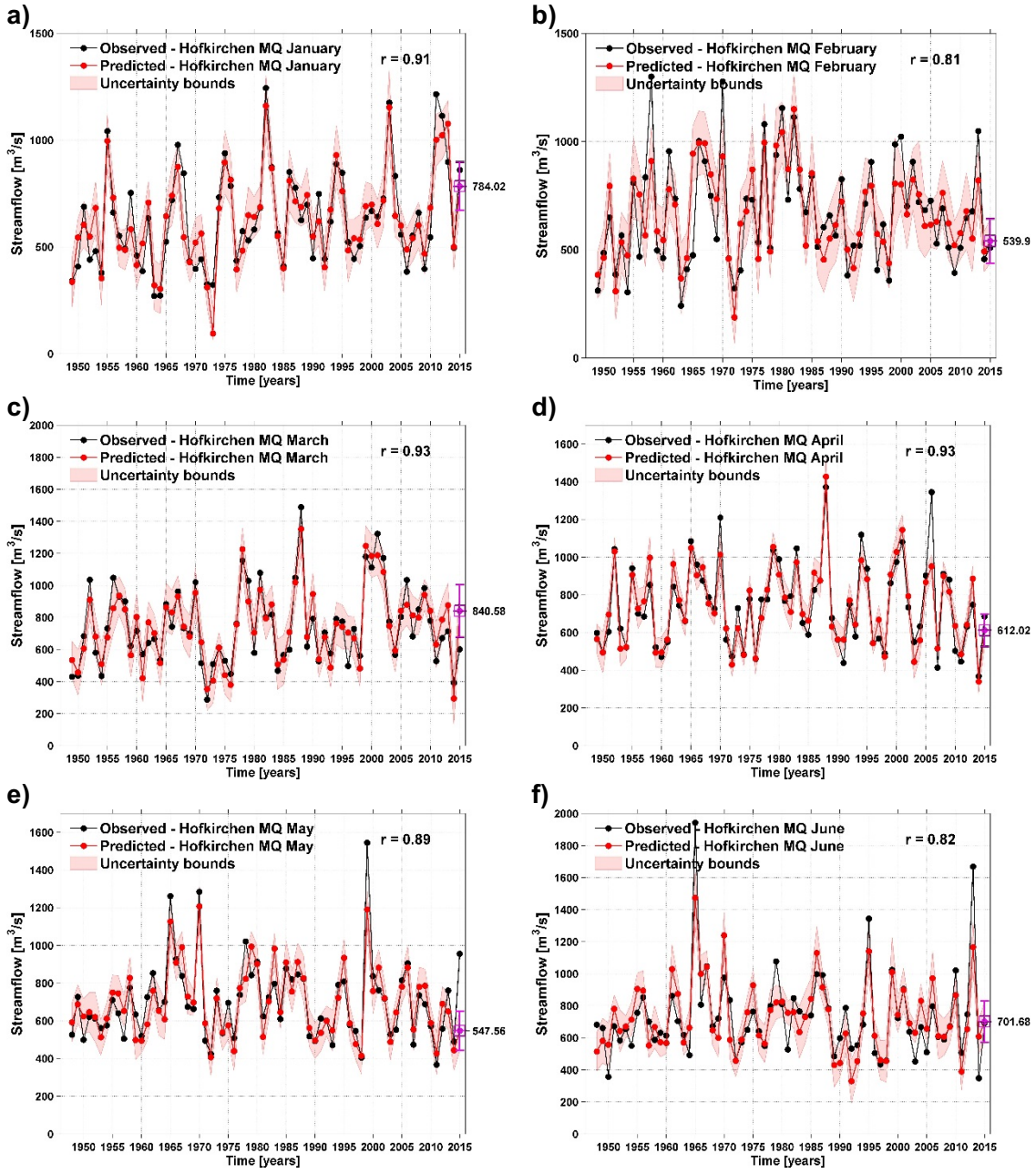

Fig. 51a: *Comparison between the observed and predicted monthly (January – June) MQ at Hofkirchen: Observed (black) and Predicted (red) values for the period 1948-2015. The light red shaded area represents the 95% uncertainty bounds.*

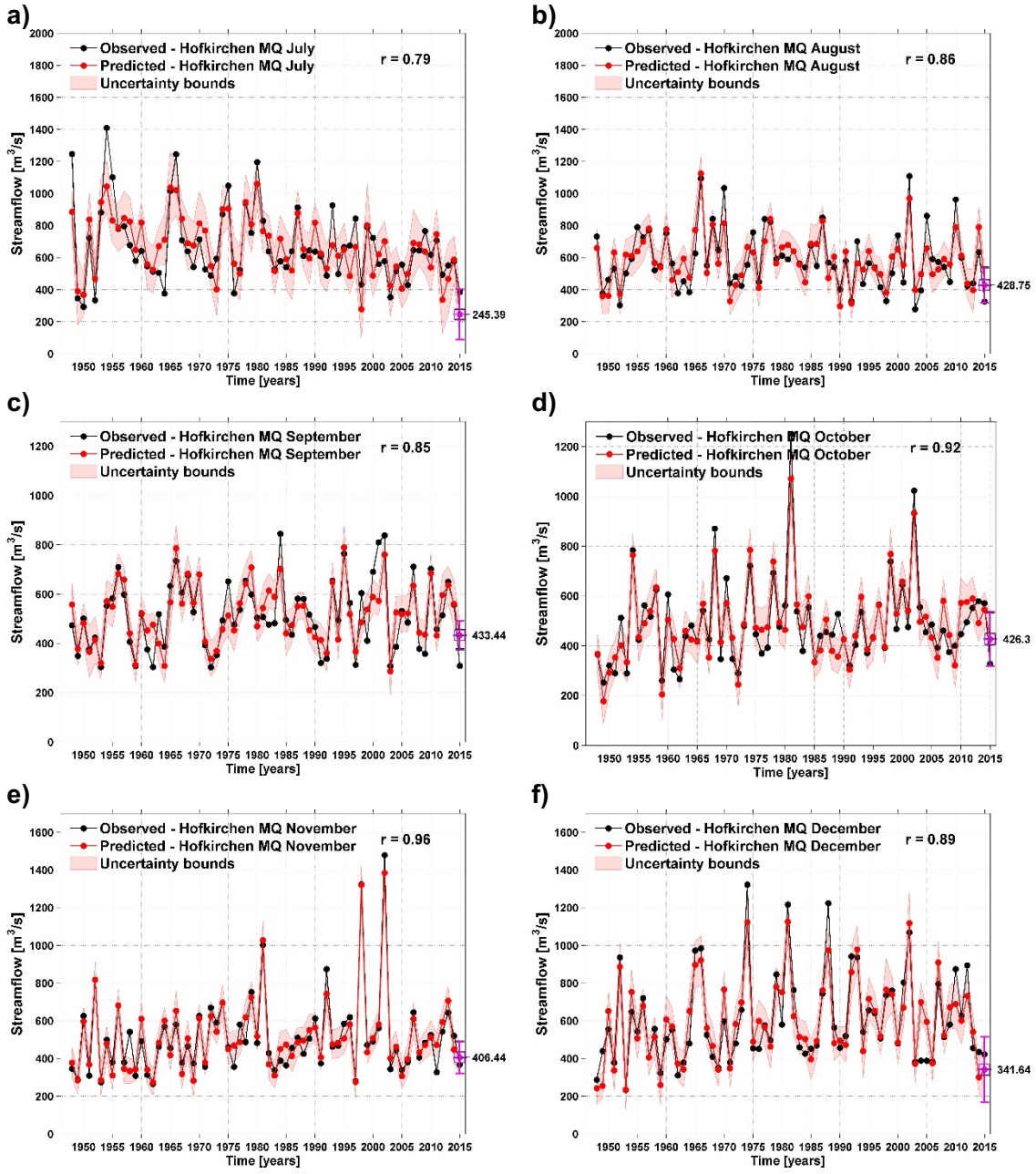

Fig. 51b: *Comparison between the observed and predicted monthly (July – December) MQ at Hofkirchen station: Observed (black) and Predicted (red) values for the period 1948-2015. The light red shaded area represents the 95% uncertainty bounds.*

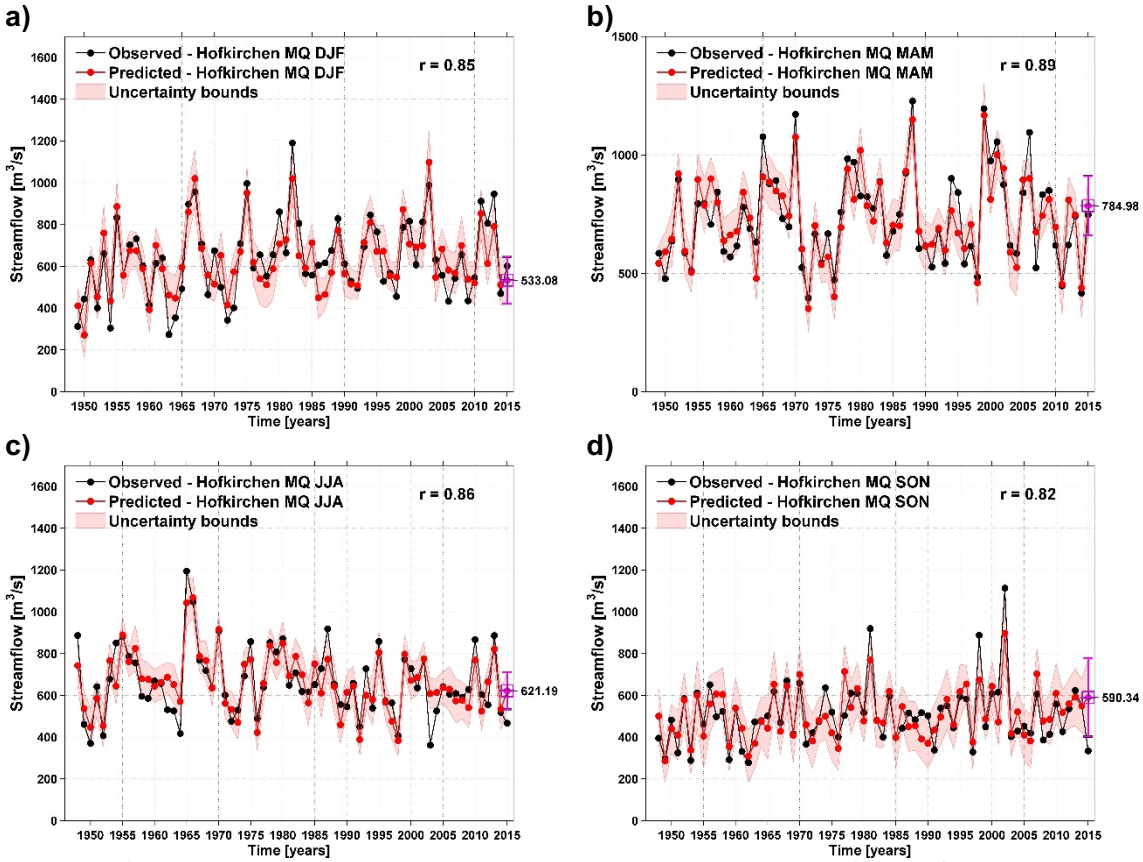

Fig. 52: *Comparison between the observed and predicted seasonal MQ at Hofkirchen station: Observed (black) and Predicted (red) values for the period 1948-2015. The light red shaded area represents the 95% uncertainty bounds.*

Mid-Range forecasting of the German Waterways streamflow Table 1: Contingency table – NM7Q Kaub

	January	February	March	April	May	June	July	August	September	October	November	December
Hit	57	62	63	55	61	40	66	38	57	51	54	63
Miss	9	4	3	11	5	26	0	28	9	15	12	3
Hit %	**86**	**94**	**95**	**83**	**92**	**61**	**100**	**58**	**86**	**77**	**82**	**95**
Miss %	**14**	**6**	**5**	**17**	**8**	**39**	**0**	**42**	**14**	**23**	**18**	**5**

Table 2: Skill parameters – NM7Q Kaub

GOF	January	February	March	April	May	June	July	August	September	October	November	December
ME	-2.88	-4.07	1.78	-0.98	-7.97	-2.58	1.5	-1.6	-4.8	-4.78	-1.98	-2.2
MAE	116.15	141.99	108.44	146.05	102.12	136.41	89.49	137.55	94.31	104.43	121.97	161.68
MSE	21350.36	34379.67	18513.35	34839.02	16676.23	28277.01	11144.39	28743.4	14268.18	17504.05	23890.94	44135.85
RMSE	146.12	185.42	136.06	186.65	129.14	168.16	105.57	169.54	119.45	132.3	154.57	210.09
NRMSE %	36.8	43.8	36.5	42.4	30.9	41.7	26.8	53.4	42	46.7	40.2	43
PBIAS %	-0.2	-0.3	0.1	-0.1	-0.5	-0.2	0.1	-0.1	-0.4	-0.5	-0.2	-0.2
RSR	0.37	0.44	0.37	0.42	0.31	0.42	0.27	0.53	0.42	0.47	0.4	0.43
rSD	0.9	0.91	0.94	0.91	0.96	0.92	0.96	0.85	0.94	0.9	0.92	0.91
NSE	**0.86**	**0.81**	**0.86**	**0.82**	**0.9**	**0.82**	**0.93**	**0.71**	**0.82**	**0.78**	**0.84**	**0.81**
mNSE	0.63	0.55	0.65	0.59	0.7	0.57	0.68	0.45	0.59	0.54	0.55	0.51
rNSE	0.86	0.77	0.83	0.81	0.89	0.78	0.91	0.69	0.77	0.79	0.81	0.78
d	**0.96**	**0.94**	**0.96**	**0.95**	**0.97**	**0.95**	**0.98**	**0.91**	**0.95**	**0.94**	**0.95**	**0.95**
md	0.81	0.77	0.82	0.79	0.85	0.78	0.84	0.7	0.79	0.75	0.77	0.75
rd	0.96	0.93	0.95	0.94	0.97	0.94	0.98	0.9	0.94	0.94	0.95	0.94
cp	0.9	0.9	0.89	0.89	0.94	0.91	0.97	0.87	0.91	0.9	0.93	0.91
r	0.93	0.9	0.93	0.9	0.95	0.91	0.96	0.84	0.91	0.88	0.91	0.9
R2	0.86	0.81	0.86	0.82	0.9	0.82	0.93	0.71	0.82	0.78	0.84	0.81
bR2	0.85	0.79	0.86	0.81	0.89	0.81	0.92	0.7	0.81	0.76	0.82	0.79
KGE	**0.88**	**0.86**	**0.91**	**0.87**	**0.94**	**0.88**	**0.94**	**0.78**	**0.89**	**0.85**	**0.88**	**0.86**
VE	0.9	0.89	0.92	0.9	0.93	0.92	0.94	0.89	0.91	0.89	0.88	0.86

Table 3: Contingency table – MQ Kaub

	January	February	March	April	May	June	July	August	September	October	November	December
Hit	62	54	61	58	64	38	57	49	61	60	51	46
Miss	5	13	6	9	4	30	11	19	7	8	17	22
Hit %	**93**	**81**	**91**	**87**	**94**	**56**	**84**	**72**	**90**	**88**	**75**	**68**
Miss %	**7**	**19**	**9**	**13**	**6**	**44**	**16**	**28**	**10**	**12**	**25**	**32**

Table 4: Skill parameters – MQ Kaub

GOF	January	February	March	April	May	June	July	August	September	October	November	December
ME	-8.44	5.13	7.22	-3.13	-14.62	1.78	0.01	-1.15	1.47	3.8	0.22	-1.89
MAE	168.28	280.14	181.41	194.09	151.13	205.34	187.09	129.32	132.12	117.38	174.81	250.34
MSE	47250.51	117308.9	50202.18	57127.13	43178.36	65772.88	58469.48	26551.8	27640.3	21315.65	48446.73	102685.4
RMSE	217.37	342.5	224.06	239.01	207.79	256.46	241.8	162.95	166.25	146	220.11	320.45
NRMSE %	33.1	48.3	34.3	38	37.2	46.4	49.3	39.2	43.7	33.3	38.5	45.6
PBIAS %	-0.5	0.3	0.4	-0.2	-0.8	0.1	0	-0.1	0.1	0.3	0	-0.1
RSR	0.33	0.48	0.34	0.38	0.37	0.46	0.49	0.39	0.44	0.33	0.38	0.46
rSD	0.94	0.87	0.94	0.92	0.94	0.88	0.87	0.92	0.89	0.94	0.92	0.89
NSE	**0.89**	**0.76**	**0.88**	**0.85**	**0.86**	**0.78**	**0.75**	**0.84**	**0.81**	**0.89**	**0.85**	**0.79**
mNSE	0.67	0.51	0.65	0.61	0.66	0.51	0.48	0.62	0.56	0.65	0.57	0.54
rNSE	0.84	0.67	0.84	0.83	0.87	0.76	0.73	0.82	0.78	0.83	0.75	0.68
d	**0.97**	**0.93**	**0.97**	**0.96**	**0.96**	**0.93**	**0.93**	**0.96**	**0.94**	**0.97**	**0.96**	**0.94**
md	0.83	0.74	0.82	0.8	0.82	0.74	0.73	0.8	0.77	0.82	0.77	0.76
rd	0.96	0.9	0.96	0.95	0.96	0.93	0.92	0.95	0.94	0.95	0.93	0.91
cp	0.92	0.88	0.91	0.91	0.91	0.88	0.9	0.92	0.9	0.94	0.94	0.88
r	0.94	0.87	0.94	0.92	0.93	0.88	0.87	0.92	0.9	0.94	0.92	0.89
R2	0.89	0.76	0.88	0.85	0.86	0.78	0.75	0.84	0.81	0.89	0.85	0.79
bR2	0.87	0.74	0.87	0.84	0.85	0.77	0.74	0.83	0.8	0.88	0.83	0.76
KGE	**0.92**	**0.82**	**0.92**	**0.89**	**0.91**	**0.84**	**0.81**	**0.89**	**0.85**	**0.92**	**0.89**	**0.84**
VE	0.9	0.84	0.9	0.89	0.92	0.9	0.9	0.92	0.9	0.91	0.87	0.85

Table 5: Contingency table – MQ Seasonal Kaub

	DJF	MAM	JJA	SON
Hit	57	56	63	61
Miss	10	11	5	7
Hit %	**85**	**84**	**93**	**90**
Miss %	**15**	**16**	**7**	**10**

Table 6: Skill parameters – MQ Seasonal Kaub

GOF	DJF	MAM	JJA	SON
ME	-7.83	0.77	-0.01	3.3
MAE	203.28	146.4	111.66	153.49
MSE	69879.31	32539.24	21961.12	33946.07
RMSE	264.35	180.39	148.19	184.24
NRMSE %	49.5	33.3	37.3	50.7
PBIAS %	-0.5	0	0	0.2
RSR	0.5	0.33	0.37	0.51
rSD	0.88	0.94	0.93	0.85
NSE	**0.75**	**0.89**	**0.86**	**0.74**
mNSE	0.51	0.67	0.64	0.45
rNSE	0.52	0.87	0.81	0.66
d	**0.93**	**0.97**	**0.96**	**0.92**
md	0.73	0.83	0.81	0.7
rd	0.86	0.96	0.95	0.9
cp	0.84	0.93	0.93	0.89
r	0.87	0.94	0.93	0.86
R2	0.75	0.89	0.86	0.74
bR2	0.73	0.88	0.85	0.73
KGE	**0.82**	**0.92**	**0.9**	**0.8**
VE	0.88	0.92	0.94	0.88

Table 7: Contingency table – NM7Q Neu Darchau

	January	February	March	April	May	June	July	August	September	October	November	December
Hit	48	53	58	51	57	37	51	66	52	59	46	56
Miss	19	14	9	17	11	31	15	0	16	9	22	12
Hit %	**72**	**79**	**87**	**75**	**84**	**54**	**77**	**100**	**76**	**87**	**68**	**82**
Miss %	**28**	**21**	**13**	**25**	**16**	**46**	**23**	**0**	**24**	**13**	**32**	**18**

Table 8: Skill parameters –NM7Q Neu Darchau

GOF	January	February	March	April	May	June	July	August	September	October	November	December
ME	0.04	1.27	-1.67	-3.64	2.42	-0.07	-0.51	0.1	-0.63	-0.08	1.3	0.74
MAE	91.57	104.45	72.37	125.68	77.95	92.08	46.87	12.39	29.34	22.02	58.95	45.62
MSE	13047.97	17571.27	7931.24	26618.73	9989.37	13531.94	3443.32	259.77	1496.74	786.7	5130.02	3295.57
RMSE	114.23	132.56	89.06	163.15	99.95	116.33	58.68	16.12	38.69	28.05	71.62	57.41
NRMSE %	35.5	46.1	33.1	49.2	42.3	52.3	38.5	10.8	28.8	20.5	32.6	26.5
PBIAS %	0	0.2	-0.2	-0.5	0.4	0	-0.1	0	-0.2	0	0.3	0.1
RSR	0.35	0.46	0.33	0.49	0.42	0.52	0.38	0.11	0.29	0.21	0.33	0.27
rSD	0.93	0.89	0.95	0.89	0.9	0.85	0.93	0.99	0.96	0.98	0.94	0.96
NSE	**0.87**	**0.78**	**0.89**	**0.75**	**0.82**	**0.72**	**0.85**	**0.99**	**0.92**	**0.96**	**0.89**	**0.93**
mNSE	0.62	0.55	0.68	0.53	0.56	0.42	0.59	0.89	0.73	0.81	0.62	0.72
rNSE	0.76	0.72	0.87	0.72	0.79	0.73	0.78	0.98	0.88	0.95	0.87	0.88
d	**0.96**	**0.94**	**0.97**	**0.93**	**0.95**	**0.91**	**0.96**	**1**	**0.98**	**0.99**	**0.97**	**0.98**
md	0.81	0.76	0.83	0.75	0.77	0.7	0.79	0.95	0.86	0.9	0.81	0.86
rd	0.93	0.92	0.96	0.92	0.94	0.92	0.94	1	0.97	0.99	0.97	0.97
cp	0.93	0.88	0.93	0.85	0.89	0.86	0.91	0.99	0.95	0.97	0.95	0.97
r	0.93	0.89	0.94	0.87	0.9	0.85	0.92	0.99	0.96	0.98	0.94	0.96
R2	0.87	0.78	0.89	0.76	0.82	0.72	0.85	0.99	0.92	0.96	0.89	0.93
bR2	0.85	0.76	0.88	0.73	0.8	0.69	0.83	0.99	0.91	0.95	0.88	0.92
KGE	**0.91**	**0.84**	**0.93**	**0.83**	**0.86**	**0.79**	**0.89**	**0.99**	**0.94**	**0.97**	**0.92**	**0.95**
VE	0.86	0.85	0.91	0.84	0.86	0.8	0.88	0.97	0.92	0.94	0.87	0.91

Table 9: Contingency table – MQ Neu Darchau

	January	February	March	April	May	June	July	August	September	October	November	December
Hit	44	47	60	52	63	30	43	51	41	60	53	45
Miss	23	20	7	16	5	38	25	17	27	8	15	23
Hit %	**66**	**70**	**90**	**76**	**93**	**44**	**63**	**75**	**60**	**88**	**78**	**66**
Miss %	**34**	**30**	**10**	**24**	**7**	**56**	**37**	**25**	**40**	**12**	**22**	**34**

Table 10: Skill parameters –MQ Neu Darchau

GOF	January	February	March	April	May	June	July	August	September	October	November	December
ME	-3.56	1.76	0.59	-0.37	-0.32	-2.33	-0.39	0.28	-0.58	-1.33	1.11	1.33
MAE	140.5	135.11	98.18	140.84	64.48	141.98	107.26	107.7	58.3	38.01	77.52	89.79
MSE	27228.86	28295.09	15183.78	37458.22	6302.53	41640.4	20358.81	22120.27	5525.03	2279.97	10253.65	12352.12
RMSE	165.01	168.21	123.22	193.54	79.39	204.06	142.68	148.73	74.33	47.75	101.26	111.14
NRMSE %	36.2	42.2	31.9	42.5	25.2	54.9	55.8	56.3	38	23.6	33.9	32.9
PBIAS %	-0.4	0.2	0.1	0	0	-0.4	-0.1	0.1	-0.1	-0.3	0.2	0.2
RSR	0.36	0.42	0.32	0.42	0.25	0.55	0.56	0.56	0.38	0.24	0.34	0.33
rSD	0.93	0.9	0.94	0.9	0.97	0.84	0.83	0.82	0.93	0.98	0.94	0.94
NSE	**0.87**	**0.82**	**0.9**	**0.82**	**0.94**	**0.69**	**0.68**	**0.68**	**0.85**	**0.94**	**0.88**	**0.89**
mNSE	0.59	0.59	0.69	0.6	0.74	0.45	0.45	0.43	0.6	0.76	0.64	0.64
rNSE	0.73	0.56	0.85	0.83	0.9	0.73	0.72	0.6	0.81	0.91	0.85	0.84
d	**0.96**	**0.95**	**0.97**	**0.95**	**0.98**	**0.9**	**0.9**	**0.9**	**0.96**	**0.99**	**0.97**	**0.97**
md	0.79	0.78	0.84	0.8	0.87	0.71	0.71	0.7	0.8	0.88	0.82	0.81
rd	0.93	0.87	0.96	0.95	0.97	0.92	0.91	0.87	0.95	0.98	0.96	0.96
cp	0.92	0.9	0.93	0.89	0.96	0.85	0.81	0.8	0.91	0.97	0.95	0.95
r	0.93	0.91	0.95	0.9	0.97	0.83	0.83	0.82	0.92	0.97	0.94	0.94
R2	0.87	0.82	0.9	0.82	0.94	0.69	0.68	0.68	0.85	0.94	0.88	0.89
bR2	0.84	0.8	0.89	0.79	0.93	0.64	0.64	0.63	0.83	0.93	0.86	0.87
KGE	**0.9**	**0.87**	**0.92**	**0.86**	**0.95**	**0.77**	**0.76**	**0.75**	**0.9**	**0.96**	**0.91**	**0.92**
VE	0.84	0.85	0.9	0.87	0.91	0.77	0.8	0.78	0.87	0.92	0.86	0.87

Table 11: Contingency table – MQ Seasonal Neu Darchau

	DJF	MAM	JJA	SON
Hit	55	57	50	54
Miss	12	10	18	14
Hit %	**82**	**85**	**74**	**79**
Miss %	**18**	**15**	**26**	**21**

Table 12: Skill parameters –MQ Seasonal Neu Darchau

GOF	DJF	MAM	JJA	SON
ME	-1.4	-0.62	1.74	0.81
MAE	100.57	96.19	92.71	63.06
MSE	15551.3	14113.8	15505.6	6272.35
RMSE	124.71	118.8	124.52	79.2
NRMSE %	35.6	37.6	54.9	38.3
PBIAS %	-0.2	-0.1	0.3	0.2
RSR	0.36	0.38	0.55	0.38
rSD	0.94	0.93	0.83	0.92
NSE	**0.87**	**0.86**	**0.69**	**0.85**
mNSE	0.64	0.64	0.48	0.62
rNSE	0.69	0.83	0.6	0.77
d	**0.96**	**0.96**	**0.9**	**0.96**
md	0.81	0.81	0.71	0.8
rd	0.91	0.95	0.87	0.94
cp	0.92	0.9	0.82	0.93
r	0.93	0.93	0.83	0.92
R2	0.87	0.86	0.69	0.85
bR2	0.85	0.84	0.66	0.83
KGE	**0.91**	**0.9**	**0.76**	**0.89**
VE	0.88	0.9	0.83	0.87

Table 13: Contingency table – NM7Q Hofkirchen

	January	February	March	April	May	June	July	August	September	October	November	December
Hit	51	51	52	38	54	56	39	57	42	45	43	48
Miss	16	16	15	29	14	12	29	11	26	23	25	20
Hit %	**76**	**76**	**78**	**57**	**79**	**82**	**57**	**84**	**62**	**66**	**63**	**71**
Miss %	**24**	**24**	**22**	**43**	**21**	**18**	**43**	**16**	**38**	**34**	**37**	**29**

Table 14: Skill parameters – NM7Q Hofkirchen

GOF	January	February	March	April	May	June	July	August	September	October	November	December
ME	-2.48	1.06	0.99	0.24	-2.37	-1.15	0.43	-0.69	0.87	0.68	0.31	-0.41
MAE	39.51	59.48	66.7	57.16	46.39	51.86	71.49	35.19	34.29	41.11	46.14	59.75
MSE	2478.76	5286.21	8069.66	5528.47	3272.07	3879.83	8011.99	1939.01	1823.07	2841.01	3499.6	6048.48
RMSE	49.79	72.71	89.83	74.35	57.2	62.29	89.51	44.03	42.7	53.3	59.16	77.77
NRMSE %	35.8	49.4	57.5	45.8	37.2	39.5	63.4	37.9	53.7	50.4	40.3	53.2
PBIAS %	-0.5	0.2	0.2	0	-0.4	-0.2	0.1	-0.2	0.2	0.2	0.1	-0.1
RSR	0.36	0.49	0.58	0.46	0.37	0.39	0.63	0.38	0.54	0.5	0.4	0.53
rSD	0.93	0.87	0.82	0.89	0.94	0.92	0.77	0.94	0.83	0.86	0.91	0.85
NSE	**0.87**	**0.75**	**0.66**	**0.79**	**0.86**	**0.84**	**0.59**	**0.85**	**0.71**	**0.74**	**0.84**	**0.71**
mNSE	0.63	0.51	0.46	0.56	0.6	0.57	0.31	0.6	0.48	0.43	0.49	0.41
rNSE	0.87	0.71	0.55	0.76	0.86	0.8	0.54	0.84	0.66	0.74	0.84	0.75
d	**0.96**	**0.92**	**0.89**	**0.94**	**0.96**	**0.96**	**0.86**	**0.96**	**0.91**	**0.92**	**0.95**	**0.91**
md	0.81	0.74	0.7	0.77	0.8	0.78	0.62	0.79	0.71	0.71	0.74	0.69
rd	0.97	0.91	0.85	0.93	0.96	0.94	0.84	0.96	0.89	0.92	0.96	0.92
cp	0.9	0.85	0.74	0.88	0.91	0.91	0.76	0.92	0.82	0.87	0.93	0.85
r	0.93	0.87	0.82	0.89	0.93	0.92	0.77	0.92	0.84	0.86	0.91	0.84
R2	0.87	0.75	0.66	0.79	0.86	0.84	0.59	0.85	0.71	0.74	0.84	0.71
bR2	0.86	0.74	0.65	0.78	0.85	0.83	0.57	0.85	0.7	0.73	0.82	0.69
KGE	**0.9**	**0.81**	**0.74**	**0.84**	**0.9**	**0.89**	**0.67**	**0.9**	**0.77**	**0.8**	**0.88**	**0.78**
VE	0.91	0.88	0.88	0.91	0.92	0.9	0.85	0.92	0.91	0.89	0.89	0.86

Table 15: Contingency table – MQ Hofkirchen

	January	February	March	April	May	June	July	August	September	October	November	December
Hit	48	49	55	44	46	36	48	43	47	48	58	51
Miss	19	18	12	23	22	32	20	25	21	20	10	17
Hit %	**72**	**73**	**82**	**66**	**68**	**53**	**71**	**63**	**69**	**71**	**85**	**75**
Miss %	**28**	**27**	**18**	**34**	**32**	**47**	**29**	**37**	**31**	**29**	**15**	**25**

Table 16: Skill parameters – MQ Hofkirchen

GOF	January	February	March	April	May	June	July	August	September	October	November	December
ME	-1.13	0.45	3.58	-1.09	-6.01	0.16	-2.05	1.53	1.83	1.46	0.58	-1.18
MAE	74.29	110.88	77.41	61.4	75.75	111.83	108.37	78.66	56.07	56.15	46.09	76.44
MSE	9251.65	20239.71	8712.24	7236.62	10906.69	22496.3	19125.3	8770.22	5405.44	4727.29	3678.19	10015.68
RMSE	96.19	142.27	93.34	85.07	104.44	149.99	138.29	93.65	73.52	68.76	60.65	100.08
NRMSE %	41.6	58.1	38.5	37.5	50.5	56.7	59.8	50.6	51.8	39.7	28.3	42.1
PBIAS %	-0.2	0.1	0.5	-0.1	-0.9	0	-0.3	0.3	0.4	0.3	0.1	-0.2
RSR	0.42	0.58	0.39	0.38	0.5	0.57	0.6	0.51	0.52	0.4	0.28	0.42
rSD	0.9	0.81	0.93	0.93	0.89	0.82	0.82	0.85	0.84	0.91	0.96	0.91
NSE	**0.82**	**0.66**	**0.85**	**0.86**	**0.74**	**0.67**	**0.64**	**0.74**	**0.73**	**0.84**	**0.92**	**0.82**
mNSE	0.6	0.44	0.6	0.66	0.5	0.36	0.37	0.44	0.51	0.54	0.68	0.59
rNSE	0.76	0.52	0.8	0.87	0.79	0.65	0.56	0.69	0.67	0.81	0.9	0.77
d	**0.95**	**0.89**	**0.96**	**0.96**	**0.92**	**0.89**	**0.88**	**0.92**	**0.92**	**0.95**	**0.98**	**0.95**
md	0.78	0.7	0.79	0.83	0.75	0.68	0.67	0.7	0.74	0.76	0.83	0.79
rd	0.93	0.85	0.94	0.96	0.94	0.89	0.86	0.9	0.9	0.95	0.97	0.93
cp	0.86	0.81	0.89	0.92	0.86	0.85	0.78	0.88	0.84	0.92	0.97	0.9
r	0.91	0.81	0.92	0.93	0.86	0.82	0.8	0.86	0.85	0.92	0.96	0.91
R2	0.82	0.66	0.85	0.86	0.74	0.67	0.64	0.74	0.73	0.84	0.92	0.82
bR2	0.81	0.63	0.84	0.85	0.72	0.65	0.61	0.72	0.72	0.83	0.91	0.8
KGE	**0.87**	**0.73**	**0.89**	**0.9**	**0.82**	**0.75**	**0.73**	**0.8**	**0.79**	**0.88**	**0.94**	**0.87**
VE	0.88	0.83	0.9	0.92	0.89	0.85	0.84	0.87	0.89	0.88	0.91	0.87

Table 17: Contingency table – MQ Seasonal Hofkirchen

	DJF	MAM	JJA	SON
Hit	41	51	49	55
Miss	26	16	19	13
Hit %	**61**	**76**	**72**	**81**
Miss %	**39**	**24**	**28**	**19**

Table 18: Skill parameters – MQ Seasonal Hofkirchen

GOF	DJF	MAM	JJA	SON
ME	-1.02	0.56	2.27	3.76
MAE	83.8	68.06	66.5	66.49
MSE	9775.14	7512.01	7018.62	7494.53
RMSE	98.87	86.67	83.78	86.57
NRMSE %	53.1	44.5	51.2	59.8
PBIAS %	-0.2	0.1	0.3	0.7
RSR	0.53	0.44	0.51	0.6
rSD	0.85	0.89	0.85	0.82
NSE	**0.71**	**0.8**	**0.73**	**0.64**
mNSE	0.42	0.57	0.48	0.36
rNSE	0.56	0.79	0.61	0.59
d	**0.91**	**0.94**	**0.92**	**0.88**
md	0.69	0.77	0.72	0.67
rd	0.86	0.94	0.88	0.86
cp	0.81	0.88	0.85	0.84
r	0.85	0.89	0.86	0.8
R2	0.71	0.8	0.73	0.64
bR2	0.7	0.79	0.73	0.63
KGE	**0.78**	**0.85**	**0.79**	**0.73**
VE	0.87	0.91	0.9	0.87

Die **Berichte zur Polar- und Meeresforschung** (ISSN 1866-3192) werden beginnend mit dem Band 569 (2008) als Open-Access-Publikation herausgegeben. Ein Verzeichnis aller Bände einschließlich der Druckausgaben (ISSN 1618-3193, Band 377-568, von 2000 bis 2008) sowie der früheren **Berichte zur Polarforschung** (ISSN 0176-5027, Band 1-376, von 1981 bis 2000) befindet sich im electronic Publication Information Center **(ePIC)** des Alfred-Wegener-Instituts, Helmholtz-Zentrum für Polar- und Meeresforschung (AWI); see http://epic.awi.de. Durch Auswahl “Reports on Polar- and Marine Research“ (via “browse”/”type”) wird eine Liste der Publikationen, sortiert nach Bandnummer, innerhalb der absteigenden chronologischen Reihenfolge der Jahrgänge mit Verweis auf das jeweilige pdf-Symbol zum Herunterladen angezeigt.

The **Reports on Polar and Marine Research** (ISSN 1866-3192) are available as open access publications since 2008. A table of all volumes including the printed issues (ISSN 1618-3193, Vol. 377-568, from 2000 until 2008), as well as the earlier **Reports on Polar Research** (ISSN 0176-5027, Vol. 1-376, from 1981 until 2000) is provided by the electronic Publication Information Center **(ePIC)** of the Alfred Wegener Institute, Helmholtz Centre for Polar and Marine Research (AWI); see URL http://epic.awi.de. To generate a list of all Reports, use the URL http://epic.awi.de and select “browse”/ ”type” to browse ”Reports on Polar and Marine Research”. A chronological list in declining order will be presented, and pdf-icons displayed for downloading.

Zuletzt erschienene Ausgaben:

Recently published issues:

711 (2017) Mid-Range forecasting of the German Waterways streamflow based on hydrologic, atmospheric and oceanic data, by Monica Ionita

710 (2017) The Expedition PS103 of the Research Vessel POLARSTERN to the Weddell Sea in 2016/2017, edited by Olaf Boebel

709 (2017) Russian-German Cooperation: Expeditions to Siberia in 2016, edited by Pier Paul Overduin, Franziska Blender, Dmitry Y. Bolshiyanov, Mikhail N. Grigoriev, Anne Morgenstern, Hanno Meyer

708 (2017) The role of atmospheric circulation patterns on the variability of ice core constitutents in coastal Dronning Maud Land, Antarctica, by Kerstin Schmidt

707 (2017) Distribution patterns and migratory behavior of Antarctic blue whales, by Karolin Thomisch

706 (2017) The Expedition PS101 of the Research Vessel POLARSTERN to the Arctic Ocean in 2016, edited by Antje Boetius and Autun Purser

705 (2017) The Expedition PS100 of the Research Vessel POLARSTERN to the Fram Strait in 2016, edited by Torsten Kanzow

704 (2016) The Expeditions PS99.1 and PS99.2 of the Research Vessel POLARSTERN to the Fram Strait in 2016, edited by Thomas Soltwedel

703 (2016) The Expedition PS94 of the Research Vessel POLARSTERN to the central Arctic Ocean in 2015, edited by Ursula Schauer

702 (2016) The Expeditions PS95.1 and PS95.2 of the Research Vessel POLARSTERN to the Atlantic Ocean in 2015, edited by Rainer Knust and Karin Lochte

701 (2016) The Expedition PS97 of the Research Vessel POLARSTERN to the Drake Passage in 2016, edited by Frank Lamy

700 (2016) The Expedition PS96 of the Research Vessel POLARSTERN to the southern Weddell Sea in 2015/2016, edited by Michael Schröder

ALFRED-WEGENER-INSTITUT
HELMHOLTZ-ZENTRUM FÜR POLAR-
UND MEERESFORSCHUNG

BREMERHAVEN

Am Handelshafen 12
27570 Bremerhaven
Telefon 0471 4831-0
Telefax 0471 4831-1149
www.awi.de

HELMHOLTZ
GEMEINSCHAFT